NASA CR-112061

DESIGN AND TESTING OF A MAGNETIC SUSPENSION AND DAMPING SYSTEM FOR A SPACE TELESCOPE

FINAL TECHNICAL REPORT

MAY 1972

SPACE DIVISION CHRYSLER CORPORATION

NASA CR-112061

DESIGN AND TESTING OF A MAGNETIC SUSPENSION AND DAMPING SYSTEM FOR A SPACE TELESCOPE

By Norman J. Ockman

Prepared under Contract No. NAS1-10776 by
CHRYSLER CORPORATION SPACE DIVISION
New Orleans, Louisiana
for
NATIONAL AERONAUTICS AND SPACE ADMINISTRATION

TABLE OF CONTENTS

TABLE OF CONTENTS (continued)

LIST OF ILLUSTRATIONS

LIST OF ILLUSTRATIONS (Continued)

SYMBOLS

a	Damping Constant for Analog Simulation ($kg/m^2 sec^2$)
a_x, $a_{\ddot{x}}$, $a_{\dot{\theta}}$	Analog Computer Scale Factors Relating Space Variables to Machine Variables (section 6)
$b(r)$	Magnetic Field Within Helmholtz Coil (Gauss)
$B(\omega)$	Hankel Transform of $b(r)$
d	Thickness of Disc Magnet (cm)
F_{1x}, F_{2x}	x Component of Damping Force on Disc Magnets No. 1 and No. 2, Respectively
F_{1y}, F_{2y}	y Component of Damping Force on Disc Magnets No. 1 and No. 2, Respectively
F_θ	Torque Exerted on Air Bearing due to Damping System
$F[\ ]$	Fourier Transform of Term in Brackets
$H[\ ]$	Hankel Transform of Term in Brackets
$H_z(z, \theta = 0)$	Magnetic Field Along Axis of Solenoid (Oersted)
$H_z(r, \theta = 0)$	Magnetic Field in Central Plane of Solenoid (Oersted)
I_z	Moment of Inertia of Air Bearing (kg/m^2)
$i(s)$	Instantaneous Current in Suspension Coils
ℓ	Distance Between Disc Magnets (Meters)
k	Stiffness of Spring Constant of Suspension (n/m)
K	Gain of Electronics in Damping System
$m(r)$	Magnetization of Disc Magnet ($Maxwell/cm^2$)
M	Mass of Air Bearing
$M(\omega)$	Hankel Transform of $m(r)$
nc	Non-conservative (used as a subscript)
r_o	Radius of Disc Magnet
r_1, r_2	Distance of Disc Magnet from its Respective Equilibrium Position
$U(r)$	Potential Energy of Disc Magnet (dynes cm)
$V(s)$	Voltage Across Suspension Coil

SYMBOLS (continued)

x, y, θ	Space Coordinates of Air Bearing
X, Y, Θ	Machine Variables (Units of Volts) Representing Space Coordinates of Air Bearing
$Z(s)$	Impedance of Suspension Coil
δ	Distance from Center of Air Bearing to Center of Mass
θ	Rotational Displacement of Air Bearing (Radians)
ω_r	Rotational Resonant Frequency (Rad/Sec)
ω_t	Translational Resonant Frequency (Rad/Sec)
$\Gamma(z)$	Gamma Function

Section 1

SUMMARY

To fully utilize the anticipated resolving power of large orbiting telescopes, it is necessary to isolate the telescope from the random disturbances created by a manned spacecraft. Such isolation reduces the complexity of the fine-pointing control system of the telescope and tends to increase pointing accuracy.

The basic equations of motion are derived for a two-dimensional, three-degree of freedom simulation of a space telescope coupled to a spacecraft by means of a magnetic suspension and isolation system. The system consists of paramagnetic or ferromagnetic discs confined to the magnetic field between two Helmholtz coils. Damping is introduced by varying the magnetic field in proportion to a velocity signal derived from the telescope.

The equations of motion are nonlinear, similar in behavior to the one-dimensional Van der Pol equation. The equations were simulated on an analog computer to determine isolation effectiveness and system response to various driving functions.

The computer simulation was verified by testing a 264-kilogram air bearing platform which simulates the telescope in a frictionless environment. The air bearing is attached to a hydraulic shaker by means of the isolation system and the shaker made according to the desired driving function.

The simulation demonstrated effective isolation capabilities for disturbance frequencies above resonance. Damping in the system improved the response near resonance and prevented the build-up of large oscillatory amplitudes. The damping is highly amplitude dependent. A damping effect equivalent to that of a linear second-order system damping ratio of 0.55 was demonstrated for translational amplitudes of 2.0 millimeters. Damping, equivalent to a damping ratio of 0.80 was demonstrated for rotational amplitudes of 1.0 arc-minute. Usable damping was obtained for rotations of 0.5 arc-minute.

Section 2
INTRODUCTION

One of the space scientific programs proposed for post-Apollo applications is the large orbital telescope, or space observatory. Such a space observatory will carry out observations much as its Earth-based counterpart, but above the obscuration of the Earth's atmosphere. The advantages of space astronomy - an increased spectral range and higher resolution - are so attractive that the eventual deployment of such an observatory is a virtual certainty.

However,to fully use the theoretical resolving power of a space telescope, perhaps as low as 0.01 arc-second, the telescope must be stabilized in attitude to a corresponding precision. To achieve this level of stability, the physical disturbances transmitted to the telescope during operation must be very small. For an unmanned telescope in synchronous orbit this is no problem; the natural space environment is practically disturbance free and the pointing control system can handle small internal disturbances. But for a manned telescope, the disturbance environment caused by man's dynamic movements and the increased complexity of the spacecraft create a serious stabilization problem, even at synchronous orbit.

The key to meeting the precise stabilization requirements is to isolate the telescope from the disturbance created by the manned spacecraft to which it is attached. Such an isolation will result in increased pointing accuracy and smaller bandwidth requirements for the fine-pointing control system.

The purpose of this study has been to analytically study, design, and test a prototype magnetic suspension and damping system. Such a system utilizes magnetic fields rather than mechanical contacts to stabilize and control the relative motions between the spacecraft and the telescope.

This system reduces the amplitude of the torques exerted on the telescope by the random spacecraft motion and provides damping to ensure that large oscillatory motions of the telescope cannot result. The magnetic suspension discussed in this report allows for real-time adjustment of suspension stiffness and, therefore, the degree of isolation. The system damping is obtained by instantaneously adjusting the stiffness to remove unwanted disturbances. The stiffness is varied according to a control signal proportional to the relative velocity between the telescope and the spacecraft.

In this report the behavior of a space telescope attached to a spacecraft by such a magnetic suspension was investigated. The differential equations of motion were derived. The equations for translational and rotational motion were found to be similar to the one-dimensional Van der Pol equation in which the damping term is proportional to the product of the velocity and the square of the displacement, rather then simply proportional to the velocity as in the case of the linear second-order system. Aside from small coupling terms between degrees of freedom, this damping term is the only nonlinear term in the equations.

The equations of motion of the telescope were simulated on an analog computer to determine the response to various spacecraft disturbances and initial conditions. The damping rate was found to be highly amplitude dependent, and for practical purposes damping can be considered to exist only for amplitudes above a certain threshold value.

The behavior of the telescope suspension was experimentally verified by tests performed on an air bearing platform floating on a smooth granite table. The air bearing platform provides an essentially frictionless environment in two dimensions, simulating in part the motion of a space telescope. The air bearing was positioned on the table by means of the magnetic suspension, and disturbances, simulating a spacecraft motion, were introduced to the system. The subsequent motion of the air bearing was then monitored.

The results of the study demonstrate that the magnetic suspension and damping system can provide suitable isolation for a space telescope and can provide damping in both the translational and rotational degrees of freedom. Anticipated problem areas in alignment and adjustment are discussed in section 9, although no difficulties have been encountered which would seriously compromise the applicability of the system.

An appendix is provided in which some of the important parameters in suspension magnet design are discussed. The relationship between the magnetic field distribution in the suspension coils and the suspension stiffness; i.e., potential energy function, is shown. Extensive descriptions or calculations relating a particular magnetic field distribution to the actual physical dimensions of the suspension coils are not included because this material is adequately covered in the literature on magnet design. It is further shown in the appendix that the physical dimensions of the coils are not critical in their effect on the stiffness vs. displacement (or shape) of the potential energy function. References are provided and the equations involving the coil sizes and the field distributions are listed. The appendix also describes a method involving the use of integral transforms to eliminate much of the computer calculations involved in the magnet design. Two examples are illustrated.

Section 3
DESCRIPTION OF TEST FACILITY

Chrysler Corporation Space Division has designed and built a facility to test the response of a suspension system to a specified set of input disturbance functions applied along one axis. The load and suspension system are free to move in a horizontal plane in both rotation and translational modes, under the influence of the applied force only. That is, there are no external restraining forces such as friction and, therefore, the response of the system to forces in any direction can be completely isolated and measured, facilitating design (see figure 3.1-1).

The basic facility consists of the following major apparatus:

- A 35-inch-diameter air bearing platform with self-contained air supply.
- A granite-surface micro-flat table on which the air bearing platform moves essentially without friction.
- A triangular frame which encloses the platform but is not attached to it. The frame rests on three channeled slip tables which allow it to move back and forth along one axis.
- A hydraulic shaker which is attached to the triangular frame and can be programmed to follow an electric waveform over a frequency range from 0.1 Hz to 1000 Hz.
- A Systron-Donner Model 80 analogue computer to provide input signals to the shaker and to process output data.

The air bearing platform corresponds to a load or system which is to be suspended. Its mass, center of gravity and moment of inertia must be compatible with those of the actual load which is to be suspended or isolated. If the platform cannot be modified to match the mass characteristics of the true load, then some type of modeling or scaling must be performed to correlate the data. This is not difficult in the cases of linear suspension systems, but becomes rather complex in the case of nonlinear systems. However, even for the nonlinear systems, it is generally possible to make assumptions and approximations which provide sufficient accuracy for most cases.

In operation, the suspension system to be tested is connected between the triangular frame and the air bearing platform. The desired displacement function for the input disturbance is generated as a voltage-time waveform and applied to the

shaker, causing the shaker and the attached frame to move in accordance with the original displacement function. Instrumentation on the platform records its displacement and acceleration in both the translational and rotational modes.

The frame has been designed to facilitate the mounting of varied types of attachment points for the suspension systems, so that the suspension systems can quickly and easily be removed, modified and returned.

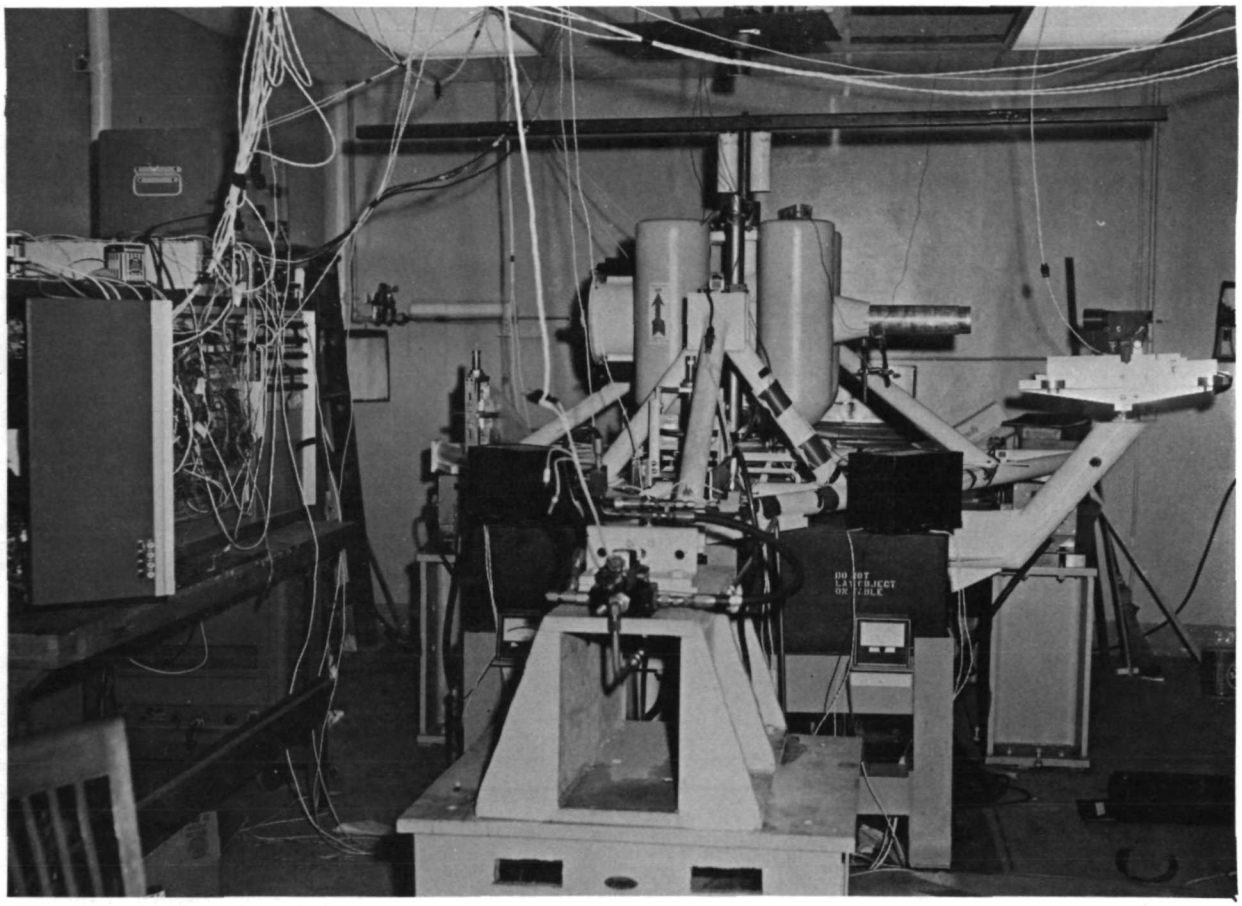

Figure 3.1-1. Isolation Test Facility

Section 4

DESCRIPTION OF MAGNETIC SUSPENSION SYSTEM

4.1 GENERAL DESCRIPTION

Under a previous NASA contract, NASA1-9674, a preliminary design of a two-dimensional magnetic suspension and damping system was tested and found to have a number of advantages over conventional spring configurations, the principal advantage being real-time adjustable spring constants and damping rates.

The magnetic suspension systems investigated were based on the fact that when a ferromagnetic or paramagnetic material experiences a force in a non-uniform magnetic field, the force tends to move the material toward the region of highest magnetic field.

Two coils were used to obtain the magnetic field for the suspension system. They were connected in parallel across a power supply and oriented so that the fields added (see figure 4.1-1).

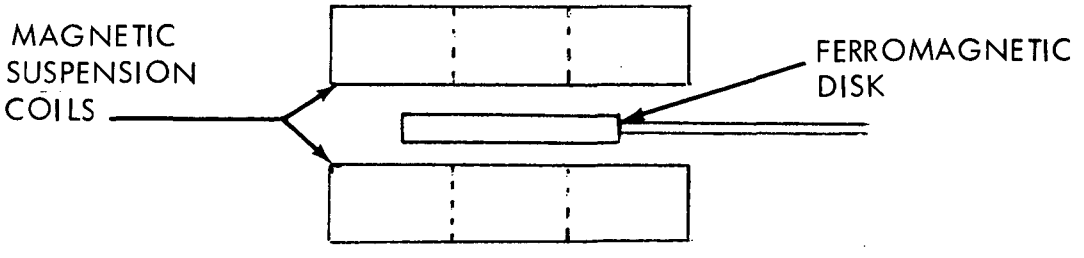

Figure 4.1-1. Magnetic Coil Geometry

The ferromagnetic disc consisted of a soft iron disc 0.7-cm thick and 5-cm in diameter which was attached to the bearing by means of a small aluminum rod. An identical suspension system was placed on the other side of the air bearing to prevent rotation. This provided a two-axis suspension system.

Damping was introduced into the system by means of a velocity sensor which changed the current through the suspension coils according to changes in the velocity of the air bearing. The velocity was sensed by two pickup coils fastened to the shaker frame. The coils were obtained from a commercial solenoid valve. A magnet positioned under the velocity sensing coils induced a voltage in the coils proportional

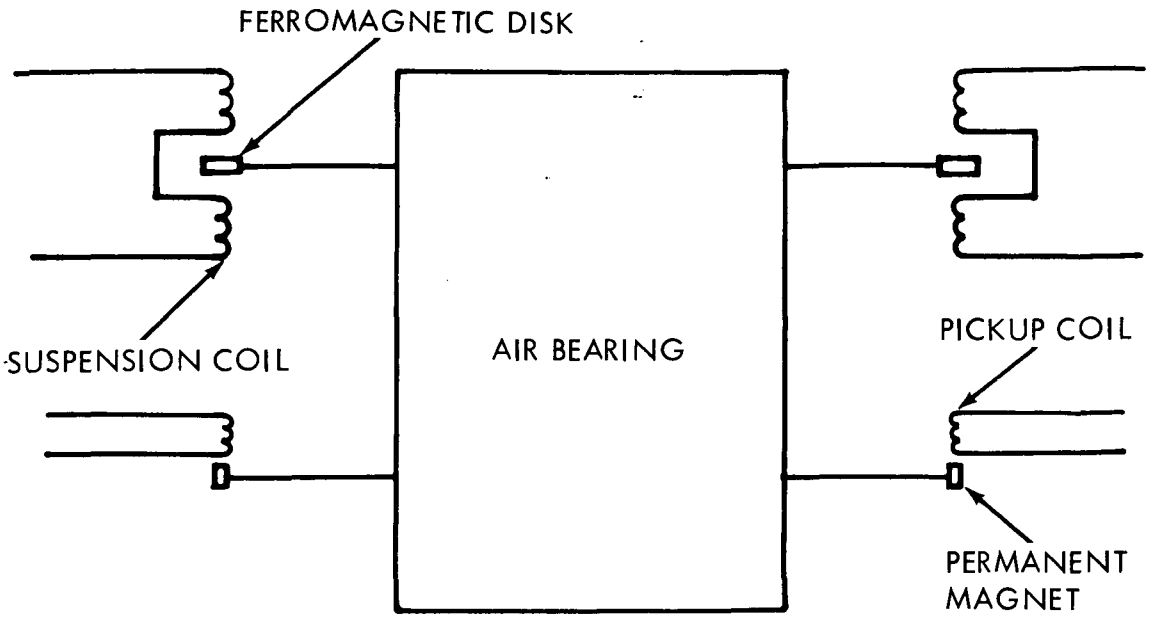

Figure 4.1-2. Suspension Geometry

to the velocity. An identical magnet and arm were fastened to the other side of the bearing (see figure 4.1-2). The magnets and pickup coils were positioned so that with current going through the suspension coils and the bearing in its equilibrium position, the small magnets in each of the arms were directly beneath the center of the pickup coils.

With the magnets and pickup coils positioned as described, the movement of any magnet induced a voltage in its respective pickup coil. The magnitude of the voltage was proportional to the velocity of the magnet (and hence to the velocity of that arm of the bearing). The induced voltage had one polarity for velocities away from equilibrium and the opposite polarity for velocities toward equilibrium.

The induced voltage from each pickup coil was amplified and used as a control signal to vary the current in the suspension coils. When the air bearing was motionless, the control signal was zero, and current in the suspension coils was at its steady-state value, I_0. The polarity of the control signal was such that when one arm of the air bearing was moving away from its equilibrium position, the control signal caused the current in the suspension coils to increase in proportion to bearing velocity away from equilibrium. This increase in current created an additional force (over and above that due to I_0) tending to return the bearing to its equilibrium position. When the bearing was moving toward equilibrium position, the current in the suspension coils was reduced below its steady-state value, I_0, creating less restoring force. The net result was a damping effect which removed energy from each oscillation, causing the amplitude to decrease with each cycle.

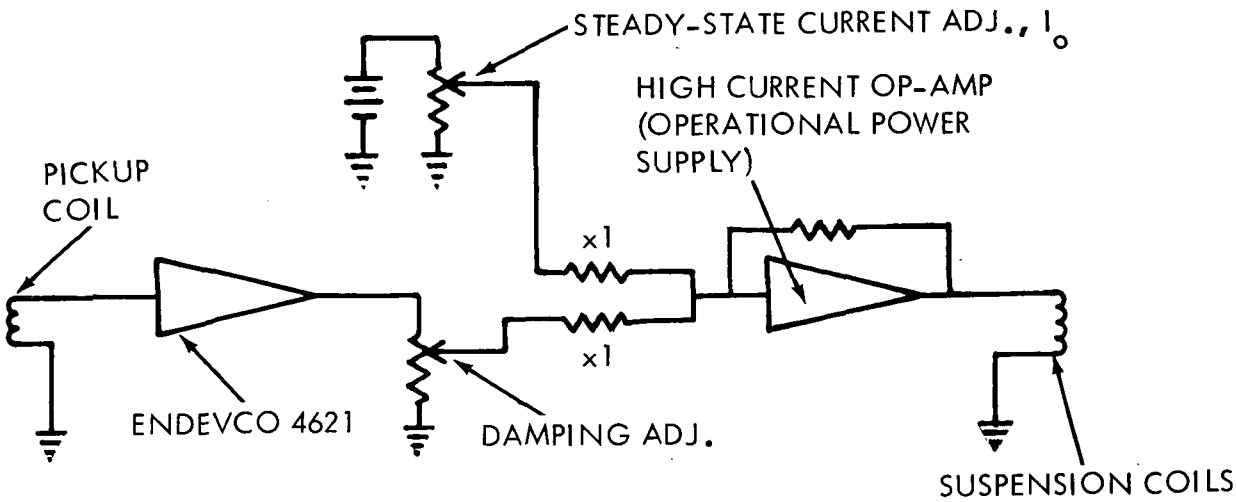

Figure 4.1-3. Damping Electronics

Figure 4.1-3 is a simplified schematic diagram of the damping electronics. The amount of damping is controlled by changing the gain, K, of the first amplifier or by varying the output potentiometer.

In the previous contract, which was a survey of different isolation concepts, no attempt was made to optimize the sizes of the magnet coils and the magnetic discs for maximum damping and isolation characteristics. One of the objectives of the present contract was to determine the significant parameters in the system design and to incorporate these parameters as much as possible in a laboratory simulation. A discussion of coil and magnet design is included in appendix A.

The major changes made in the system described in this report were the reduction in diameter of the suspension and velocity pickup coils and in replacing the ferromagnetic disc by a permanent ceramic magnet (see figure 8.1-1). The permanent magnet allowed the use of a smaller suspension coil current. Various combinations of magnets and coil separation were also used in order to increase the magnitude of the velocity signal and to obtain a tighter control of the air bearing for small movements.

4.2 DAMPING TECHNIQUES

The output of the velocity sensing coil is shown in figures 4.2-1a and 4.2-1b for positive and negative velocities. The system studied operates only in the linear portion of the curve about $X = 0$. The curve represents the output voltage of the pickup coil, and, therefore, the change in the effective spring constant, as a function of the air bearing position. The output can be represented by $V = -bx\dot{x}$.

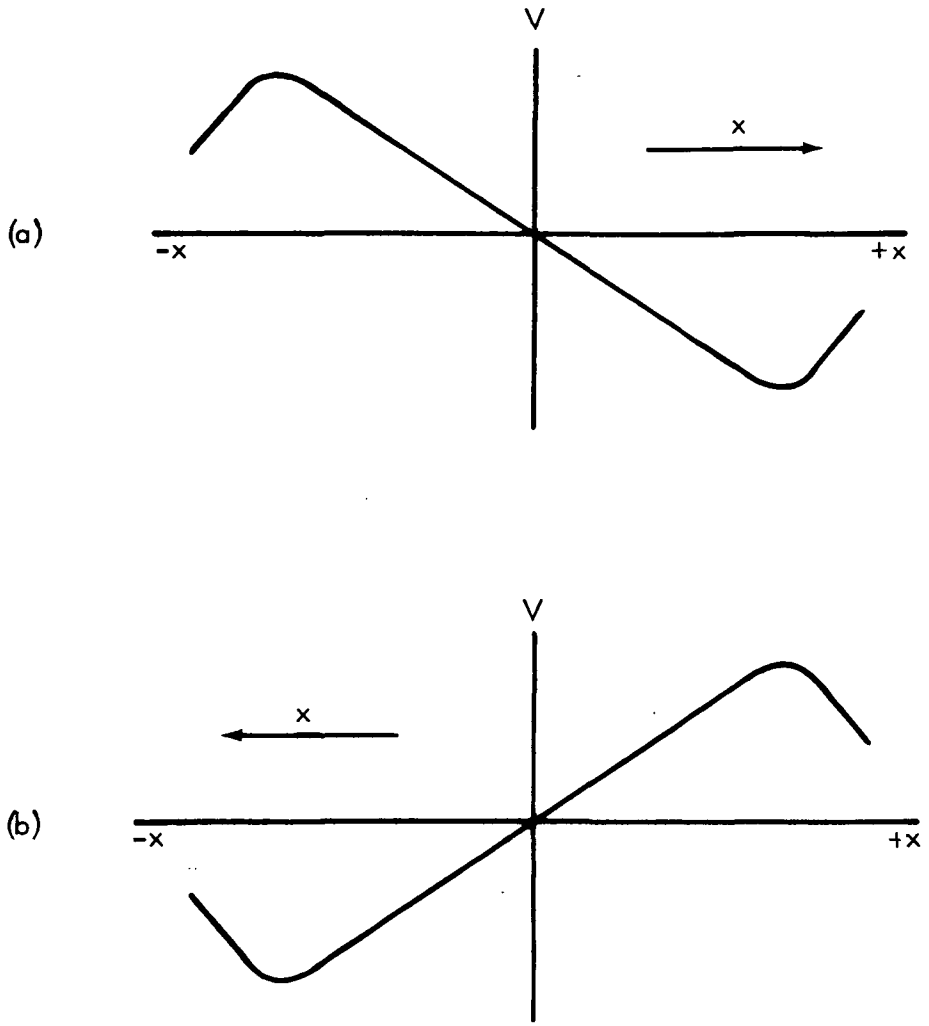

Figure 4.2-1. Output Voltage of Velocity Sensing Coils

The slope of the center portion of the curve is proportional to the velocity, $\dot{x}$. It should be pointed out that operation at amplitudes beyond the nonlinear portion of the curve does not drastically alter the system characteristics or produce instabilities. Operation in this region only reduces the effectiveness of the damping. The extent of the nonlinear portion is a function of the pickup coil geometry and size.

Figure 4.2-2 is a schematic of the electronics in the damping control circuit. The circuit is essentially a high-gain amplifier and a low-pass filter with the transfer functions

$$\frac{K}{(\tau_1 s + 1)(\tau_2 s + 1)}$$

$\tau_1 = 1.0$ sec

$\tau_2 = 0.1$ sec

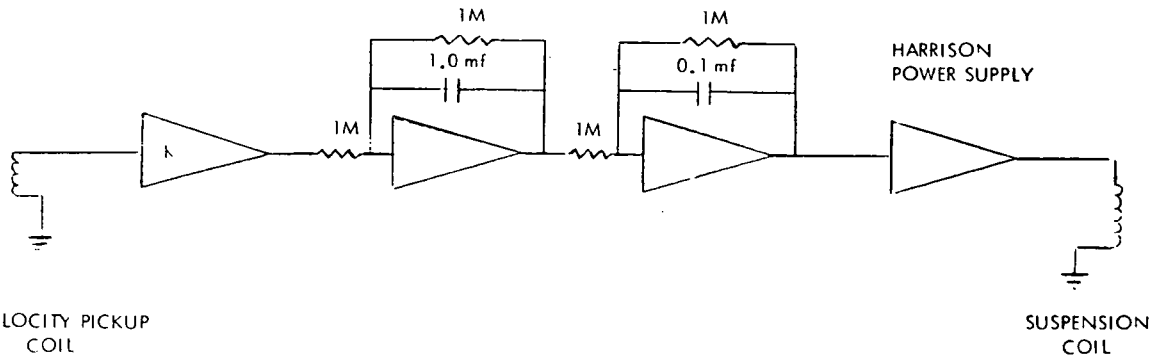

Figure 4.2-2. Damping Control Electronics

Typical values for the open loop gain, K, were between 100,000 and 1,000,000. The amplified velocity signal was then fed into a Harrison model 6823A power supply/ amplifier to provide current for the suspension coils.

4.3 ONE-DIMENSIONAL EQUATIONS OF MOTION

For operation in the linear portion of the pickup coil, the effective spring constant of the system is proportional to the sum of the amplified pickup coil signal and the steady-state current through the suspension coils.

$$k = ax\dot{x} + cI_o$$

or

$$k = ax\dot{x} + k_o$$

The differential equation for one-dimensional oscillator with magnetic damping is then

$$m\frac{d^2x}{dt^2} + ax^2\left|\frac{dx}{dt}\right| + k_o x = F_x(t)$$

The major difference in behavior from a simple linear oscillator is in the nonlinear second term. For a constant velocity, the nonlinear damping should be more efficient than simple linear damping, because due to the x^2 term there is a greater damping force near the peak of the displacement than there is for the linear damper.

For large amplitudes this equation is similar to the Van der Pol equation:

$$m\ddot{x} + c(x^2 - 1)\dot{x} + kx = F_x(t)$$

If misalignments are considered such as the velocity pickup coil not being placed directly over the disc magnets when the system is in equilibrium, then the one-dimensional equation of motion actually becomes Van der Pol's equation. This equation has the general property that the damping is negative for small displacements. As the displacement becomes sufficiently large, the damping becomes positive and limits further increases in amplitude.

The schematic diagram of the two-dimensional suspension system under investigation is shown in figure 4.3-1. Each of the disc magnets experiences a restoring force tending to return it to its equilibrium position ($\bar{r}_1 = 0$ and $\bar{r}_2 = 0$). Damping occurs when either of the magnets has a velocity component along $\bar{r}_1$ or $\bar{r}_2$. The damping force is

$$ar_1^2 \frac{dr_1}{dt} \hat{r}_1$$

where $\hat{r}_1$ is a unit vector along $\bar{r}_1$. A similar term involving $\bar{r}_2$ acts on the disc. It can be seen that the magnetic damping system has a damping effect on the rotational motion because a damping force is applied to each of the ferromagnetic discs rather than to the center-of-mass of the air bearing. The two damping forces along $\bar{r}_1$ and $\bar{r}_2$ act as a couple which produces a damping torque opposing the angular velocity and, therefore, removes rotational energy from the system.

In the mathematical analysis and analog simulation of the following sections of this report, the damping constant, a, will be used to designate the suspension system response. All analytical data in this report will be characterized by the constant, a, having the mks units $kg/m^2\ sec^2$. Because of the nonlinear nature of the equations of motion, a nondimensional damping ratio, ξ, as used to describe a linear second-order differential equation, cannot be found. In general, the larger the value of the damping constant, a, the greater the overall damping effect. For a = 0 all equations reduce to the linear second-order form.

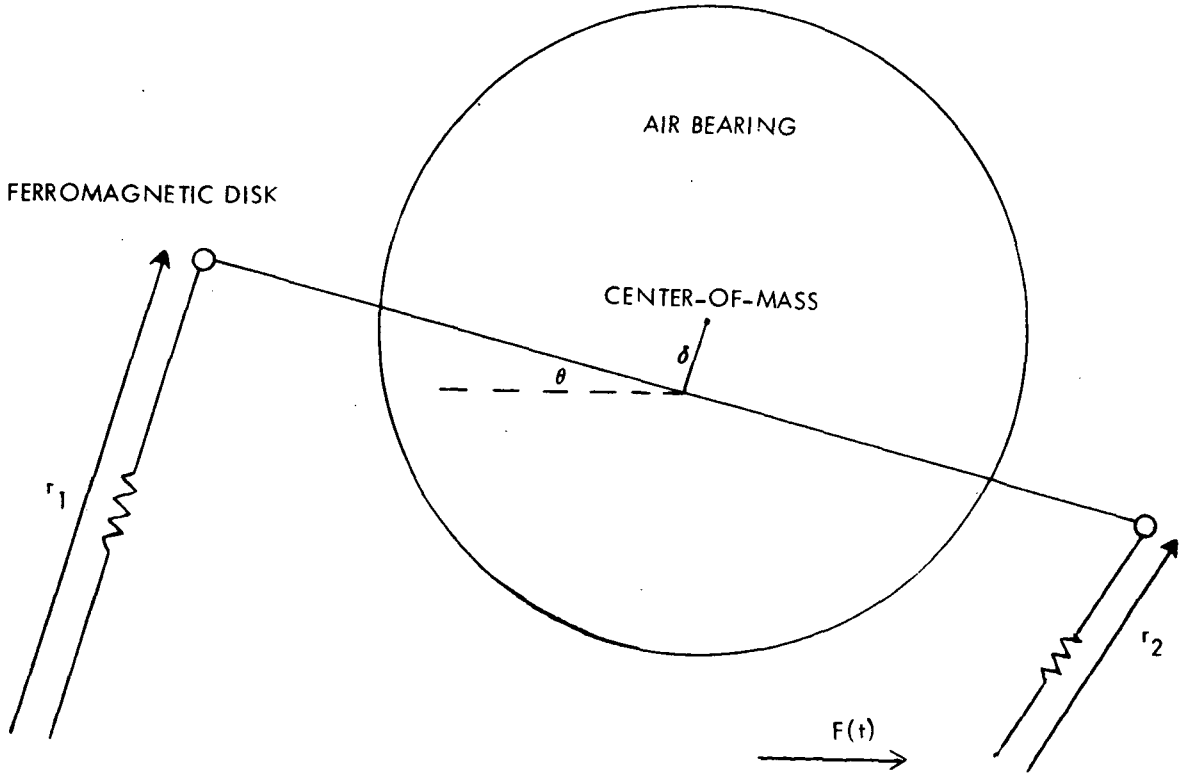

Figure 4.3-1. Schematic Diagram of Suspension System

Section 5
EQUATIONS OF MOTION

The suspension system geometry is shown in figure 5.1-1. The equilibrium position of the center-of-mass of the air bearing coincides with the origin. The disc magnets (or ferromagnetic discs) each extend a distance $\frac{1}{2}\bar{\imath}$ from the center-of-mass. At equilibrium the magnets coincide with the points $\frac{1}{2}\bar{\imath}$ and $-\frac{1}{2}\bar{\imath}$ on the x-axis. These points will be considered to be the centers of force for each suspension magnet coil; i.e., the forces on each of the disc magnets will be in the direction of the vectors $\bar{r}_1$ and $\bar{r}_2$. The generalized coordinates will be x, y, and θ which correspond to the Cartesian coordinates of the center-of-mass and the angular rotation of the air bearing as measured from the x-axis.

The more general case is that in which the center-of-mass does not lie on the straight line between the two points of application of the suspension forces. In figure 5.1-1 the center-of-mass "offset" is denoted by δ.

The kinetic energy is given by

$$T = \frac{1}{2}M(\dot{x}^2 + \dot{y}^2) + \frac{1}{2}I_z\dot{\theta}^2 + M\dot{\theta}\left[(\dot{y}\bar{X} - \dot{x}\bar{Y})\cos\theta - (\dot{x}\bar{X} + \dot{y}\bar{Y})\sin\theta\right] \quad (5.1)$$

where $\bar{X}$ and $\bar{Y}$ are the coordinates of the center-of-mass in the air bearing coordinate system with the origin midway between the two disc magnets. In this discussion only center-of-mass offsets perpendicular to $\bar{\imath}$ will be considered since these will have the most pronounced effect. Hence $\bar{X} = 0$ and $\bar{Y} = -\delta$. The kinetic energy is then

$$T = \frac{1}{2}M(\dot{x}^2 + \dot{y}^2) + \frac{1}{2}I_z\dot{\theta}^2 + M\delta\dot{\theta}(\dot{x}\cos\theta + \dot{y}\sin\theta) \quad (5.2)$$

Using the approximations $\sin\theta = \theta$ and $\cos\theta = 1 - \frac{1}{2}\theta^2$, the equation for kinetic energy can be written as

$$T = \frac{1}{2}M(\dot{x}^2 + \dot{y}^2) + \frac{1}{2}I_z\dot{\theta}^2 + M\delta\dot{\theta}\dot{x} - \frac{1}{2}M\delta\theta^2\dot{\theta}\dot{x} + M\delta\theta\dot{\theta}\dot{y} \quad (5.3)$$

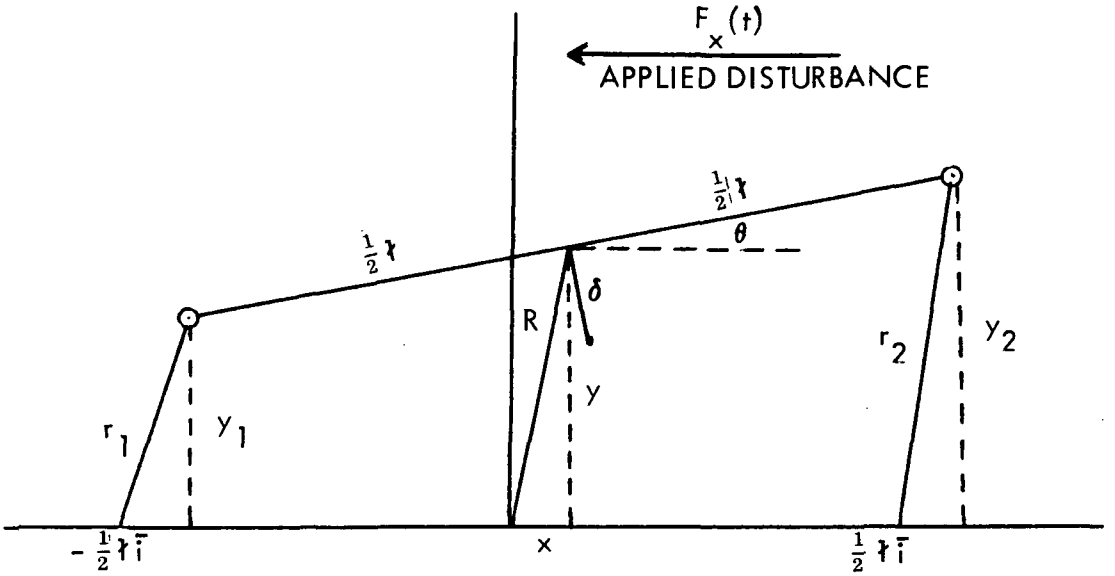

Vector Relationships

$$\bar{R} = -\tfrac{1}{2}\bar{i}\ell + \bar{r}_1 + \tfrac{1}{2}\bar{\ell}$$

$$\bar{R} = \tfrac{1}{2}\bar{i}\ell + \bar{r}_2 - \tfrac{1}{2}\bar{\ell}$$

$$2\bar{R} = \bar{r}_1 + \bar{r}_2$$

$$2x = x_1 + x_2$$

$$2y = y_1 + y_2$$

$$x_1 = x - \tfrac{1}{2}\ell\cos\theta + \tfrac{1}{2}\ell$$

$$y_1 = y - \tfrac{1}{2}\ell\sin\theta$$

$$x_2 = x + \tfrac{1}{2}\ell\cos\theta - \tfrac{1}{2}\ell$$

$$y_2 = y + \tfrac{1}{2}\ell\sin\theta$$

Figure 5.1-1. Suspension System Geometry

The following derivatives will be needed:

$$\frac{\partial T}{\partial x} = 0$$

$$\frac{\partial T}{\partial \dot{x}} = M\dot{x} + M\dot{\theta}\delta - 2M\dot{\theta}\theta^2\delta$$

$$\frac{d}{dt}\left(\frac{\partial T}{\partial \dot{x}}\right) = M\ddot{x} + \delta M\left(\ddot{\theta} - \frac{1}{2}\theta^2\ddot{\theta} - \theta\dot{\theta}^2\right) \quad (5.4) \qquad (5.4)$$

$$\frac{\partial T}{\partial y} = 0$$

$$\frac{\partial T}{\partial \dot{y}} = M\dot{y} + \delta M\theta\dot{\theta}$$

$$\frac{d}{dt}\left(\frac{\partial T}{\partial \dot{y}}\right) = M\ddot{y} + \delta M\left(\dot{\theta}^2 + \theta\ddot{\theta}\right) \quad (5.5) \qquad (5.5)$$

$$\frac{\partial T}{\partial \theta} = M\dot{\theta}\delta\left(\dot{y} - \dot{x}\theta\right)$$

$$\frac{\partial T}{\partial \dot{\theta}} = I_z\dot{\theta} + M\delta\left(\dot{x} + \dot{y}\theta - \frac{1}{2}\dot{x}\theta^2\right)$$

$$\frac{d}{dt}\left(\frac{\partial T}{\partial \dot{\theta}}\right) = I_z\ddot{\theta} + M\delta\left(\ddot{x} + \ddot{y}\theta + \dot{y}\dot{\theta} - \frac{1}{2}\ddot{x}\theta^2 - \dot{x}\dot{\theta}\theta\right) \qquad (5.6)$$

Using the Lagrange relationships

$$\frac{d}{dt}\left(\frac{\partial T}{\partial \dot{q}_i}\right) - \frac{\partial T}{\partial q_i} = \frac{\partial V}{\partial q_i} + F_{q_i} + F(t) \qquad q_i = x, y, \theta \qquad (5.7)$$

we can obtain the differential equations of motion. The quantity $-\frac{\partial V}{\partial q_i} + F_{q_i}$ represents the force applied to the air bearing by the magnetic suspension. The quanity $-\partial V/\partial q_i$ represents the conservative forces and F_{q_i} represents the damping or nonconservative forces.

The forces acting on the air bearing due to the suspension system are:

$$-k\bar{r}_1 - ar_1^2 \frac{dr_1}{dt} \hat{r}_1 \tag{5.8}$$

acting along r_1, and

$$-k\bar{r}_2 - ar_2^2 \frac{dr_2}{dt} \hat{r}_2 \tag{5.9}$$

acting along r_2. The origin of these terms involving the damping constant, a, was discussed in the preceeding section.

The quantity k represents the effective spring constant of the magnetic suspension with no damping. The damping force $ar^2 \frac{dr}{dt} \hat{r}$, is always directed along the direction $\bar{r}$ ($\hat{r}$ is a unit vector in the direction of $\bar{r}_1$ or $\bar{r}_2$). The damping is proportional to the velocity but also proportional to r^2.

The total forces acting in the x, y, and θ directions must be found and inserted in equation (5.7). The conservative component of the force can be written as a potential in terms of the generalized coordinates:

$$\begin{aligned} V &= \frac{1}{2} kr_1^2 + \frac{1}{2} kr_2^2 \\ &= \frac{1}{2} k\left(r_1^2 + r_2^2\right) \\ &= k\left(x^2 + y^2 + \frac{1}{4} \ell^2 \theta^2 + \frac{1}{16} \ell^2 \theta^4\right) \end{aligned} \tag{5.10}$$

$$\begin{aligned} \frac{\partial V}{\partial x} &= 2kx \\ \frac{\partial V}{\partial y} &= 2ky \end{aligned} \tag{5.11}$$

$$\frac{\partial V}{\partial \theta} = \frac{1}{2} k\ell^2 \theta + \frac{1}{4} k\ell^2 \theta^3 \tag{5.12}$$

The nonconservative force components cannot be expressed in terms of a potential but must be expressed in terms of the generalized coordinates x, y and θ.

$$F_{1x} = -ar_1^2 \frac{dr_1}{dt} \cos\alpha$$

$$F_{1x} = -a\left(x_1^2 + y_1^2\right) \frac{x_1 \frac{dx_1}{dt} + y_1 \frac{dy_1}{dt}}{\sqrt{x_1^2 + y_1^2}} \cdot \frac{x_1}{\sqrt{x_1^2 + y_1^2}}$$

$$F_{1x} = -a\left(x_1^2 \frac{dx_1}{dt} + x_1 y_1 \frac{dy_1}{dt}\right) \tag{5.13}$$

and a similar term for F_{2x}

$$F_{2x} = -ar_2^2 \frac{dr_2}{dt} \cos\beta$$

$$F_{2x} = -a\left(x_2^2 \frac{dx_2}{dt} + x_2 y_2 \frac{dy_1}{dt}\right) \tag{5.14}$$

$$F_{x(nc)} = F_{1x} + F_{2x} = -a\left(x_1^2 \frac{dx_1}{dt} + x_2^2 \frac{dx_2}{dt} + x_1 y_1 \frac{dy_1}{dt} + x_2 y_2 \frac{dy_2}{dt}\right) \bar{i} \tag{5.15}$$

where $F_{x(nc)}$ denotes the total non-conservative force in the x-direction.

This must be expressed in terms of x, y and θ, where

$$x_1 = x - \frac{1}{2} l \cos\theta + \frac{1}{2} l \approx x + \frac{1}{4} \theta^2 l$$

$$y_1 = y - \frac{1}{2} l \sin\theta \approx y - \frac{1}{2} l \theta^2$$

$$x_2 = x + \frac{1}{2} l \cos\theta - \frac{1}{2} l \approx x - \frac{1}{4} l \theta^2$$

$$y_2 = y + \frac{1}{2} l \sin\theta \approx y + \frac{1}{2} l \theta$$

A similar procedure is used for the y component of the force:

$$F_{1y} = -ar_1^2 \frac{dr_1}{dt} \sin\alpha$$

$$F_{2y} = -ar_2^2 \frac{dr_1}{dt} \sin\beta$$

The final result is

$$-\frac{F_{x(nc)}}{a} = 2x(x\dot{x} + y\dot{y}) + \frac{1}{4}\ell^2\theta\left[2x\dot{\theta} - \theta^2\dot{y} + 2x\theta^2\dot{\theta} - y\theta\dot{\theta} + \frac{1}{2}\dot{x}\theta^3\right] \tag{5.16}$$

$$-\frac{F_{y(nc)}}{a} = 2y(x\dot{x} + y\dot{y}) + \frac{1}{4}\ell^2\theta\left[4y\dot{\theta} + y\theta^2\dot{\theta} + 2\dot{y}\theta - 2x\theta\dot{\theta} - \dot{x}\theta^2\right] \tag{5.17}$$

The only approximations have been the trigonometric approximations for sine and cosine

$$\sin\theta \approx \theta \qquad \cos\theta \approx 1 - \frac{1}{2}\theta^2 \tag{5.18}$$

These approximations should be suitable for rotations up to twenty degrees or more. In addition to the generalized damping forces F_x and F_y we must also find the generalized force, $F_{\theta nc}$, which is actually the torque applied to the air bearing by the suspension system. From figure 5.1-2 the generalized force in the θ direction is:

$$F_\theta = \text{torque}$$

$$F_{\theta nc} = \frac{1}{2}\ell\left(F_{1x}\sin\theta - F_{2x}\sin\theta + F_{2y}\cos\theta - F_{1y}\cos\theta\right)$$

$$F_{\theta nc} = \frac{1}{2}\ell\left[\left(F_{1x} - F_{2x}\right)\sin\theta - \left(F_{1y} - F_{2y}\right)\cos\theta\right] \tag{5.19}$$

$$\sin\theta \approx \theta \qquad \cos\theta \approx 1 - 1/2\theta^2$$

$$F_\theta = \frac{1}{2}\ell\left[-(F_{1y} - F_{2y}) + (F_{1x} - F_{2x})\,\theta + (F_{1y} - F_{2y})\,\theta^2/2\right]$$

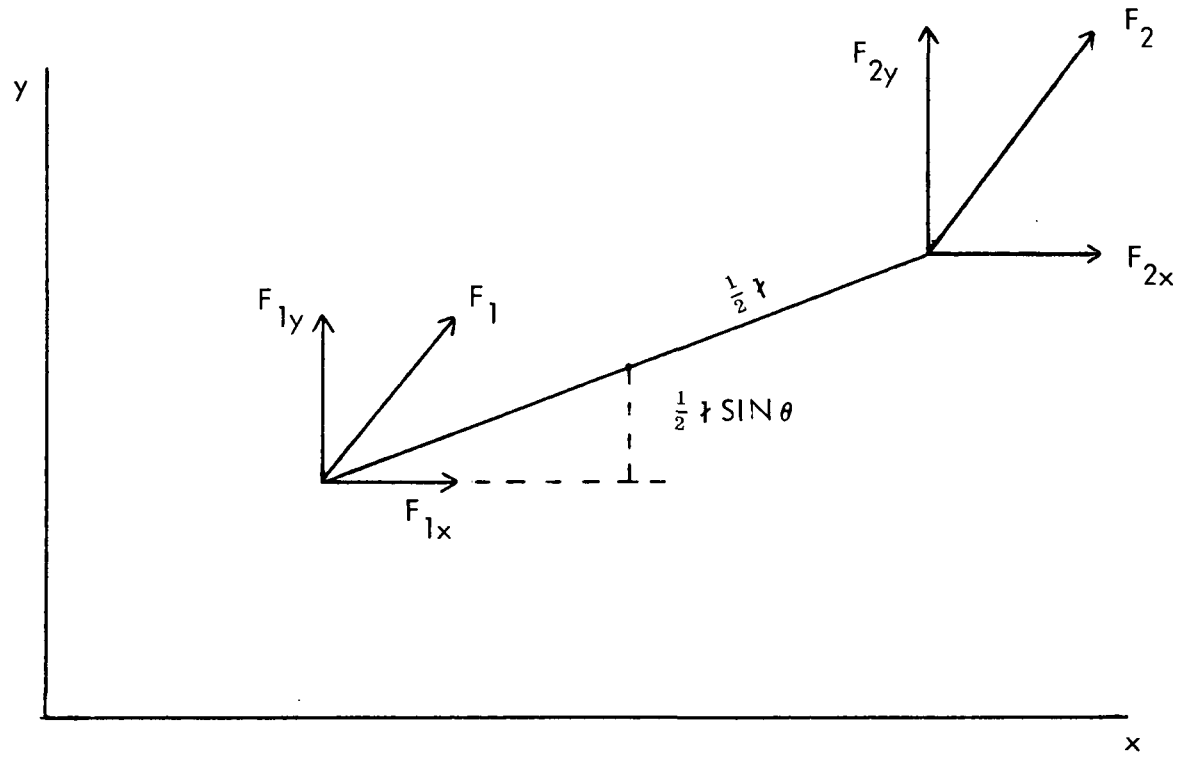

Figure 5.1-2. Forces at Suspension Points

The final result after inserting the forces expressed in terms of the generalized coordinates is:

$$\frac{2F_\theta}{a\,ł^2} = -y^2\dot{\theta} + \theta(2xy\dot{\theta} - 2y\dot{y} - x\dot{x}) + \theta^2\left(\frac{1}{2}y^2\dot{\theta} + \frac{1}{2}y\dot{x} + x\dot{y} - x^2\dot{\theta} - \frac{1}{4}ł^2\dot{\theta}\right)$$

$$+ \frac{1}{2}\theta^3(y\dot{y} - xy\dot{\theta} - x\dot{x}) - \theta^4\left(\frac{1}{8}ł^3\dot{\theta} + \frac{1}{2}y\dot{x}\right) \qquad (5.20)$$

$$\frac{2F_\theta}{a\,ł^2} = -\frac{d}{dt}(x^2 + y^2) + \frac{d}{dt}(xy\theta^2) + \frac{1}{2}y\dot{x}\theta^2 - y^2\dot{\theta} + \theta x\dot{x} - \frac{1}{4}ł^2\theta^2\dot{\theta} \qquad (5.21)$$

The final equations of motion are, therefore;

$$M\ddot{x} + \delta M\left(\ddot{\theta} - \frac{1}{2}\theta^2\ddot{\theta} - \theta\dot{\theta}^2\right) + 2kx = -a\left[2x\frac{d}{dt}(x^2 + y^2) + \frac{1}{4}\ell^2\theta(2x\dot{\theta} - \theta^2\dot{y} - y\theta\dot{\theta})\right] + F_x(t)_{appl.} \tag{5.22}$$

$$M\ddot{y} + \delta M(\theta\ddot{\theta} + \dot{\theta}^2) + 2ky = -a\left[2y\frac{d}{dt}(x^2 + y^2) + \frac{1}{4}\ell^2\theta(4y\dot{\theta} + 2\dot{y}\theta - 2x\theta\dot{\theta} - \dot{x}\theta^2)\right] + F_y(t)_{appl.} \tag{5.23}$$

$$I_z\ddot{\theta} + \delta M\left(\ddot{x} + \theta\ddot{y} - \frac{1}{2}\ddot{x}\theta^2\right) + 1/2\, k\ell^2\theta = \frac{1}{2}a\ell^2\left[-y^2\dot{\theta} + \theta(2xy\dot{\theta} - 2y\dot{y} - x\dot{x} + \frac{1}{2}y\dot{x}\theta + x\dot{y}\theta - \frac{1}{4}\ell^2\theta\dot{\theta})\right] + F_\theta(t)_{appl.} \tag{5.24}$$

$F_x(t)_{appl.}$, $F_y(t)_{appl.}$, $F_\theta(t)_{appl.}$ = externally applied forces and torques

For analog computer simulation, $\theta \leq$ ½degree and terms in θ^2 and $\theta\dot{\theta}$, can be eliminated. The equations of motion become:

$$\ddot{x} + \delta\ddot{\theta} + \frac{2k}{M} x = -\frac{a}{M} 2x \frac{d}{dt}(x^2 + y^2) + \frac{F_x(t)}{M} \tag{5.25}$$

$$\ddot{y} + \frac{2k}{M} y = -\frac{a}{M} 2y \frac{d}{dt}(x^2 + y^2) + \frac{F_y(t)}{M} \tag{5.26}$$

$$\ddot{\theta} + \frac{\delta M}{I_z}(\ddot{x} + \ddot{y}\theta) + \frac{k\ell^2\theta}{2I_z} = -\frac{a\ell^2}{2I_z}(y^2\dot{\theta} + 2y\dot{y}\theta + x\dot{x}\theta - \frac{1}{4}\ell^2\theta^2\dot{\theta}) \tag{5.27}$$

Section 6

ANALOG SIMULATION

6.1 EQUATIONS OF MOTION

The equations of motion were programmed on a Systron Donner 40/80 analog computer. This machine has a ±100-volt capability. After eliminating the non-significant terms, the equations of motion become:

$$\ddot{x} = -2(k/M)x - 4(a/M)x^2\dot{x} - 4(a/M)xy\dot{y} - \delta\ddot{\theta} + F_x(t)/M \tag{6.1}$$

$$\ddot{y} = -2(k/M)y - 4(a/M)xy\dot{x} - 4(a/M)y^2\dot{y} \tag{6.2}$$

$$\ddot{\theta} = -(k/2I_z)\ell^2\theta - (a/2I_z)\ell^2 x\dot{x}\theta - (a/I_z)\ell^2 y\dot{y}\theta - \delta(M/I_z)\ddot{x} - (a\ell^4/8I_z)\theta^2\theta \tag{6.3}$$

For initial conditions in which y = 0, it can be seen from equation (6.2) that there is no coupling of motion from the x coordinate to the y coordinate; i.e., when $y(t=0) = 0$, then $\ddot{y} = \dot{y} = y = 0$. Thus the equation of motion for the y coordinate has the same form as the equation of motion for the x coordinate, indicating a symmetric system with identical behavior along each axis. For this reason it was not necessary to program the y equation of motion on the computer, because for all practical purposes, the solution is the same as that of the x equation. Therefore, after setting y, $\dot{y}$, and $\ddot{y}$ equal to zero, the equations of motion are (within the accuracy of the computer):

$$\ddot{x} = -2(k/M)x - 4(a/M)x^2\dot{x} - \delta\ddot{\theta} + (F_x(t)/M) \tag{6.4}$$

$$\ddot{\theta} = -(k/2I_z)\ell^2\theta - (a/2I_z)\ell^2 x\dot{x}\theta - \delta(M/I_z)\ddot{x} - (a\ell^4/8I_z)\theta^2\dot{\theta} \tag{6.5}$$

Converting to machine variables X, Y, and θ, having the ranges ±100 volts, the programmed equations become:

$$\ddot{X} = -2(k/M)(a_{\ddot{x}}/a_x)X - 4(a/M)(a_{\ddot{x}}/a_x^2 a_{\dot{x}})X^2\dot{X} - \delta(a_{\ddot{x}}/a_{\ddot{\theta}})\ddot{\Theta} + (a_{\ddot{x}}/M)F(t) \tag{6.6}$$

$$\ddot{\Theta} = -(k/2I_z)\ell^2(a_{\ddot{\theta}}/a_{\dot{\theta}})\Theta - (a/2I_z)\ell^2(a_{\ddot{\theta}}/a_\theta a_x a_{\dot{x}})X\dot{X}\Theta - \delta(M/I_z)(a_{\ddot{\theta}}/a_{\ddot{x}})\ddot{X}$$

$$- (a\ell^4/8I_z)(a_{\ddot{\theta}}/a_\theta^2 a_{\dot{\theta}})\Theta^2\dot{\Theta} \tag{6.7}$$

with the following values for the scale factors and telescope parameters:

a_x =	10^4 volts/meter	a_θ =	10^5 volts/radian
$a_{\dot{x}}$ =	10^5 volts/meter per sec	$a_{\dot{\theta}}$ =	10^5 volts/rad per sec
$a_{\ddot{x}}$ =	10^5 volts/meter per sec^2	$a_{\ddot{\theta}}$ =	10^6 volts/rad per sec^2
M =	264.1 kg	$(a_{\ddot{x}}/M)F(t)$ =	379 volts/newtons
I_z =	29.2 kg m^2	=	4.4 volts/mm of space-craft motion in x direction
ℓ =	1.0 meter		
k =	5.8 newton/meter		
δ =	0 to 0.02 meter		

The suspension stiffness, k, (spring constant) was selected to provide an undamped period of 30 seconds, which is within the capability of the experimental air bearing simulation.

The computer circuit is shown in figure 6.1-1. The sinusoidal driving functions were obtained from a Hewlett Packard Model 202A Function Generator.

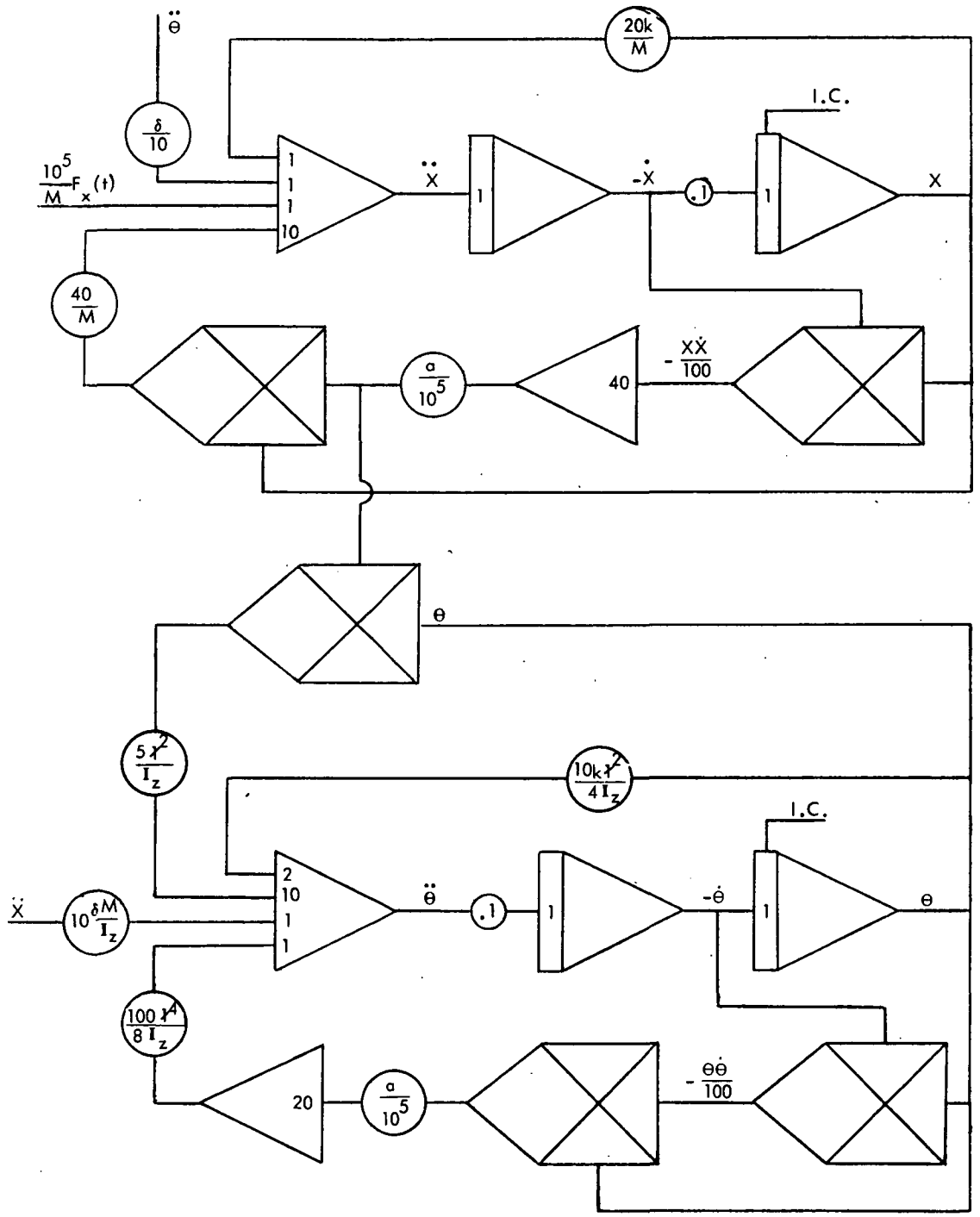

Figure 6.1-1. Circuit Diagram for Computer Setup

6.2 RESULTS OF ANALOG SIMULATION

6.2.1 TRANSFER FUNCTIONS

The transfer functions for the suspension system with various values of the damping constant, a, are shown in figures 6.2-1 through 6.2-4. The transfer functions were measured in two ways: first, as the ratio of the peak output displacement to the peak input displacement; second, as the ratio of the peak output acceleration to the peak input acceleration. Of course, for a linear system these two ratios would be the same at all frequencies, as seen in figure 6.2-1 where a = o. However, in the magnetic suspension system, damping adds nonlinear terms to the equations, resulting in nonsinusoidal waveforms.

For a telescope isolation system, the transmissibility of the displacement is more important. The mathematical operation of differentiation to obtain the acceleration from the displacement amplitude essentially acts as a high-pass filter. Therefore, the transfer functions composed of the input and output acceleration ratios are weighted more toward the higher frequencies appearing in the output. Hence, in figures 6.2-2 through 6.2-4 the differences between the two curves are a measure of the harmonic distortion in the output waveform.

There was no significant difference in transmissibility for values of center-of-mass offset, δ , between 0 and 1.0 millimeters. With a sinusoidal driving frequency, the angular disturbance transmitted by the center-of-mass offset increased almost directly as a function of δ. However, the magnitude of the disturbance for a fixed value of δ remained relatively independent of the damping constant, a. This is to be expected because an angular rotation on the order of arcseconds does not result in sufficient velocity of the suspension disc magnets to induce a useable damping signal. For this reason, relatively large angular motions resulted when the translational driving frequency was the same as the natural rotational frequency of the systems.

Figure 6.2-5 shows a typical system response for the system with a center-of-mass offset, δ , of 1.0 millimeter and a damping constant, $a = 2 \times 10^8$. In this figure, the disturbance frequencies range from .01 Hz to .08 Hz at an amplitude of 1.0 millimeter peak to peak. No large amplitude build up can be seen as the disturbance frequency approaches the translational resonant frequency of approximately 0.03 Hz. However, a large angular disturbance does occur at the rotational resonant frequency of 0.05 Hz.

Figure 6.2-6 shows the response of the same system, but with zero damping, a = o. In this case as the driving frequency is increased from 0.01 Hz, the response of the system steadily increases as resonance, 0.03 Hz, is approached.

6.2.2 INITIAL CONDITIONS

Figure 6.2-7 shows the response of the system after it has been released from rest at $x_o = 2$ mm and $\theta_o = 0$. The figure shows the response for various values the damping constant a. The damping is strongly dependent on amplitude. Large amplitudes are damped much more rapidly than the smaller amplitudes, as can be seen from the envelope of the response. There is a very rapid decrease in amplitude followed by a much slower decrease.

An estimate of the large amplitude damping can be obtained by measuring the percent overshoot as defined by (see figure 6.2-8):

$$\frac{\text{max value reached in first overshoot - steady state value}}{\text{steady state value}} \times 100$$

The percent overshoot as a function of damping constant, a, is shown in figure 6.2-9. Above the graph is shown the value of the damping ratio for a linearly damped second-order system with the same overshoot. It is seen that for relatively large amplitudes of 2 millimeters a damping ratio of at least 0.55 can be obtained.

Figure 6.2-10 shows the time required for the system to reach $1/\epsilon$ of the distance to its steady-state value.

Figure 6.2-11 is a typical system response with the initial condition x_o = 2.0 millimeters. The damping constant is $a = 2 \times 10^7$ and the center-of-mass offset is $\delta = 1.0$ millimeter. The response is shown first at an accelerated time scale in which each horizontal division represents 100 seconds. There is a very large damping effect within the first cycle, after which the amplitude decreases less rapidly. The second portion of the figure shows the same response but at a slower time scale in which each horizontal division represents 10 seconds. Here the detailed waveforms can be seen for the first few cycles.

Figure 6.2-12 shows the effect of damping constant on the angular motion. In this figure the center-of-mass offset, δ, is 2.0 millimeters and the system is released with the initial condition X_o = 2.0 millimeters. The effect of the damping constant, a, on the resultant angular motion can readily be seen. The difference in the resultant angular disturbance between zero damping and $a = 2 \times 10^8$ is more than a factor of ten.

6.2.3 RAMP DISTURBANCES

Figure 6.2-13 shows the system response to ramp input disturbances. The systems showed very little response to applied ramp functions, except for a gradual displacement in the x-direction to the final value. For the case a = o, some translational oscillatory motion at the natural frequency was excited. However, this was small and disappeared with the application of damping. No significant angular disturbance was recorded for the ramp functions, except for the case of high damping in which an angular disturbance of 4.0 arc-seconds resulted. The center-of-mass offset in all three cases was 1.0 mm.

6.2.4 ROTATIONAL DAMPING

Figure 6.2-14 illustrates the effect of the damping constant, a, on angular response. The figure shows the translational and rotational responses of the system released with the initial conditions x_o = 2.0 millimeters and θ_o = 1.0 arc-minute. When compared to the translational response, the rotational damping is relatively small for rotational amplitudes below 30 arc-seconds.

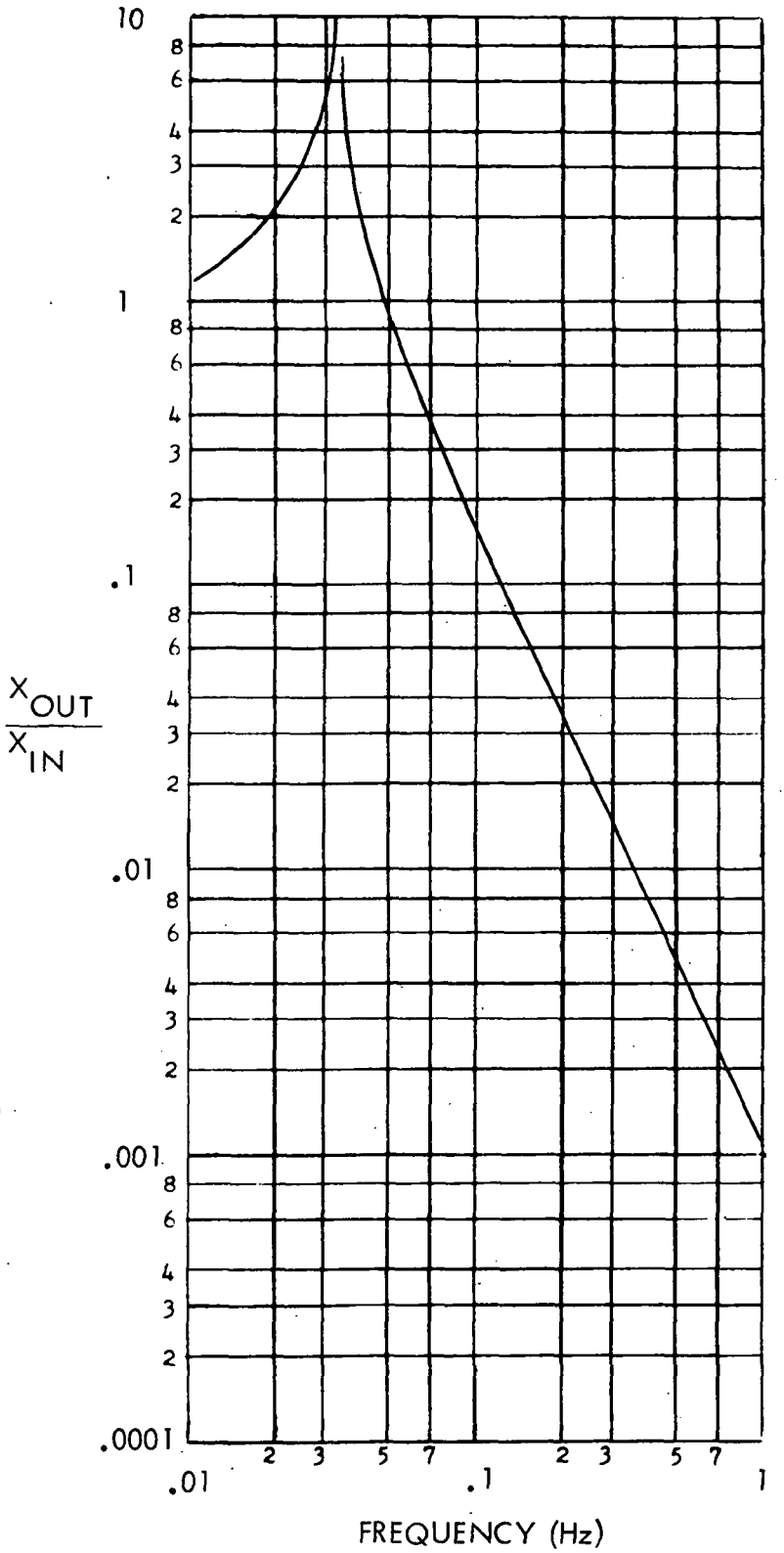

Figure 6.2-1. Analog Simulation of Transfer Function for Damping Constant a = 0

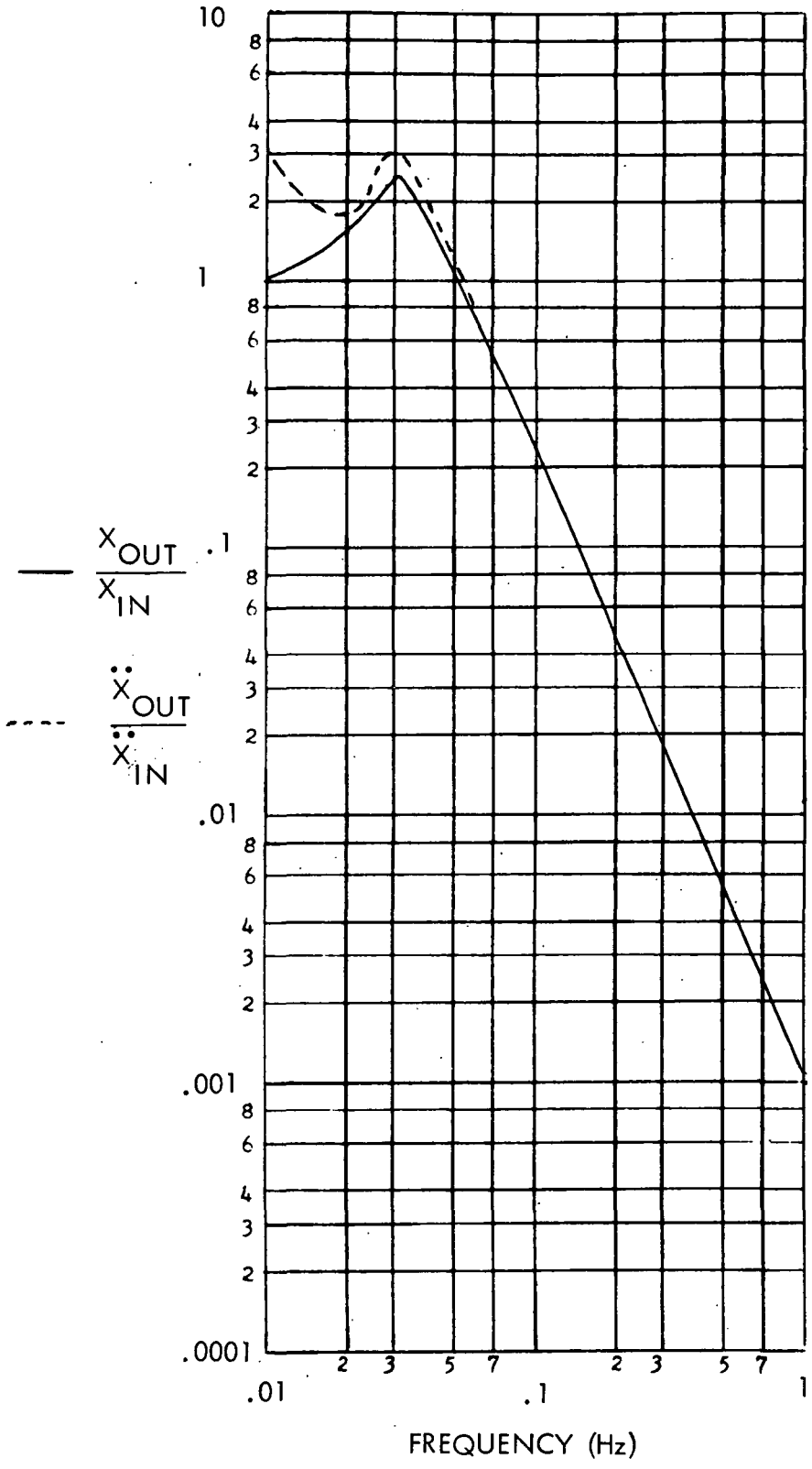

Figure 6.2-2. Analog Simulation of Transfer Function for Damping Constant $a = 2 \times 10^7$ kg/m^{2}sec^2

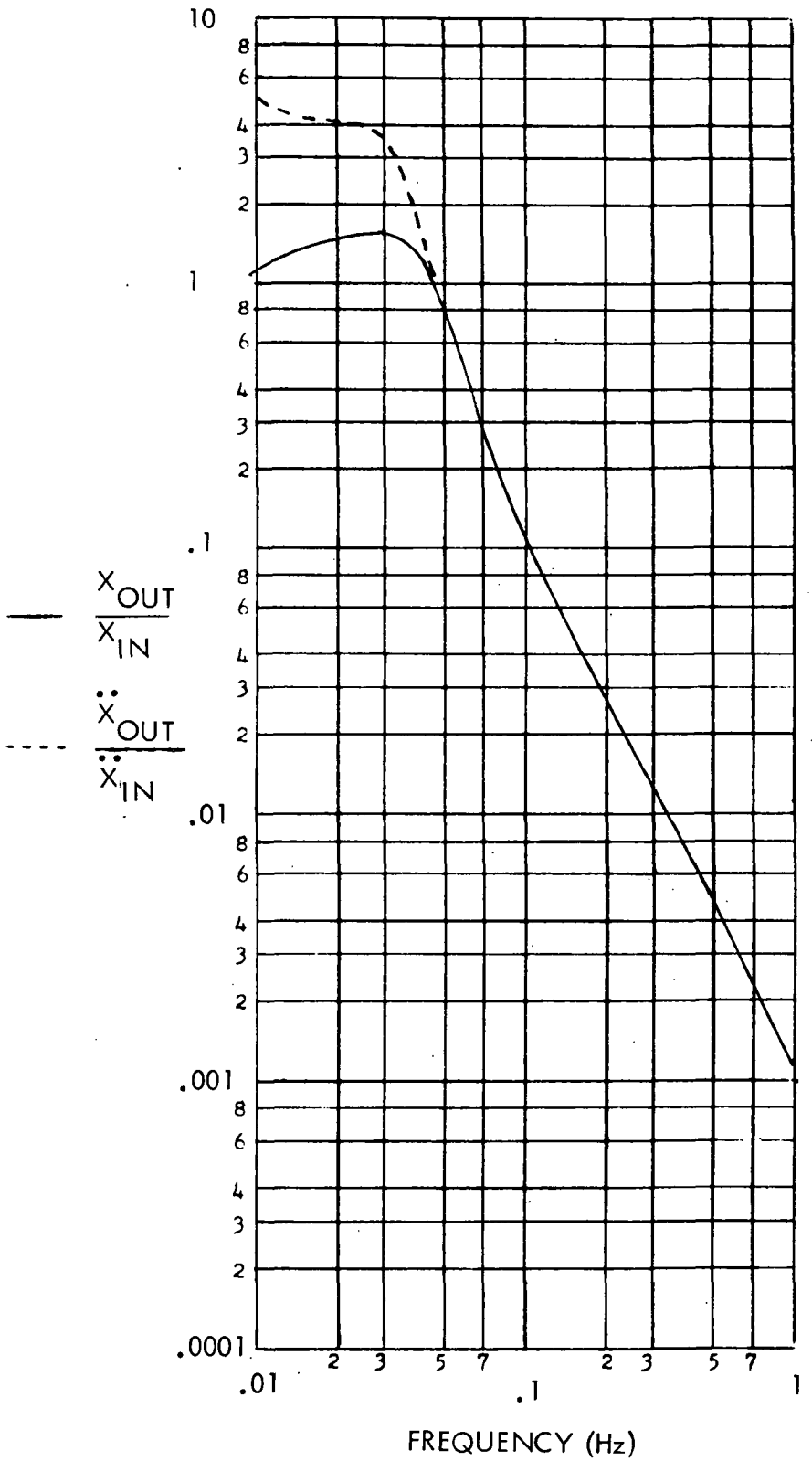

Figure 6.2-3. Analog Simulation of Transfer Function for Damping Constant $a = 10^8$ kg/m^2 sec^2

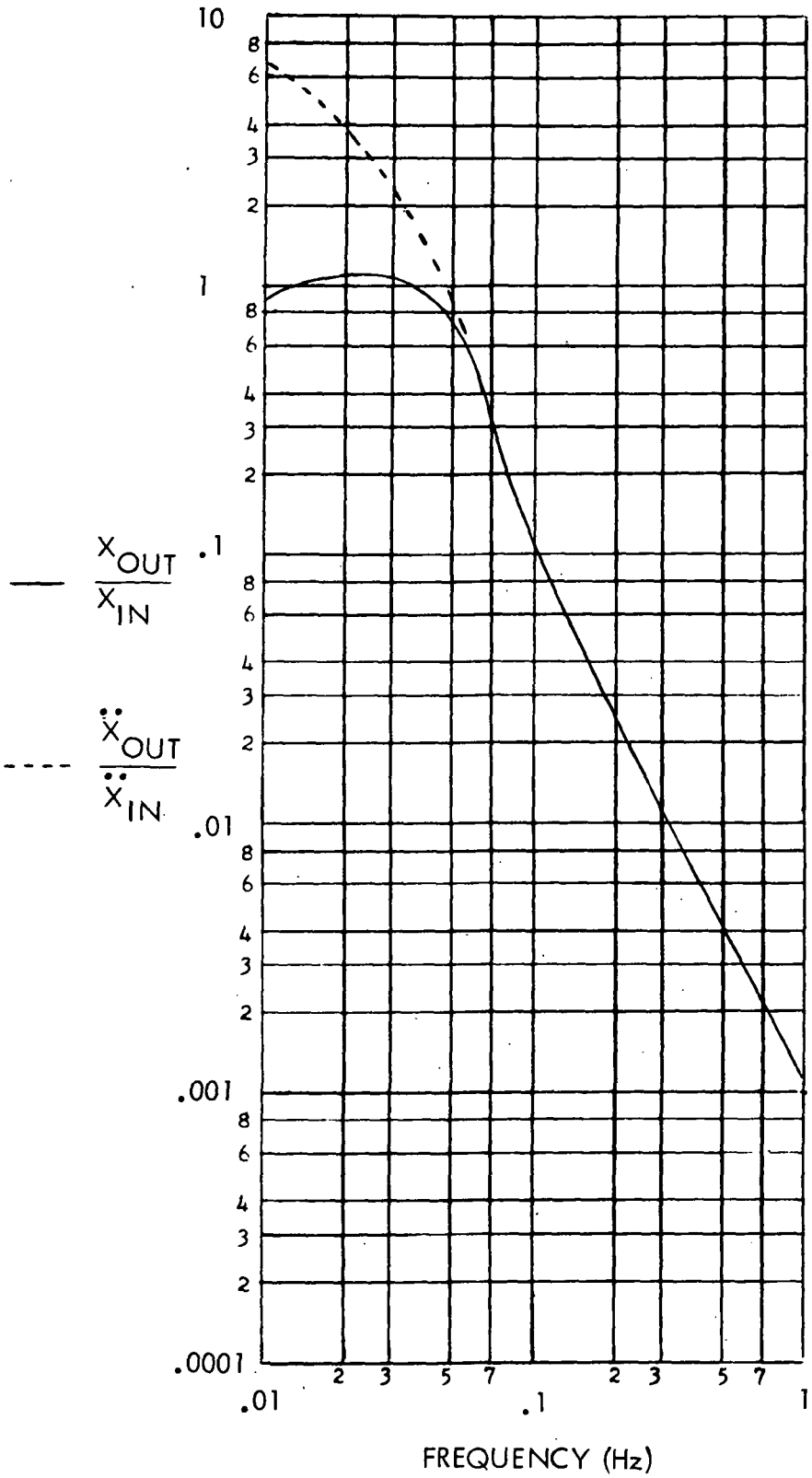

Figure 6.2-4. Analog Simulation of Transfer Function for Damping Constant $a = 2 \times 10^8$ kg/m^2 sec^2

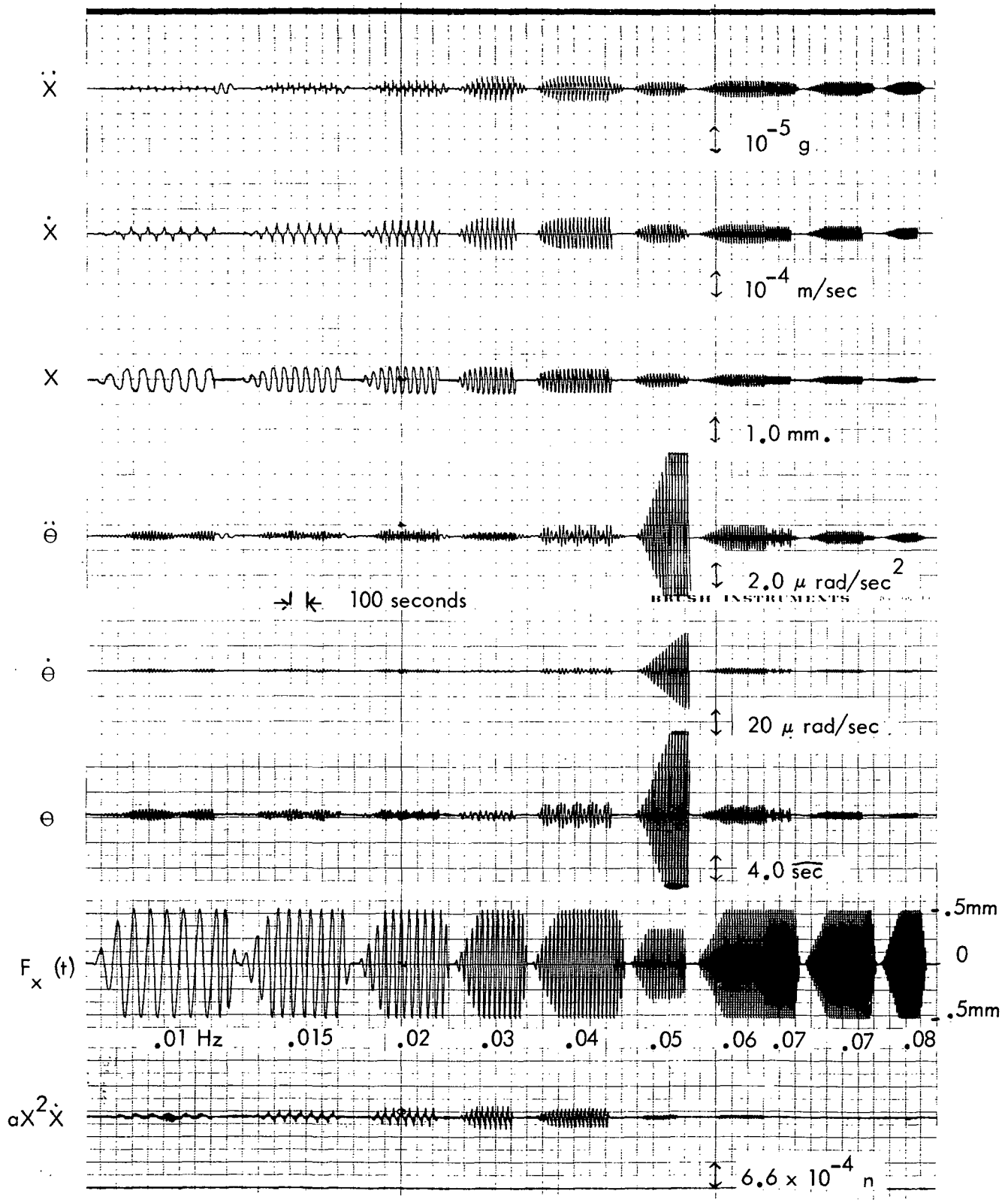

Figure 6.2-5. Sinusoidal Response for Frequencies 0.01 to 0.08 Hz., Damping Constant, $a = 2 \times 10^8$ kg/m^2 sec^2, $\delta = 1.0$ mm

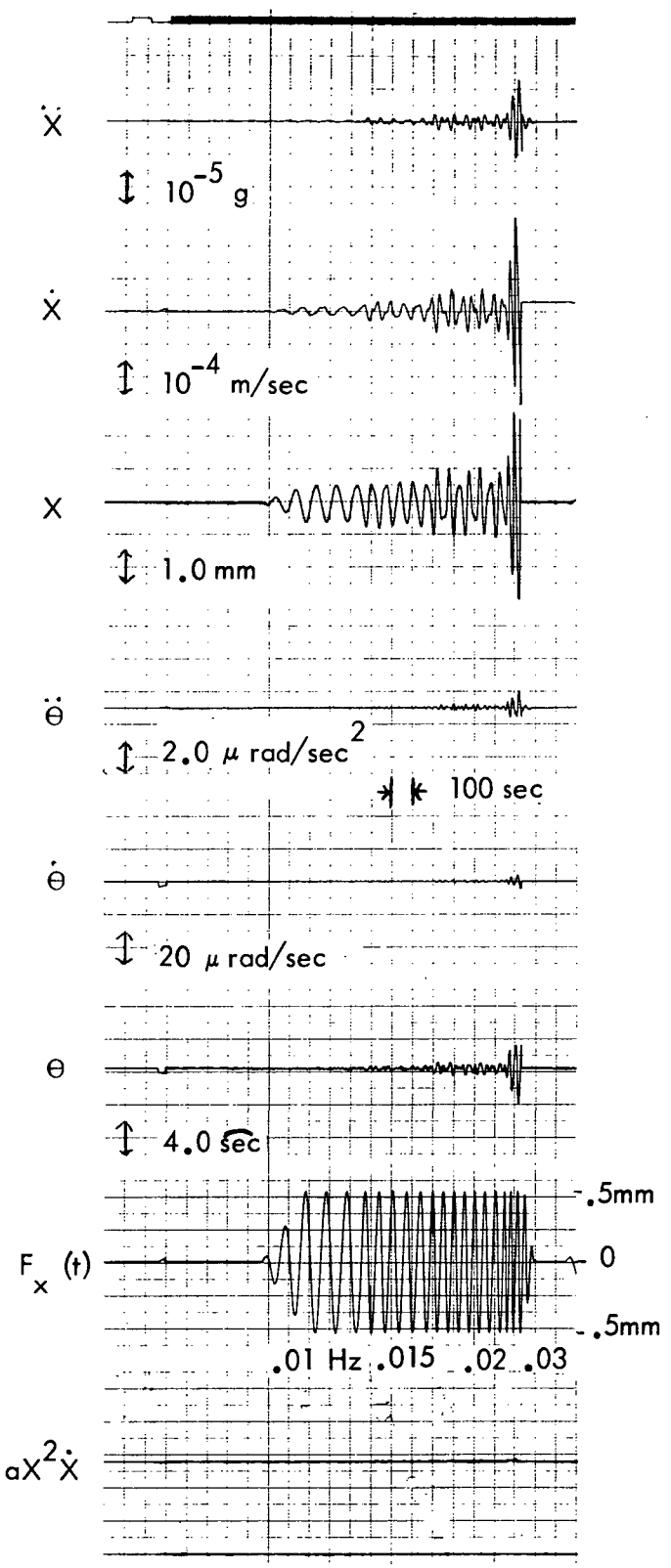

Figure 6.2-6. Sinusoidal Response for Zero Damping, a = 0, δ = 1.0 mm

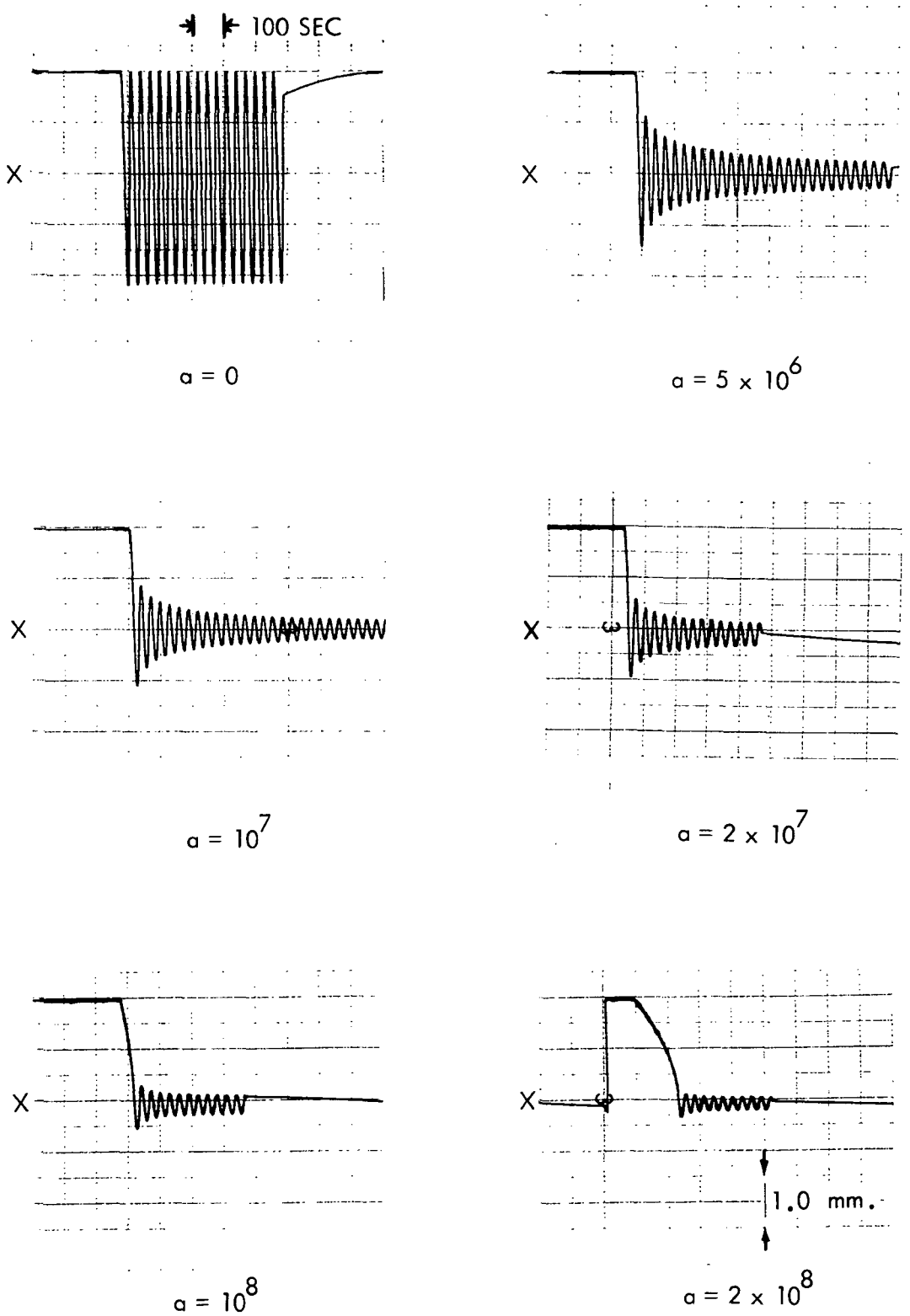

Figure 6.2-7. Translation Responses for Various Values of Damping Constant, a. Initial conditions: $x_o = 2.0$ mm., $\theta_o = 0$

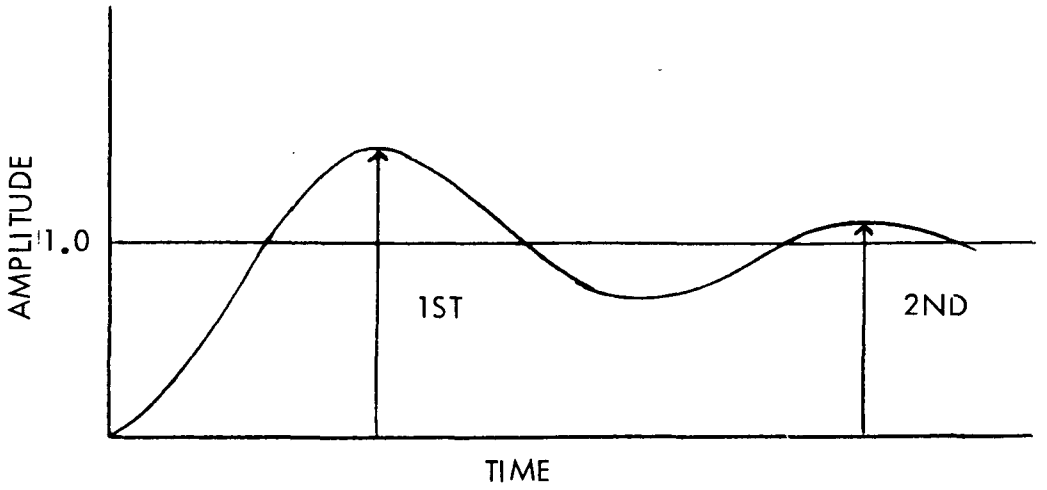

Figure 6.2-8. Illustration of Percent Overshoot

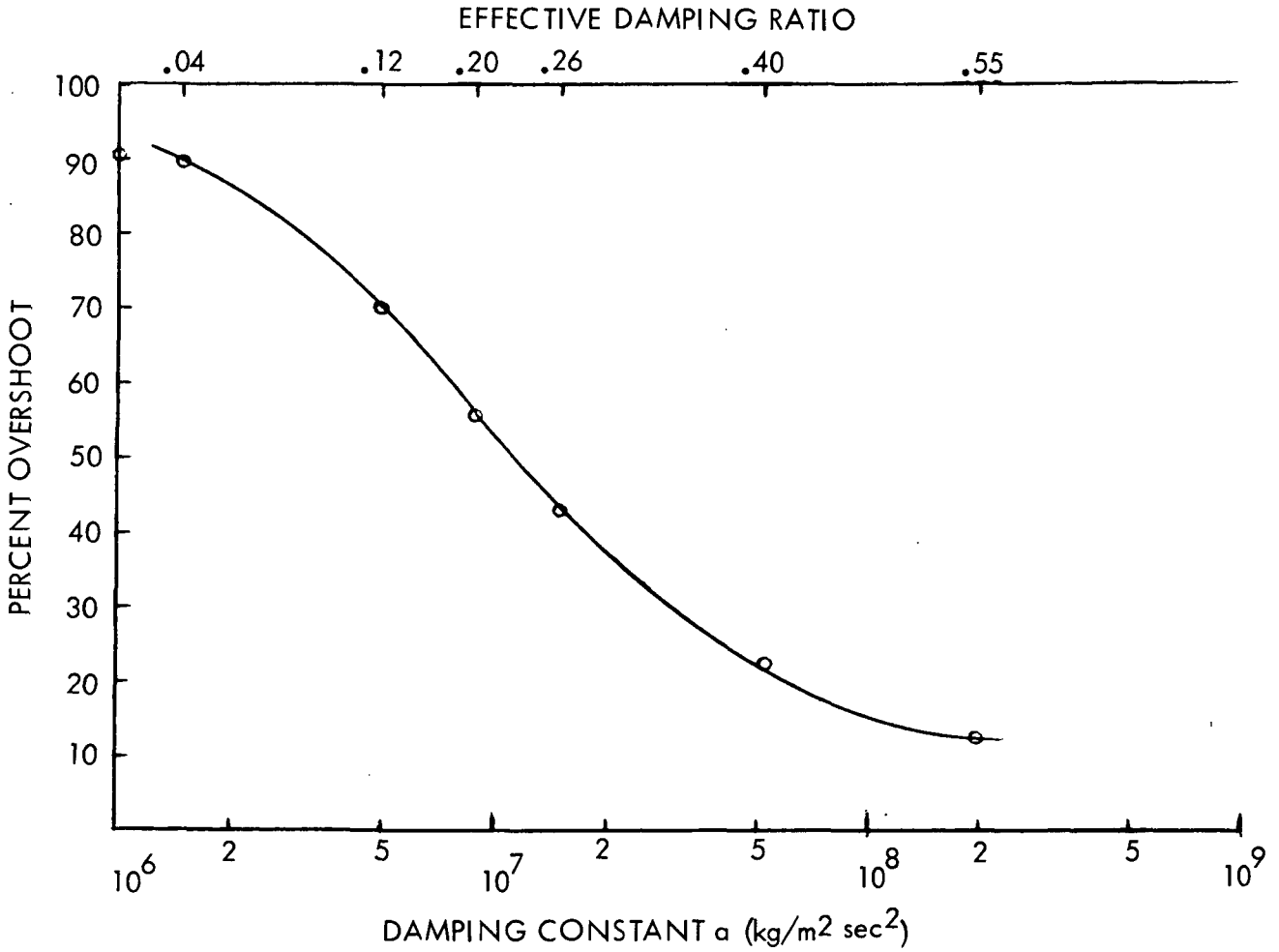

Figure 6.2-9. Percent Overshoot vs. Damping Constant

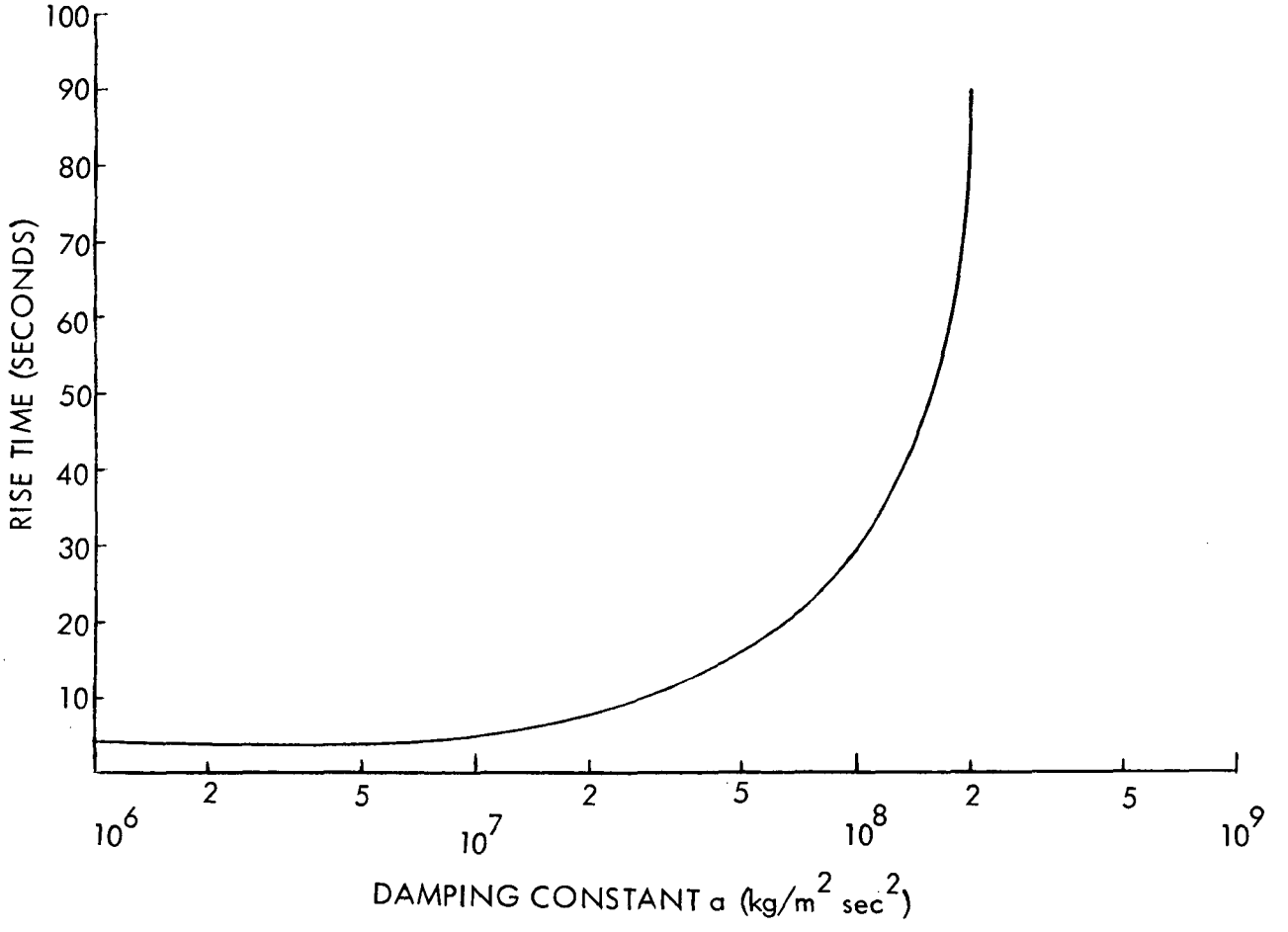

Figure 6.2-10. Rise Time (Zero to 1/e) vs. Damping Constant

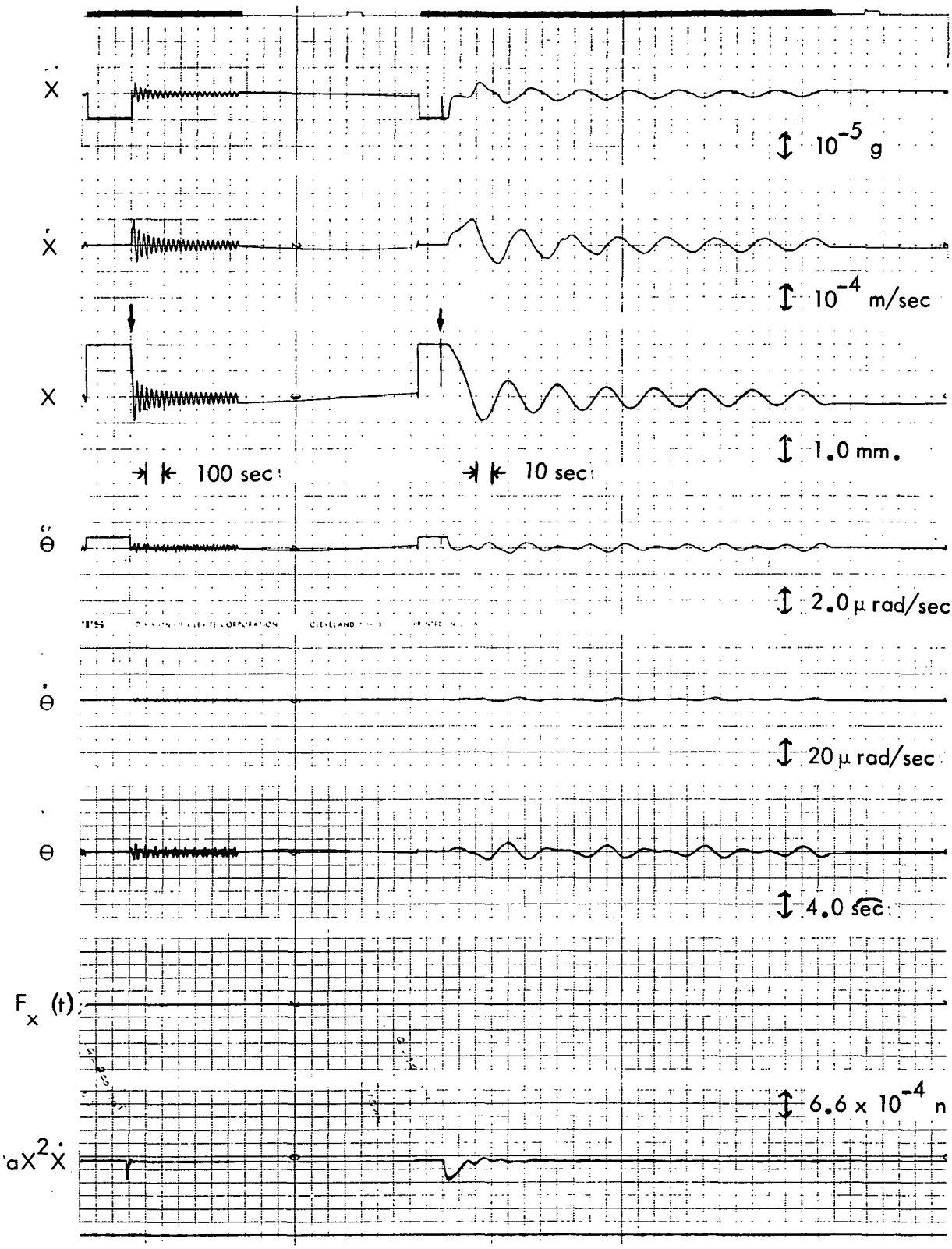

Figure 6.2-11. Response for Initial Conditions x_o = 2.0 mm., δ = 1.0 mm, a = 2 x 10^7 kg/m^2 sec^2.

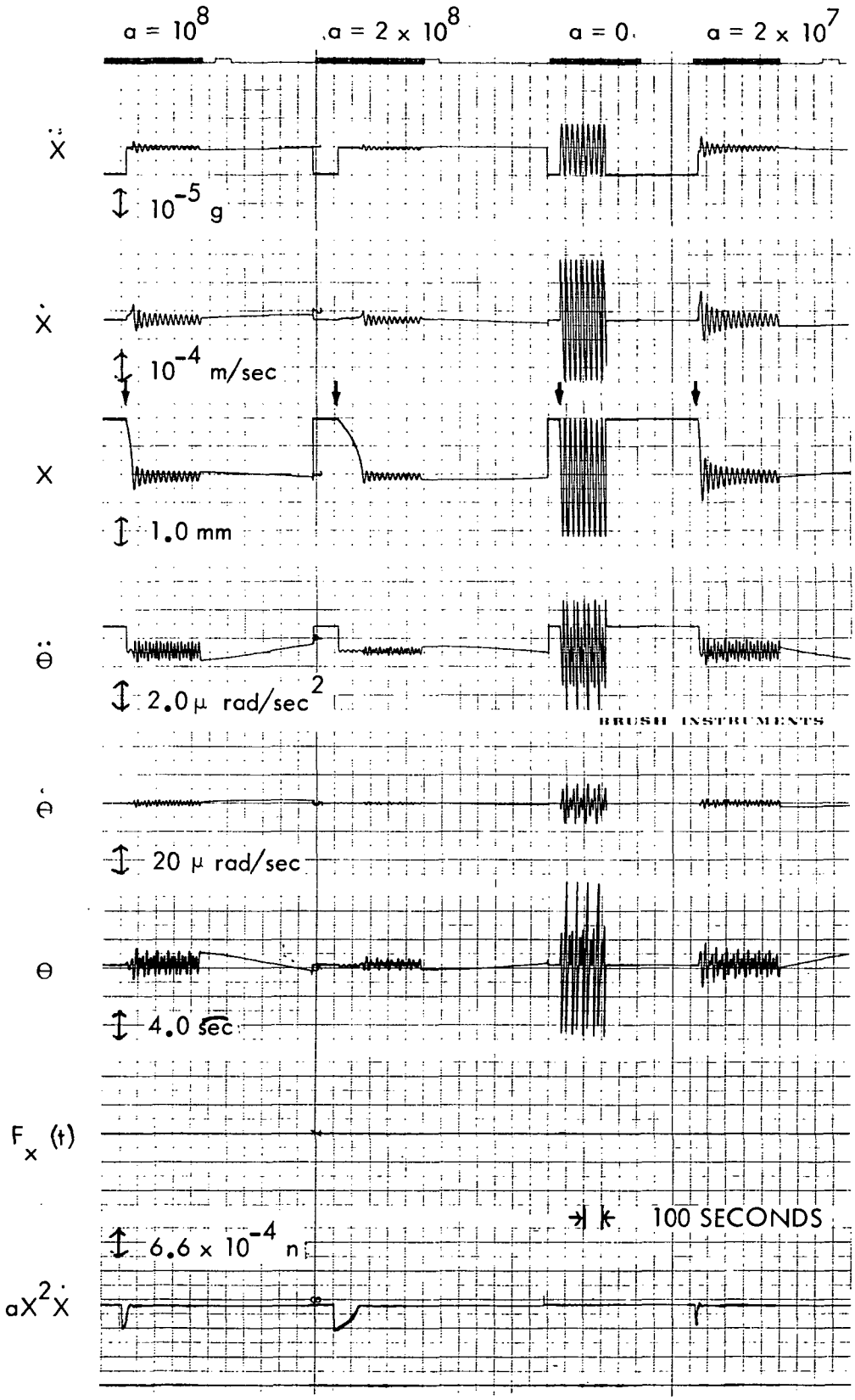

Figure 6.2-12. Responses for Various Values of Damping Constant, a. Initial Conditions: $x_0 = 2.0$ mm., $\delta = 2.0$ mm.

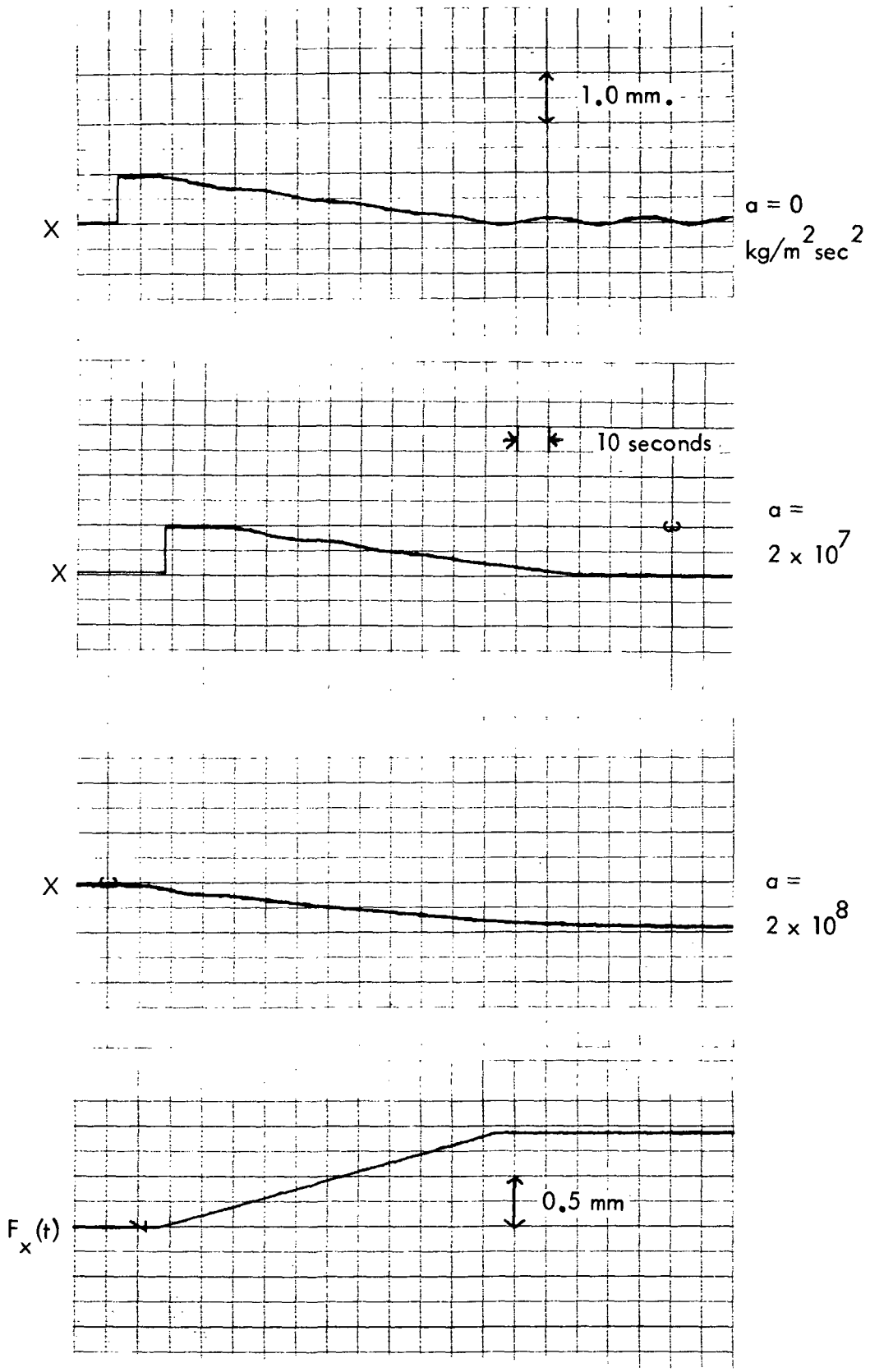

Figure 6.2-13. Ramp Responses for Different Values of Damping Constant

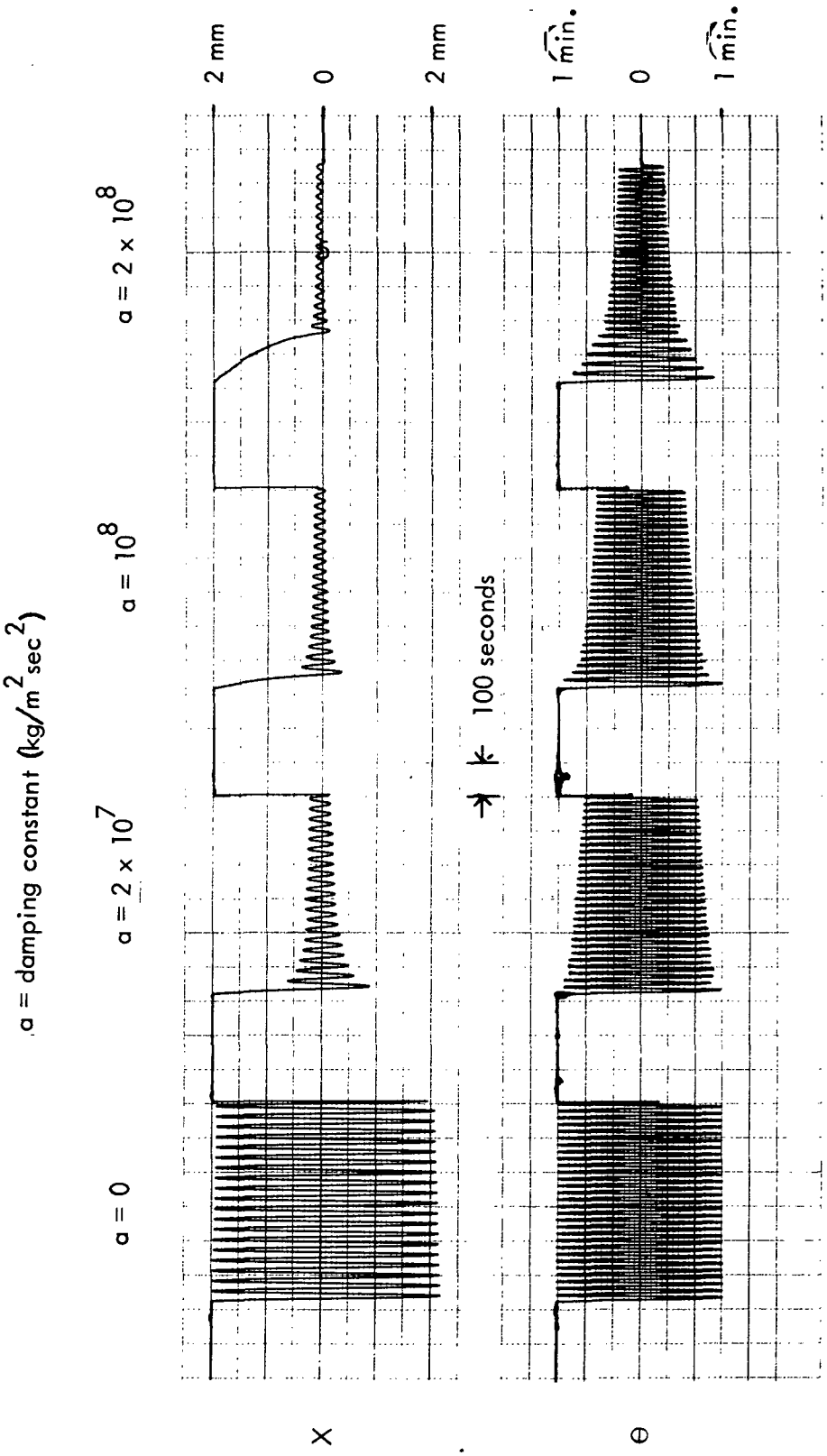

Figure 6.2-14. Translational Responses for Initial Conditions x_o = 2 mm., θ_o = 1.0 arc min.

Section 7

TEST DESCRIPTION

7.1 MEASURED PARAMETERS

For all tests, six major parameters were measured to define the suspension/platform characteristics.

These parameters were:

- Acceleration in the line of shaker motion ($\ddot{X}$)
- Acceleration transverse to the line of shaker motion ($\ddot{Y}$)
- Rotational acceleration in the horizontal plane ($\ddot{\Theta}$)
- Translation in the line of shaker motion (X)
- Damping control signals (voltage across suspension coils)
- Rotation in the horizontal plane (Θ)

The parameters were recorded as a function of time for all disturbances and suspension systems specified in this report.

7.2 INSTRUMENTATION

7.2.1 LOCATION ON PLATFORM

The location of the sensors and accelerometers described in this section is shown in figure 7.2-1. Figure 7.2-2 is a photograph of the three accelerometers. Accelerometer no. 2 is in the foreground, with nos. 1 and 3 on the left- and right-hand sides, respectively.

7.2.2 SHAKER SIGNAL CIRCUIT

The electrical disturbance signals and zero position signals to the hydraulic shaker were fed into a servo amplifier (one of the amplifiers in the analog computer). This amplifier operates a solenoid valve in the hydraulic line of the shaker mechanism, so that the shaker responded to a signal applied to the servo amplifier.

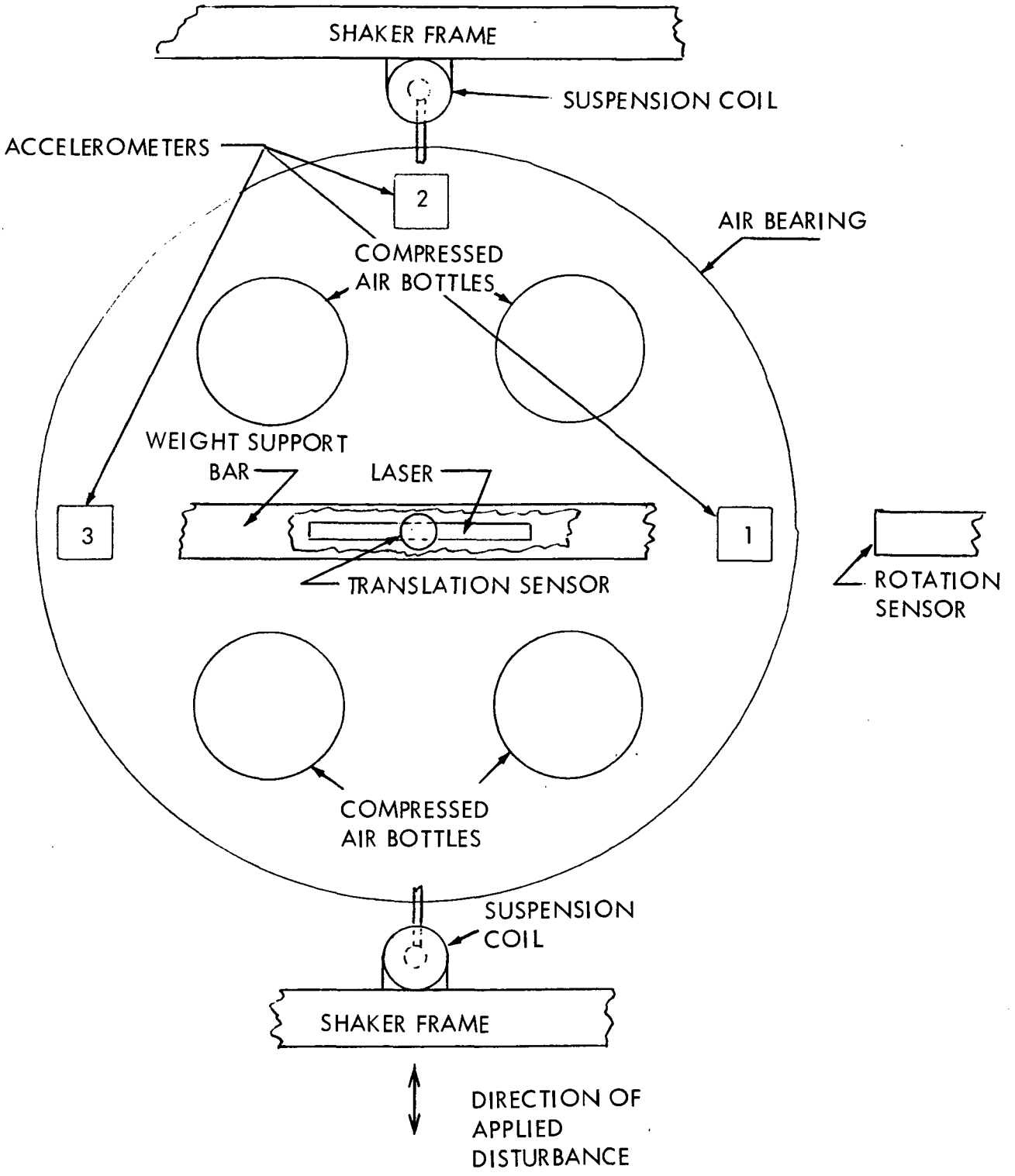

Figure 7.2-1. Location of Sensors and Accelerometers

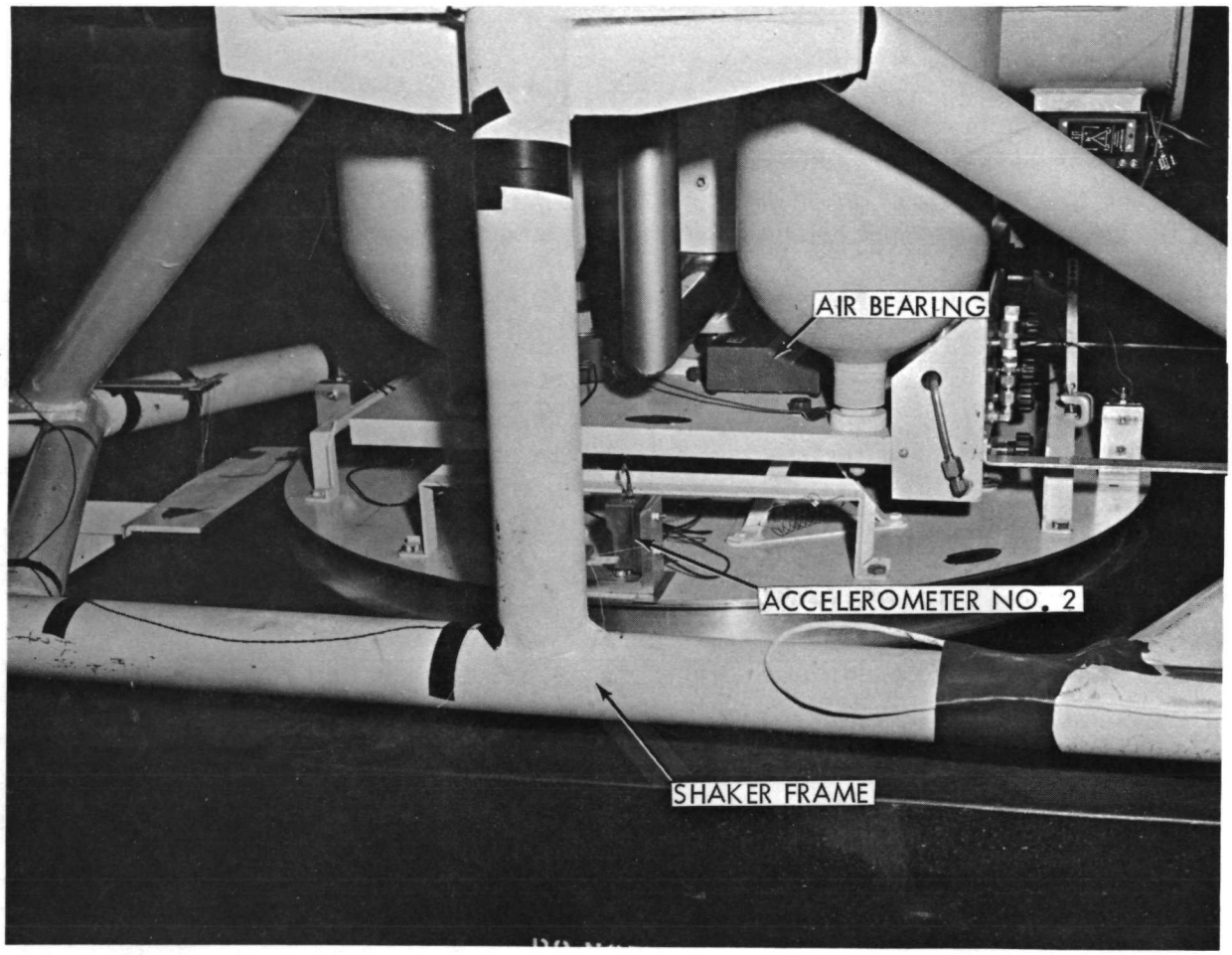

Figure 7.2-2. Accelerometers on Air Bearing

The fidelity with which the shaker followed the electrical waveform was verified by applying square electrical impulses to the amplifier and recording the actual physical motion of the shaker. The rise times recorded from the shaker displacements were much shorter than the time constants of any of the accelerometer electronics or any time constant involved in the entire test. Therefore, the shaker movement is considered to be an exact reproduction of the electrical input signal.

Sine wave signals for the transfer function curves were obtained from a Hewlett Packard model 202A Low Frequency Function Generator. This instrument was the source of all sine-and square-wave disturbance inputs.

Step function inputs were obtained by simply switching a DC voltage across the input of the servo amplifier. No problems with contact bounce were observed.

Ramp functions were obtained from one of the integrating amplifiers of the analog computer.

7.2.3 TRANSLATION SENSOR

The position of the air bearing was measured by means of an optical system incorporating a United Detector Technology, SC/25 two-axis position sensor. This solid-state device produces two electrical signals proportional to the X and Y position of a light spot focused on the surface of the detector.

The light source consisted of a Metrologic model ML 310 Laser with a one-millimeter beam diameter. By means of a beam splitter and two mirrors mounted on the air bearing, the light beam was positioned as in figure 7.2-3 so that it coincided with a vertical line through the center-of-mass. The two-axis position sensor was mounted on the ceiling of the test cell. The position of the air bearing is, therefore, measured with respect to an inertial reference rather than with the shaker frame/spacecraft.

7.2.4 ROTATION SENSOR

The laser light source was also used for the rotation measurements. Part of the laser beam was separated from the translation light path by means of the beam splitter and directed toward a small 137-mm focal length telescope with a 50-mm aperture as shown in figure 7.2-3. Another UDT position sensor was mounted in the focal plane of the telescope, providing an electrical signal proportional to the position of the focused light spot. This arrangement provided an angular rotation signal independent of the translational position of the air bearing.

7.2.5 ACCELEROMETER COMPUTER CIRCUITS

The acceleration of the air bearing was measured by means of three Accumetric Corporation accelerometers mounted on the bearing as shown in figures 7.2-1 and 7.2-2. These instruments are of the self-generating non-forcebalance type. Their frequency

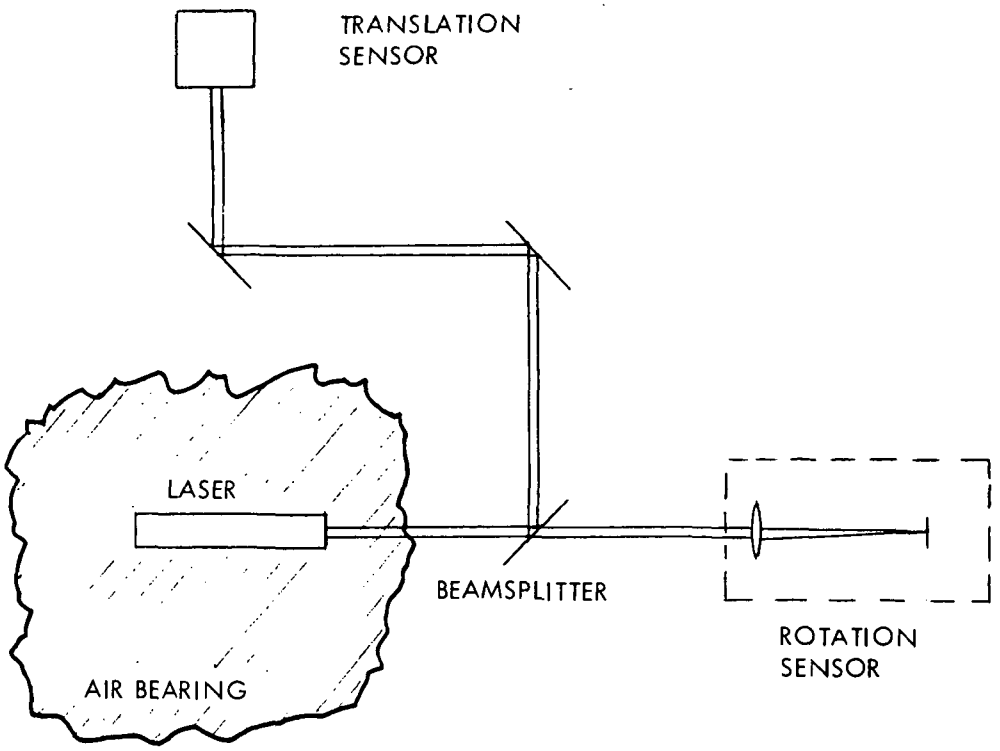

Figure 7.2-3. Optical Path for Sensor Bearing

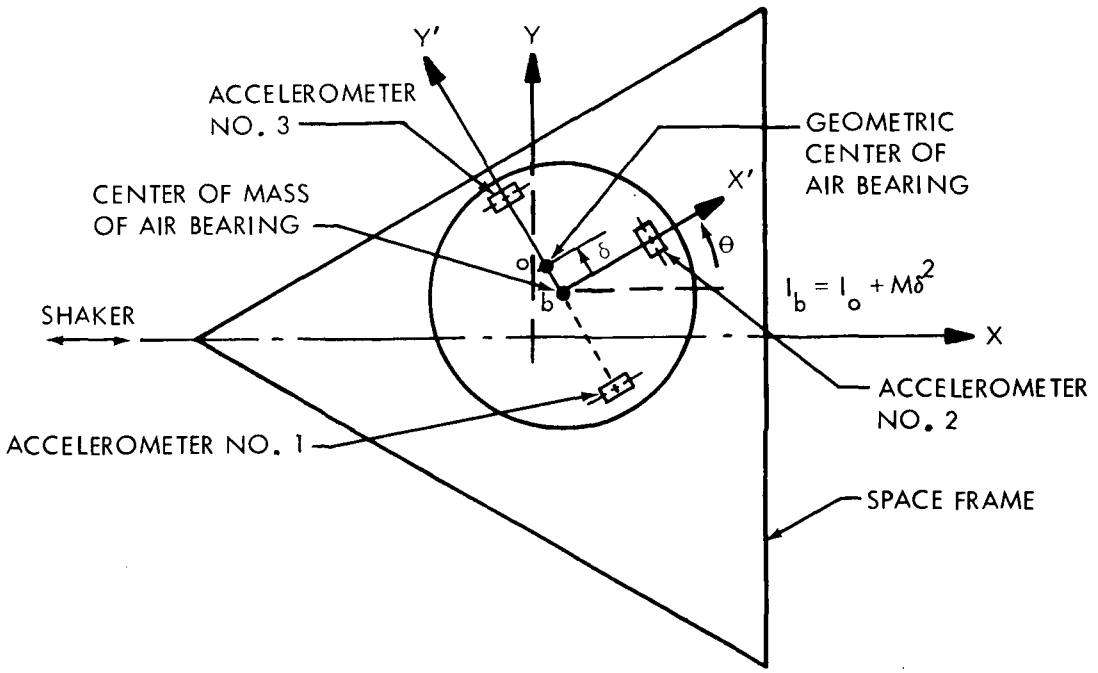

X, Y - AXES SET FIXED TO SPACE FRAME. THE FOUR ISOLATION SYSTEM ATTACHMENT POINTS ON THE SPACE FRAME ARE ASSUMED TO BE LOCATED ON THESE AXES.

X', Y' - AXES SET FIXED TO AIR BEARING. ALIGNED RELATIVE TO ACCELEROMETERS (1), (2), AND (3) AS SHOWN IN THE FIGURE.

Figure 7.2-4. Reference Axes for System

response is flat within ± 2% from 0.016 to 10 Hz. A closeup view of accelerometer no. 2 is shown in figure 7.2-2.

7.2.5.1 Relationship of Accelerometer Readings to $\ddot{X}$, $\ddot{Y}$ and $\ddot{\Theta}$

With the accelerometers positioned as shown in figure 7.2-4, there is an interaction between the translational and rotational measurements for each accelerometer. That is, both rotational and translational accelerations will be measured without separation. In order to remove this ambiguity, the outputs of the three individual accelerometers were combined as described in the following paragraphs.

Assigning a positive X direction from West to East and positive Y direction from South to North, the accelerometers were positioned so that instruments 1 and 3 measured acceleration in the positive X direction and instrument 2 measured acceleration in the positive Y direction. Then calling a_1, a_2, a_3, the outputs from accelerometers 1, 2, 3 respectively, the following equations apply:

$$a_1 = \ddot{X} + \ddot{R}\Theta \tag{7.1}$$

$$a_2 = \ddot{Y} + \ddot{R}\Theta \tag{7.2}$$

$$a_3 = \ddot{X} - \ddot{R}\Theta \tag{7.3}$$

where R is the distance from the axis of rotation of the bearing to the accelerometers (this distance is the same for all three accelerometers) and $\ddot{\Theta}$ is the angular acceleration of the bearing with counterclockwise rotation assigned as positive.

Then adding equations (7.1) and (7.3) above, we obtain: $\ddot{X} = \dfrac{a_1 + a_3}{2}$ (7.4)

Subtracting equations (7.1) and (7.3), we obtain: $\ddot{\Theta} = \dfrac{a_1 - a_3}{2R}$ (7.5)

And substituting equation (7.5) in equation (7.2): $\ddot{Y} = a_2 - \dfrac{(a_1 - a_3)}{2}$ (7.6)

The individual outputs from the accelerometers were thus combined to provide, except for constant multipliers, the terms specified in equations (7.4), (7.5) and (7.6). These final signals were applied to a Brush Company recorder and appear on the first three tracks of the output data tape.

Actually, the input signals to the first three recorder tracks are, respectively:

$$\ddot{X} = \frac{k\,a_1 + k\,a_2}{2} \tag{7.7}$$

$$\ddot{\Theta} = \frac{k\,a_3 - k\,a_1}{2R} \tag{7.8}$$

$$\ddot{Y} = \frac{k a_1 - k a_3}{2} - k a_2 \qquad (7.9)$$

where k is the gain for each of the three accelerometer filter amplifiers described below.

7.2.5.2 Ancillary Electronic Circuitry for Accelerometers

It was discovered that a ground vibration of approximately 15 Hz was being transmitted through the table to the accelerometers from other equipment located within the plant. To simplify the data analysis a low-pass filter was inserted in the output of each accelerometer. The filters incorporated three operational amplifiers in the analog computer, and were designed for cutoff frequency of 3.2 Hz. The response of the filters was essentially flat out to a frequency of 0.3 Hz and was down less than 10 percent at 1.0 Hz. Correction factors for the response falloff were applied to the readings for 0.5, 0.7 and 1.0 Hz. With the filters, the ground noise was reduced to the level of the internal noise of the accelerometers.

The outputs of the accelerometers were then combined in the analog computer to give the values of $\ddot{X}$, $\ddot{Y}$ and $\ddot{\Theta}$ on the Brown Recorder.

7.3 SYSTEM GEOMETRY AND MASS CHARACTERISTICS

The weight and center of gravity of the air platform were determined by three load cells which were positioned beneath the platform. The load cells were positioned at known points near the circumference of the platform and readings taken for several values of pressure (and hence weight) for the compressed air system used to float the platform. From these data the coordinates of the center-of-mass and the total weight of the platform were obtained. Variations due to changes in air pressure were found to be relatively small, and the values obtained for 1000 psi were used throughout the study.

The moment of inertia of the platform was obtained by activating the magnetic suspension system and measuring the translational and rotational resonant frequencies. From the translational period, the stiffness, k, of the suspension can be measured. This stiffness in each of the magnetic suspension coils also provides the restoring force for angular rotation so that the torsional stiffness is directly proportional to the translational stiffness. Hence,

$$\omega_t^2 = \frac{k}{M} \quad , \quad \omega_R^2 = \frac{K'}{I_z} = \frac{k\ell^2}{4I_z}$$

k = translational stiffness

K'= rotational stiffness

Therefore, $$I_z = \frac{M\ell^2}{4}\left(\frac{\omega_t}{\omega_R}\right)^2$$

This method was found to give more consistent results than the previously used methods of supporting the air bearing by a torsion shaft of known modulus.

In order to assess the effects of changes in moment-of-inertia and force-moment-arm on system characteristics, a slotted angle bar was attached to the air platform so as to lie along the Y'-axis. By positioning weights at different positions along this bar, the moment-of-inertia and the center-of-gravity along the Y'-axis could be changed. Because the disturbing forces are applied along the X'-axis, the applied moment arm is the distance $\bar{Y}'$, and therefore, only variations in $\bar{Y}'$were affected.

Two weight configurations were selected:

- Both weights at the center of the bar. Because of the vertical center rod through the bar, the weights could not be placed at the exact center, but rather were positioned about each arm of the bar 5.1-cm from the center. $I_z = 21.9$ kg.m^2
- A weight on each arm of the bar, 0.92 meters from the center. This arrangement is W_2. $I_z = 29.2$ kg.m^2

These weight arrangements are diagrammed in figure 7.3-1.

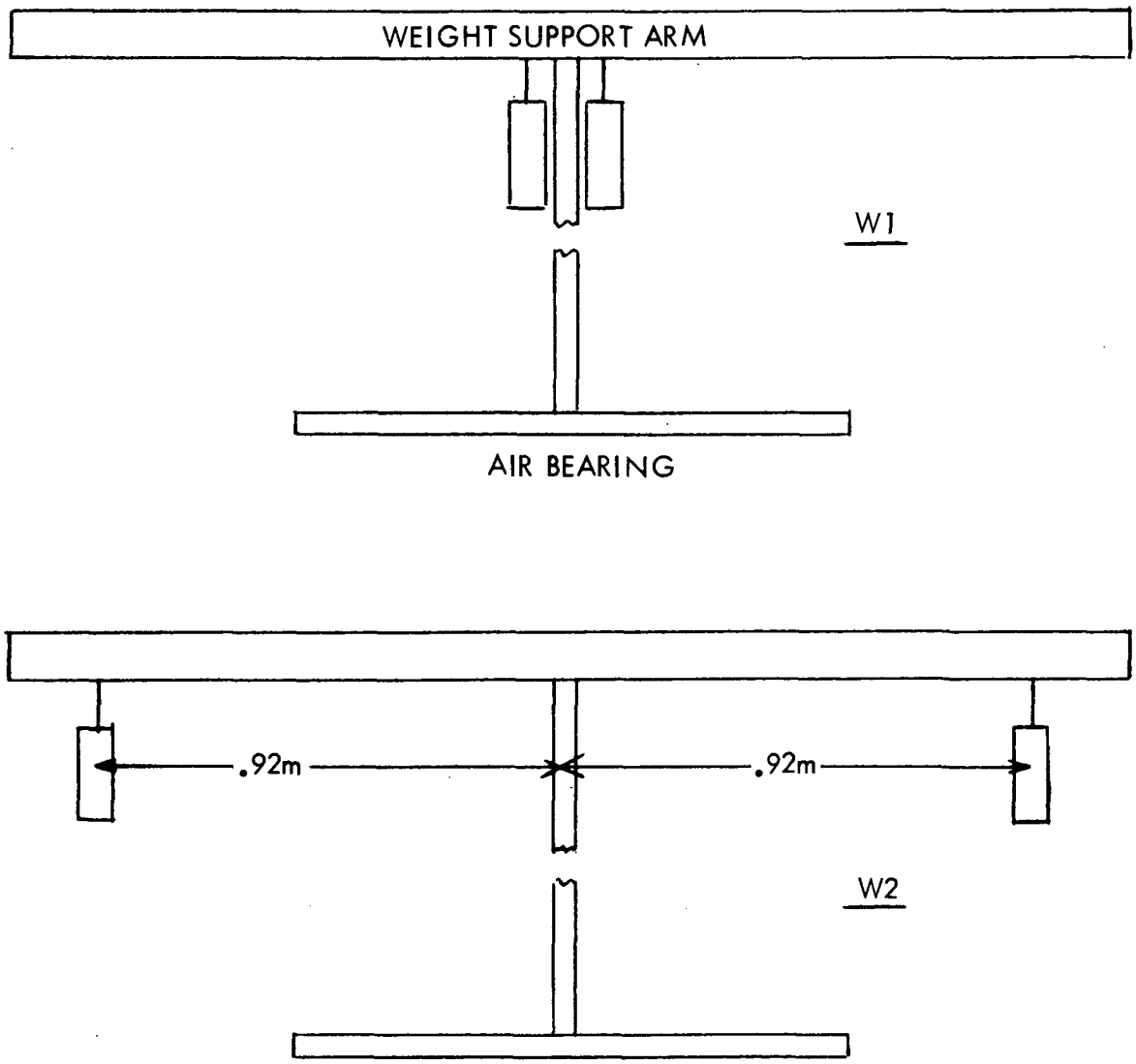

Figure 7.3-1 Weight Configurations

Section 8

TEST RESULTS

This section describes the results of the suspension system tests utilizing the floating air bearing discussed in sections 4 and 7.

8.1 BASIC MAGNETIC SUSPENSION

The basic magnetic suspension system is that described in section 4 of this report. It consists of two sets of suspension coils and two velocity pickup coils. The geometry of the suspension and velocity coils are shown in figure 8.1-1. An improvement in performance could have been obtained by using a smaller separation between the suspension coils and the disc magnet. However, the large separations were maintained since this separation would be required to allow for motion in a three-dimensional suspension system.

The electronics for the two control systems (one system for each of the two sets of suspension and velocity pickup coils) is shown in the schematic, section 4, figure 4.2-2. The constant, K, represents the total voltage gain of the electronics between the coils. The damping is proportional to this constant and, hence, the curves and data presented in this section will be designated with the value of K used in the experimental simulation. The values ranged between K = O, for an undamped system, to K = 1, 000, 000 for the most damping obtainable with the present equipment. This gain is directly proportional to the damping constant, a. The constant of proportionality is dependent on the dimensions of the suspension coil and magnet strengths.

Also shown in the schematic is a low-pass filter with the transfer function:

$$\frac{1}{(\tau_1 s + 1)\ (\tau_2 s + 1)}$$

$$\tau_1 = 1.0 \text{ sec.}$$

$$\tau_2 = 0.1 \text{ sec.}$$

Since the natural frequency of the system had a period appreciably larger than the time constant of the filter, the filter had a relatively small effect on the behavior of the system. The filters were found to be desirable because of the large gains required in the damping electronics and the resultant noise associated with the large gains. No difference in system behavior to the step disturbances were observed with and without the filters. However, for the sinusoidal responses for the systems utilizing a very large gain in the damping electronics, the filters were found to be necessary to prevent overloading of the electronics at the higher disturbance frequencies. Due to the small values of transmissibility at frequencies above 0.1 H_z, it was necessary to drive the system

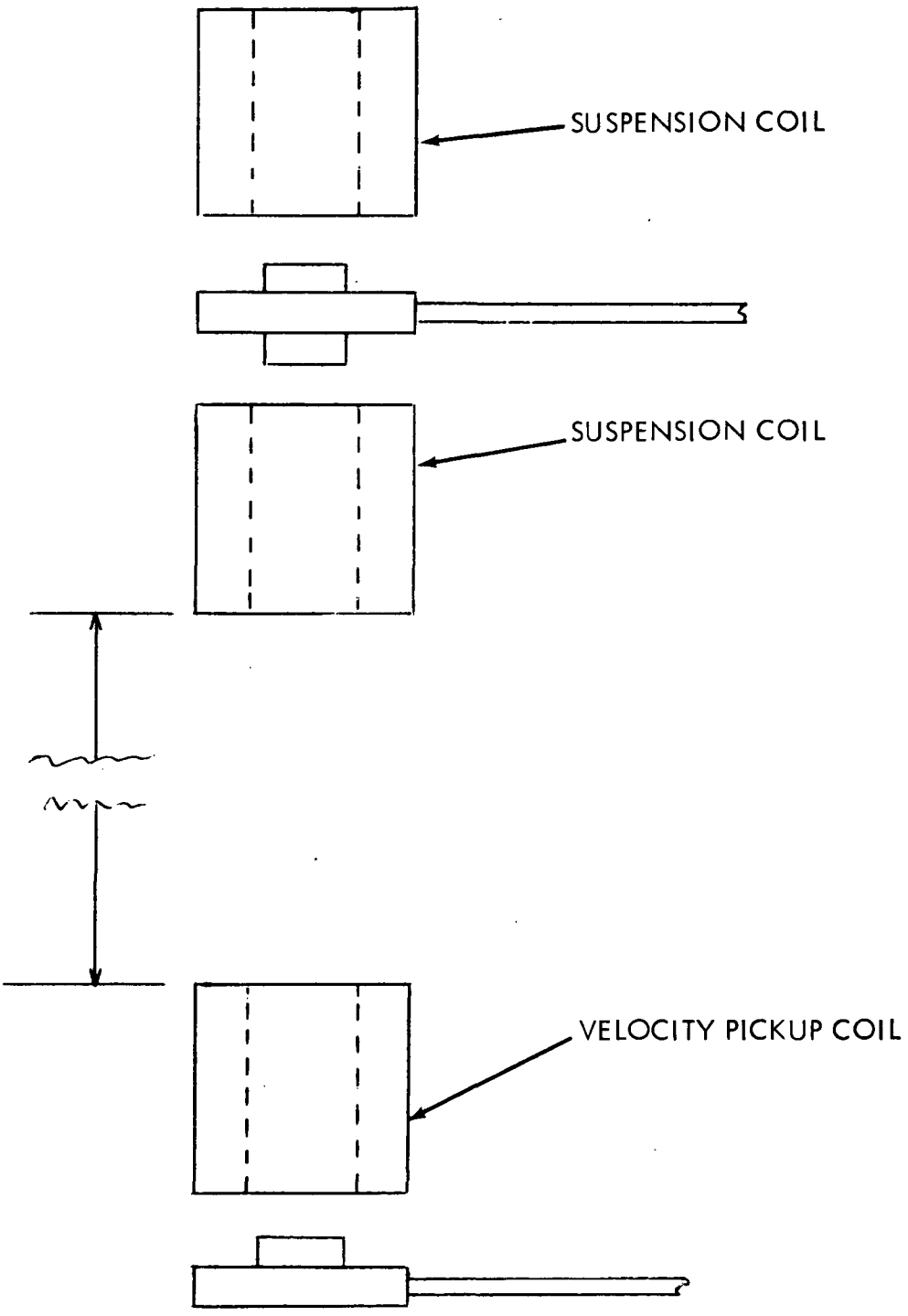

Figure 8.1-1. Suspension Coil Geometry

with relatively large amplitudes to obtain a detectable output. Thus at the higher frequencies an amplitude of one millimeter peak-to-peak was necessary. This large amplitude resulted in very large signals in the damping electronics, requiring the low-pass filters.

8.2 TRANSFER FUNCTIONS

The transfer functions for the experimental system are shown in figures 8.2-1 and 8.2-2 for two values of damping (i.e., two different gains in the damping control electronics). Since the system is nonlinear in nature these are not transfer functions in the strict sense, but ratios of the peak-to-peak output disturbance (usually non-sinusoidal) to a sinusoidal input disturbance. However, these curves do give an adequate indication of the effectiveness of the isolation at various frequencies. The behavior of the system is similar to that of a second-order spring suspension with damping. The effective transmissibility increases with an increase in the damping constant.

A difference can be noted between the two curves of figures 8.2-1 and 8.2-2 at the higher driving frequencies. The transfer function shown in the first figure was taken with the low-pass filter disconnected from the damping electronics. The behavior is similar to a linear oscillator in that the transmissibility versus driving frequency approached a straight line (on a log-log scale) for the higher frequencies.

On the system represented by figure 8.2-2, the transmissibility decreases more rapidly with increasing frequency. In this case the filter was inserted in the damping electronics. The result is that the damping signal is frequency dependent, and the damping decreases with an increase in driving frequency. As expected, by analogy with a linear oscillator, a decrease in damping results in a decrease in transmissibility. The use of such filters is seen to be an advantage since it allows one to tailor the transmissibility versus frequency curve for a particular application. The only major requirement is that the filter or filters not have an appreciable phase shift at the system resonant frequency. In such a case the damping signal would be partially or completely out of phase with the disturbance or natural oscillations, and the net result would be an effective negative damping constant.

Figure 8.2-3 is typical of the response to sinusoidal driving functions. Note the nonsinusoidal form of the output acceleration, $\ddot{X}$. The transfer functions described in this section utilized the peak-to-peak value of this function.

8.3 STEP RESPONSES

Figure 8.3-1 shows the response of the system after being released from rest at a point 2.0 millimeters away from equilibrium. In the laboratory simulation it was not possible to physically release the air bearing without creating unwanted disturbances. To obtain the responses described in this section it was necessary to allow the air bearing to come to rest at its equilibrium position and then suddenly apply a 2.0-mm step in position to the shaker/spacecraft. Such a step implies an infinite velocity impulse. This impulse in the damping electronics is usually large enough to disturb the motion of the air bearing. To eliminate this transient, the damping electronics was disconnected for approximately one second after the application of the step. The final result very accurately simulated the response of a system released from rest from a non-equilibrium position.

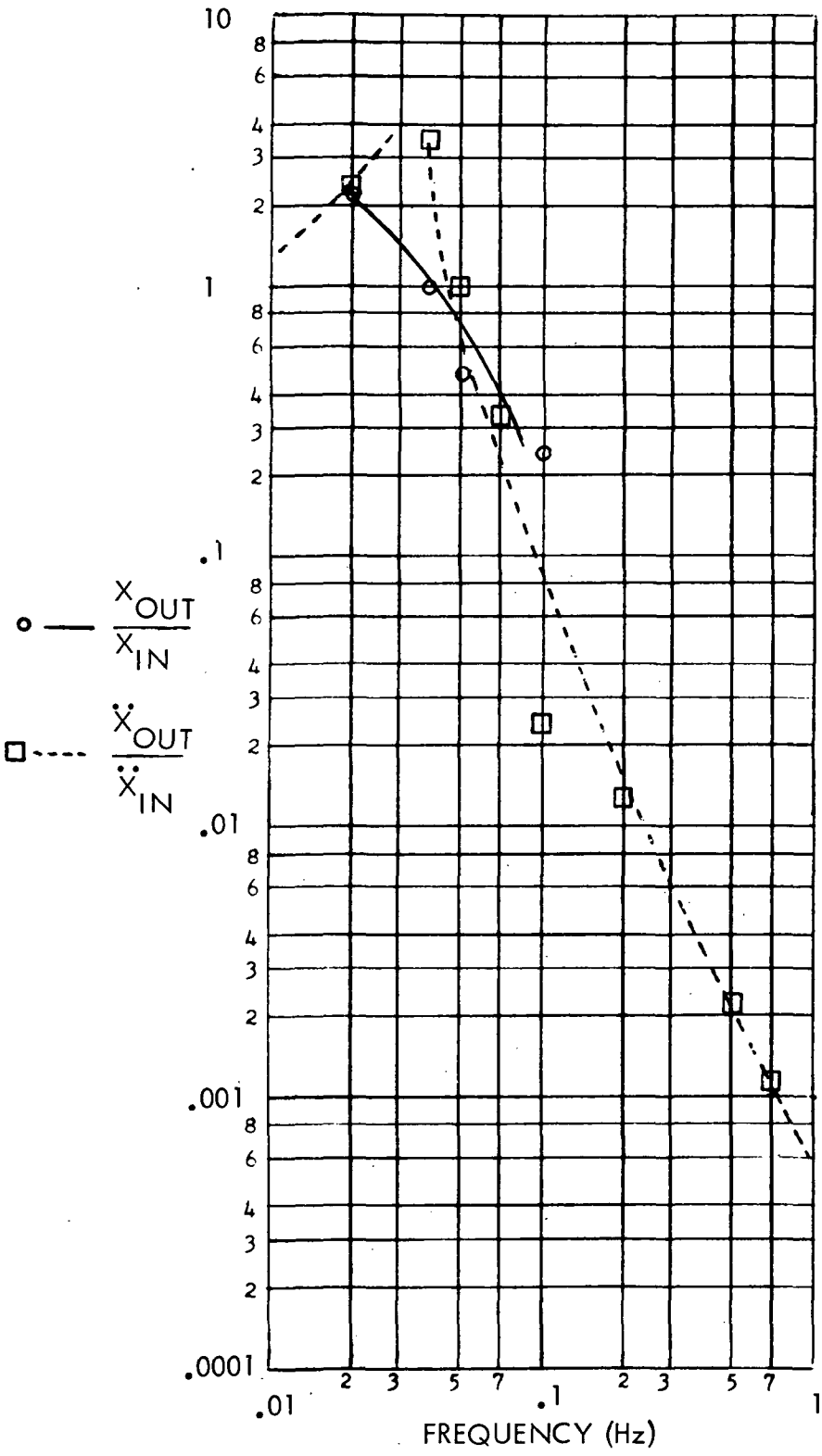

Figure 8.2-1. Experimental Transfer Function, Electronic Gain K = 100,000

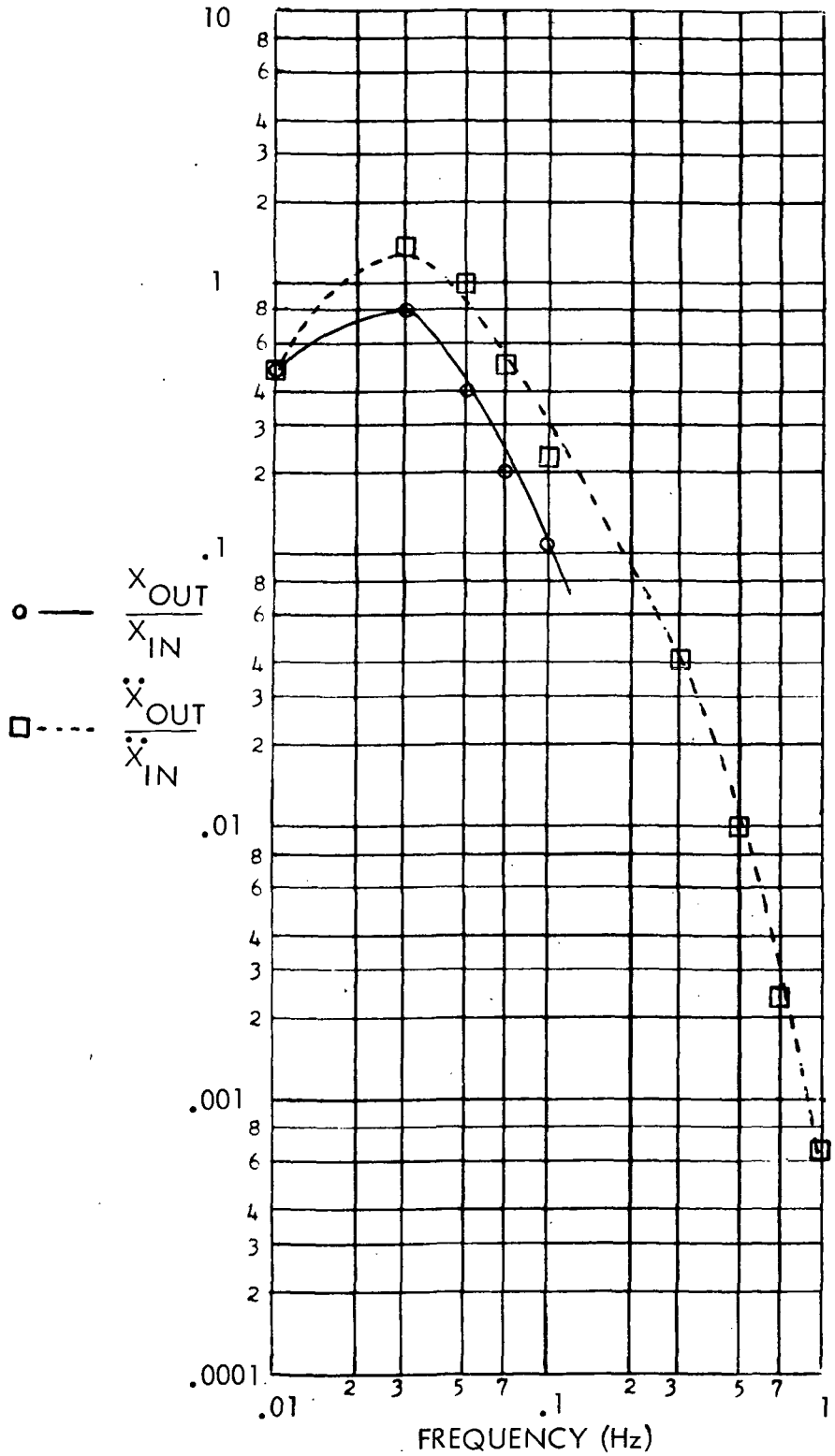

Figure 8.2-2. Experimental Transfer Function, Electronic Gain K = 300,000

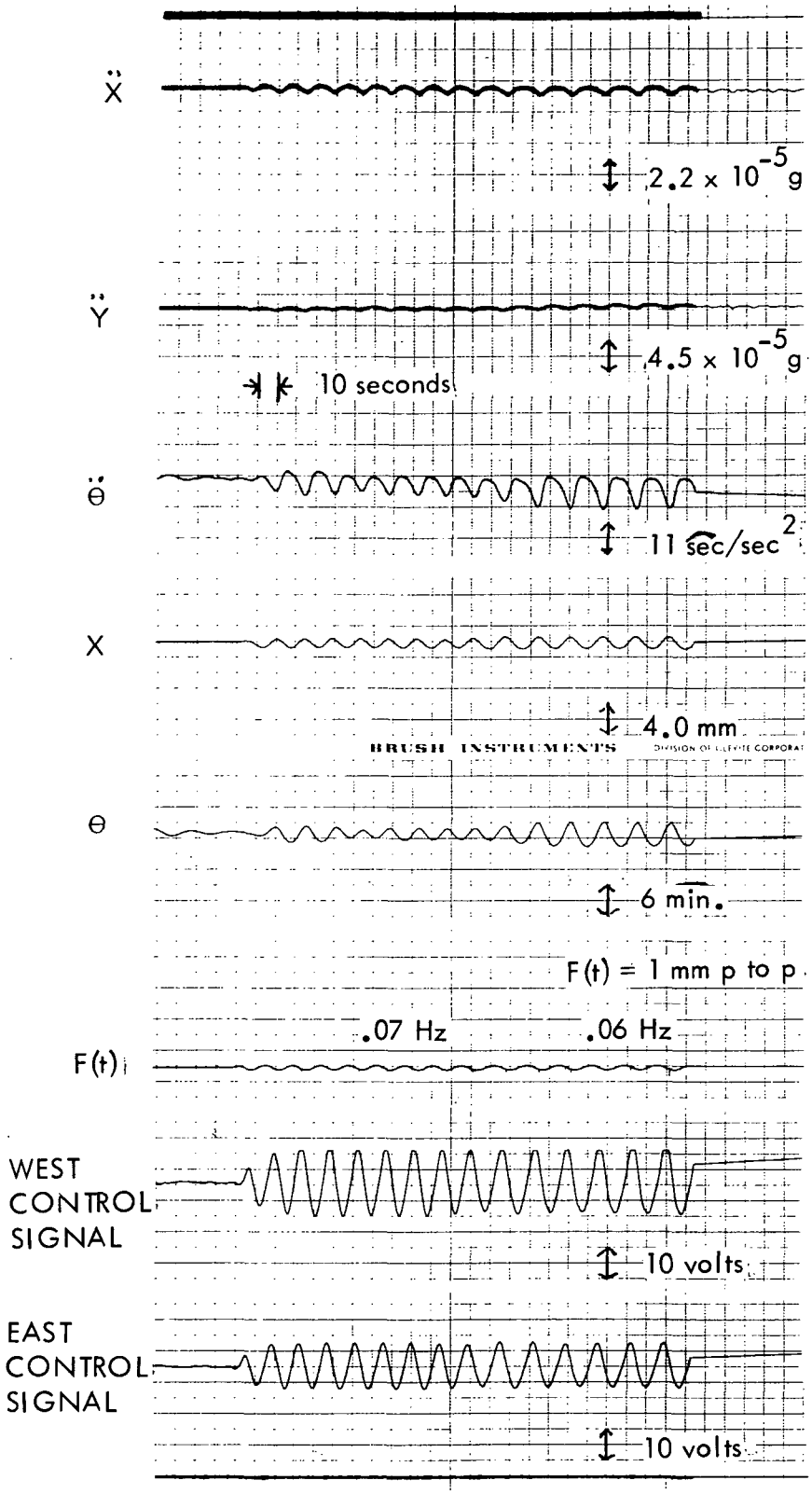

Figure 8.2-3. Response of Air Bearing to Sinusoidal Disturbances of 0.07 and 0.06 Hz.

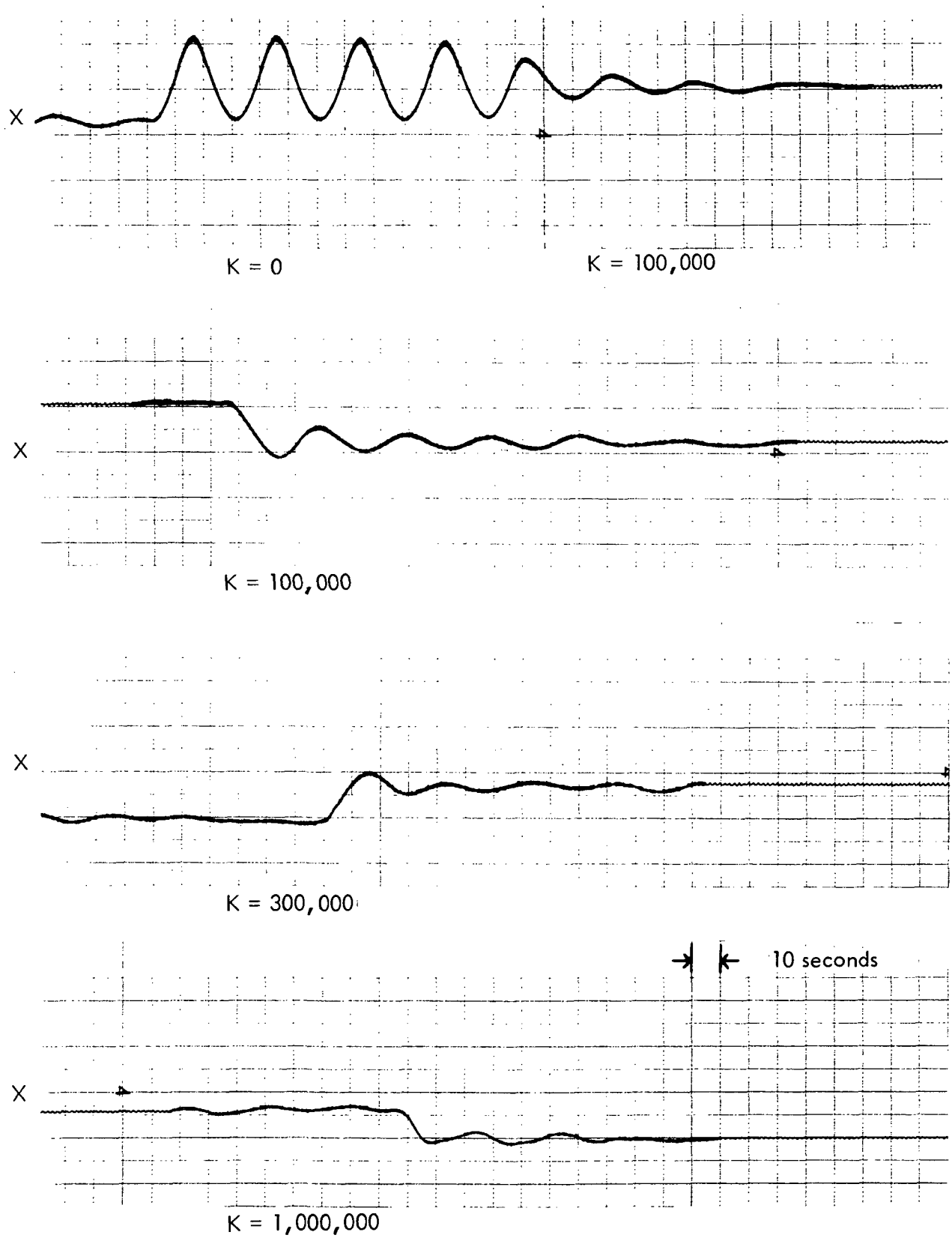

Figure 8.3-1. Translational Responses for Initial Condition x_o = 2.0 mm.

The four responses shown in figure 8.3-1 are those of the air bearing released from a point 2.0 millimeters from its equilibrium position. Each of the four responses is for a different value of damping as shown by the value of the constant, K. (This constant is the total gain of the damping electronics.) The first response is that for zero damping or K = 0. The response is that of a simple undamped oscillator. However, after approximately 3-1/2 cycles damping, K = 100,000 was introduced into the system and the amplitude quickly diminished. The following three curves show the response with increasing values of damping as shown in each figure.

Figure 8.3-2 is a graph of the percent overshoot (as described in section 6.2-2) as a function of amplifier gain, K.

The numbers at the top of the graph are values of the damping constant that a linear damped oscillator would have for the same value of overshoot.

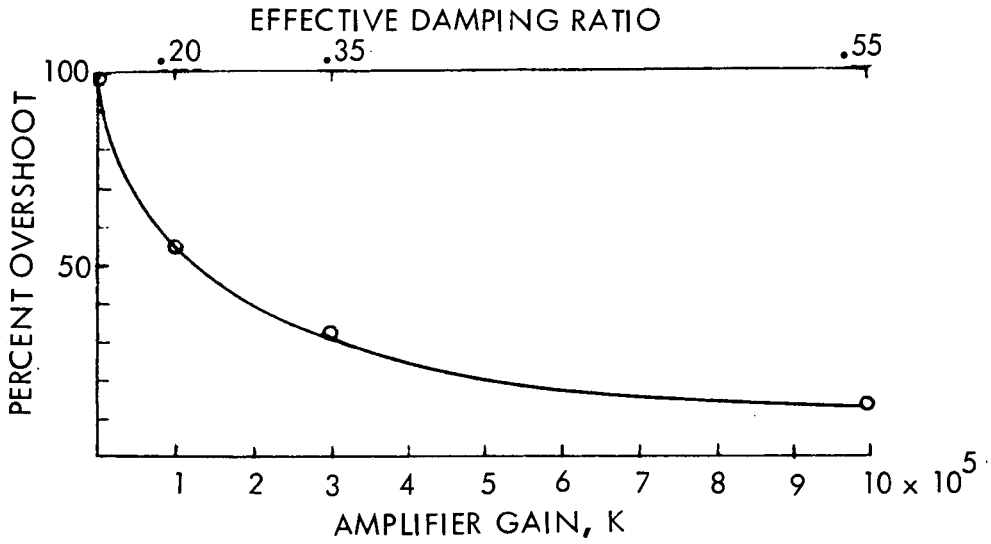

Figure 8.3-2. Percent of Overshoot as a Function of Amplifier Gain, K

Figure 8.3-3 is a typical system response to a 2.0-millimeter step input. As described previously in this section this response is not the same as the response of the system being released 2.0 millimeters from equilibrium. The damping electronics in this case was not turned off with the application of the step. The transient response to the velocity impulse can be seen in the large initial spikes in the two control signals. Since the transient responses of both damping systems were not exactly the same, these transients introduced an initial angular disturbance which would not occur if the system were simply released 2.0 millimeters from equilibrium.

A typical response to a ramp input is shown in figure 8.3-4. The ramp corresponds to a shaker/spacecraft velocity of 0.02 mm/second with respect to the air bearing/telescope. Very little change in angular motion can be observed until near the end of the ramp in which the air bearing struck one of the protective stops on the table.

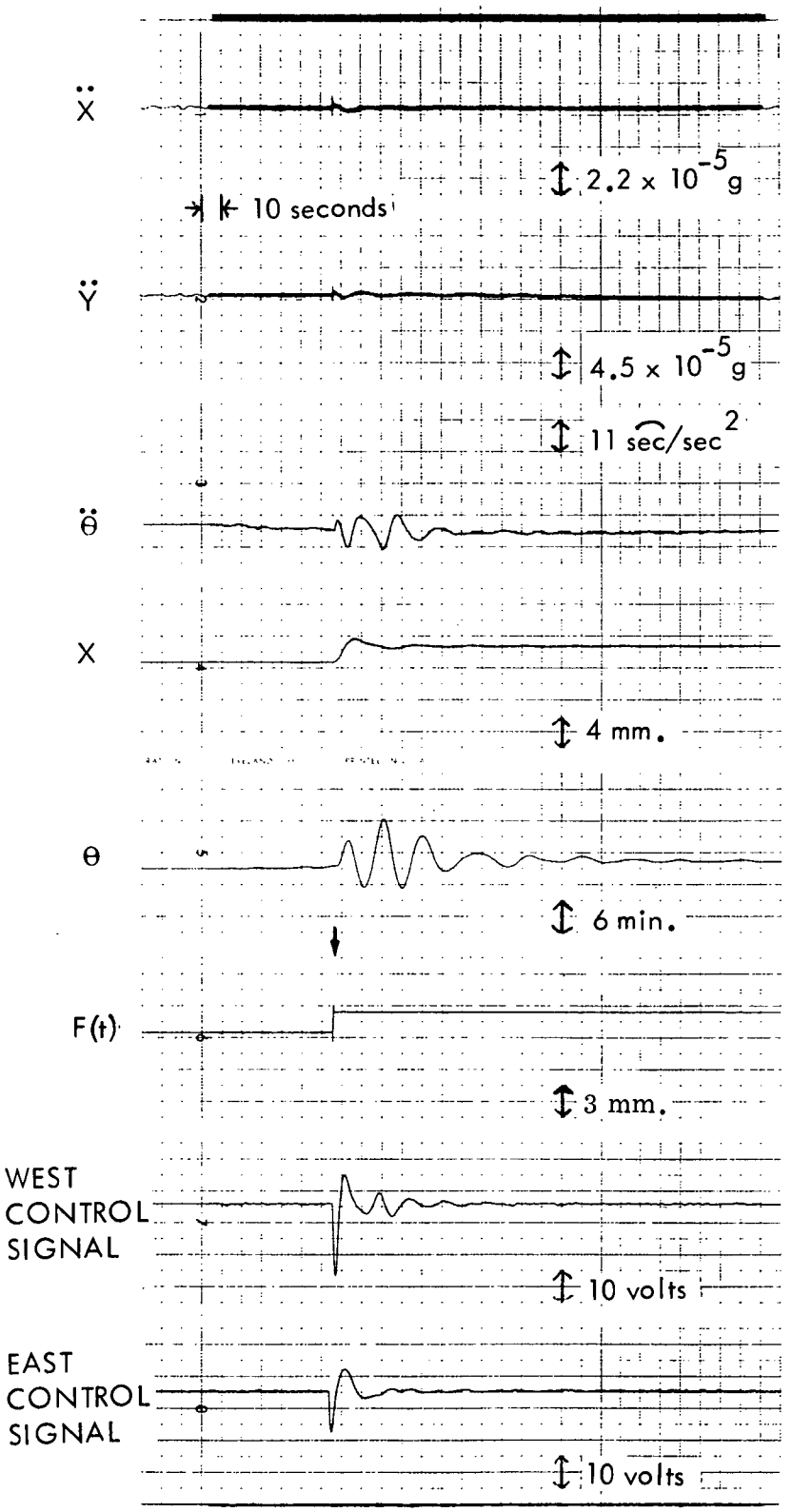

Figure 8.3-3. Typical Experimental Step Response at Amplitude = 2.0 mm.

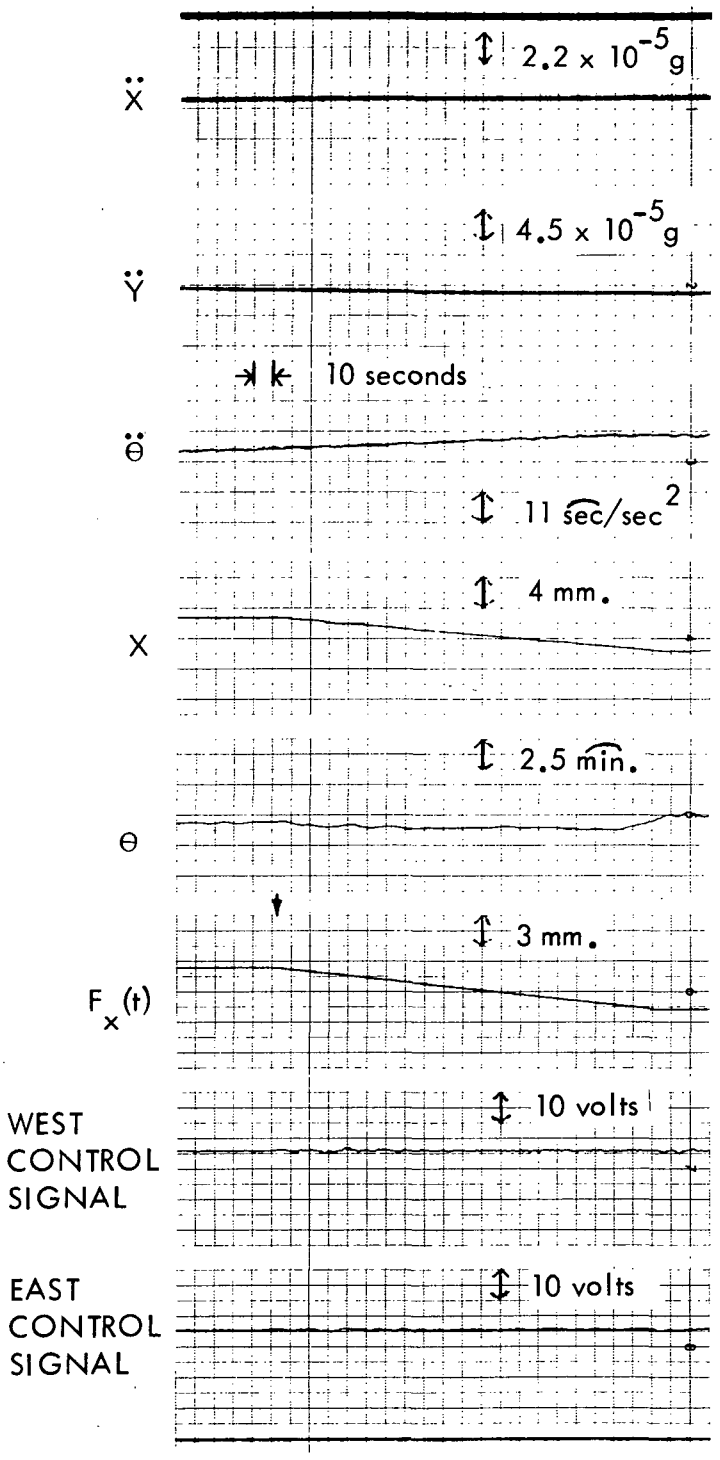

Figure 8.3-4. Typical Response to a Ramp Input Disturbance

Section 9

SUSPENSION SYSTEM MODIFICATIONS

9.1 MODIFICATION ONE - DAMPING WITH ZERO SPRING CONSTANT

The magnetic suspension system without the damping control loop behaves in almost an identical manner as a spring configuration with the added advantage that the spring constant can be adjusted during operation. However, by replacing the ferromagnetic disc by a permanent magnet, it is possible to either attract or repel the magnet, depending on the direction of current flow in the suspension coils. In other words, it is possible to obtain both a negative and a positive spring constant.

If the steady-state value of the suspension coil current is zero, but the damping control system is used to vary the instantaneous value of the current about its zero value, a damping effect could be obtained even though the average spring constant is zero. This would have an effect similar to friction damping but without physical contact and friction. Thus, it is possible to use the suspension coils and control loop as a damper to dissipate energy in any type of suspension system, e.g., a spring system. The amount of energy removed can be readily controlled by adjusting the gain of the control loop.

To determine the feasibility of using this magnetic damping described in this report with non-magnetic suspension systems, a helical spring suspension was attached to the air bearing. The springs used in this test were simple helical springs arranged in pairs at each of four suspension points as shown in figures 9.1-1 and 9.1-2. The included angle between each pair of springs was approximately 82 degrees. The linear spring constant or stiffness of the suspension was 3.50 newton/meter (0.02 lbf/in.). The equilibrium position of the spring suspension was carefully adjusted to coincide with the equilibrium position of the magnetic suspension. The steady-state current in the suspension coils was reduced to zero and the gain of the amplifiers adjusted for the desired damping constant, K.

The response of this system was nearly identical to that of the complete magnetic suspension/damping system, indicating that this type of magnetic damping can be used on other types of suspensions.

Figure 9.1-3 illustrates the response of the system after being released from a point 2.0 millimeters from equilibrium. The only difficulty encountered with this

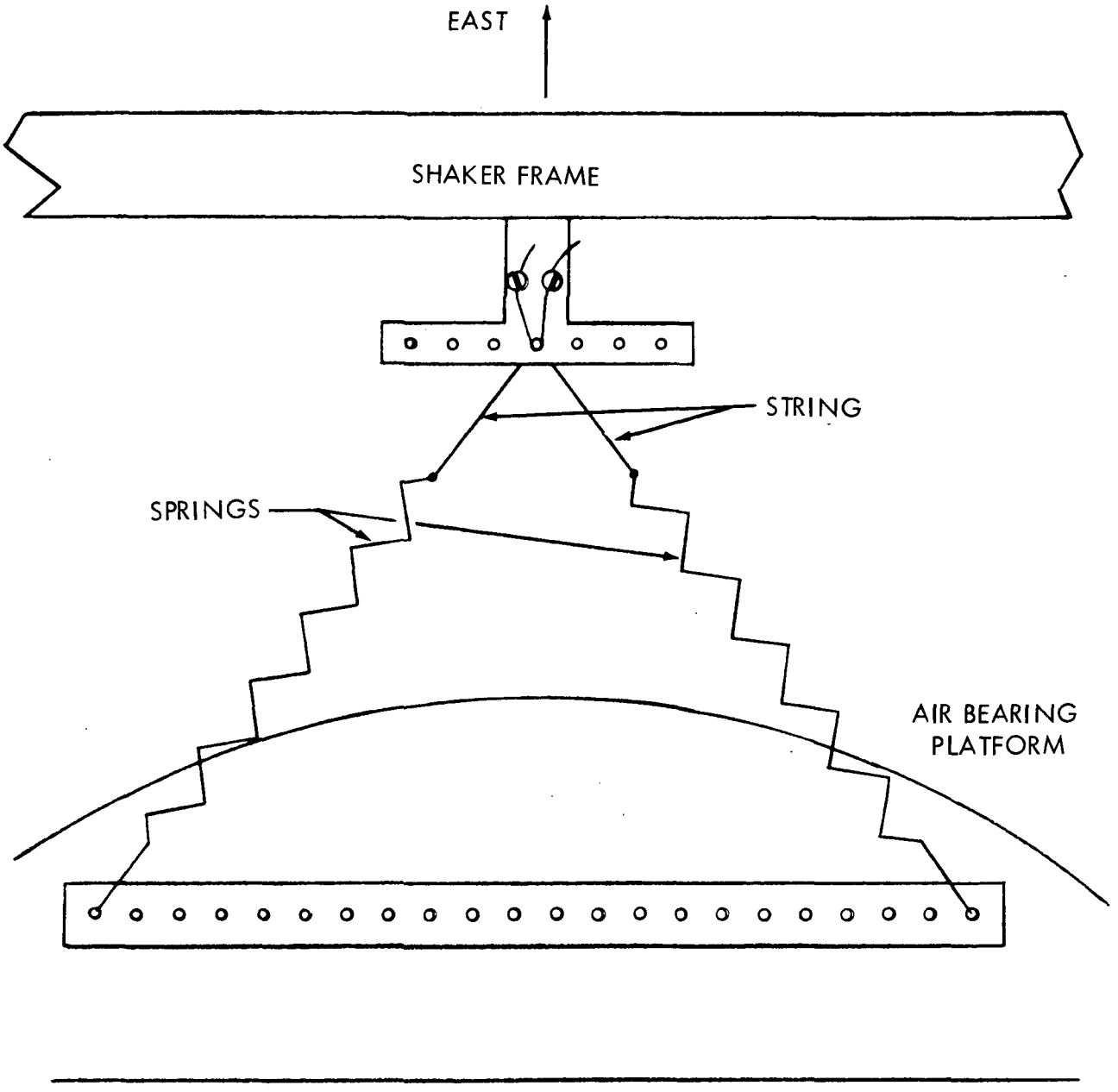

Figure 9.1-1. Spring Suspension Attachment

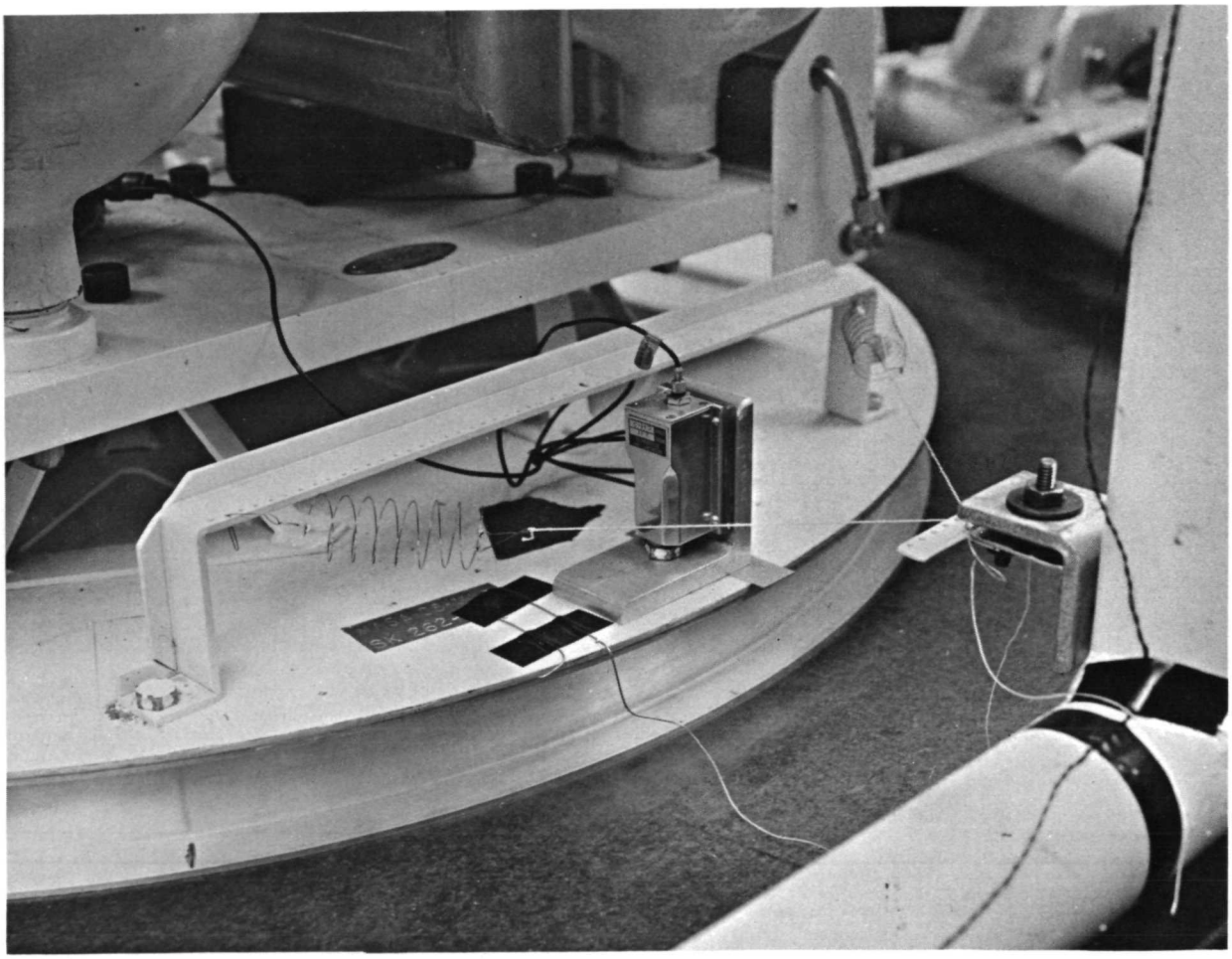

Figure 9.1-2. Spring Suspension

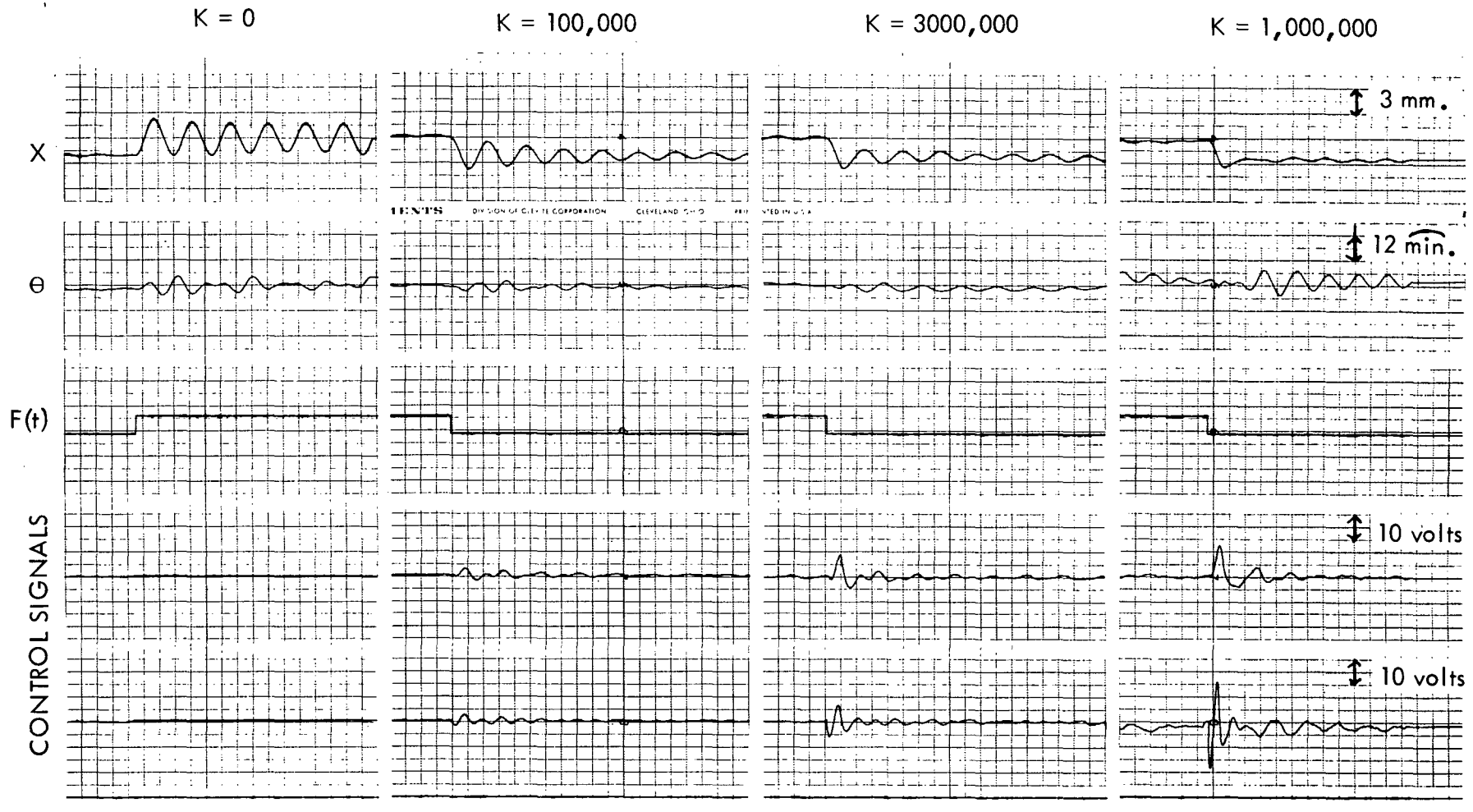

Figure 9.1-3. Response of Magnetic Damping System with Spring Suspensions, x_o = 2.0 mm., K = Amplifier Gain

system was the necessity of having the two equilibrium positions for both the spring and the magnetic systems coincide; otherwise, there would exist a small region in which the damping signal would not have the correct polarity or phase. The result would be an increase in smallest amplitude in which effective damping could be obtained. The tolerance for this positioning increased with increasing gain in the damping electronics.

9.2 MODIFICATION TWO - CONCENTRIC SUSPENSION AND VELOCITY PICKUP COILS

One disadvantage encountered with the system is the necessity for a separate arm and pickup coil in addition to the suspension coils. Besides increasing the number of components, there exists the problem of maintaining a close relative positional tolerance between the ferromagnetic disk and the permanent magnet on the velocity sensing arm. This magnet must be accurately positioned such that the magnet is directly under the center of the pickup coil $X = 0$, when the air bearing is in equilibrium. If there is a small error in this positioning, the control signal will have the opposite polarity for portions of the cycle, thus reducing the effective damping. This has been observed in the laboratory.

For this reason it would be advantageous to mount the velocity pickup coil inside and concentric with the suspension coils. However, the proximity of the two coils would allow a changing suspension coil current to induce an additional emf in the pickup coil, which would be confused with a velocity signal. This could be avoided by using two identical pickup coils wound in opposition, such that the induced emfs cancel. The double pickup coil would also reduce stray pickup from nearby electrical circuits.

For this modification each of the two sets of suspension coils was modified as follows, (see figure 9.2-1). Two small velocity pickup coils consisting of 2000 turns of no. 40 gauge copper wire were mounted within each of the suspension coils. As shown in the figure the pickup coils were arranged such that the pickup in the upper suspension coil was in the vicinity of the moving disc magnet attached to the air bearing. Thus an induced voltage proportional to the air bearing velocity would be induced in the upper pickup coil. The second pickup coil, used as a reference, was mounted in the lower end of the lower suspension coil. This coil is far enough removed from the magnets that there is no significant induced voltage, i.e., only the upper pickup coil contains the induced velocity signal.

The coils were connected in opposition as shown in the diagram of figure 9.2-2. In such an arrangement the induced voltages caused by changing currents in the suspension coils would cancel, while only the induced velocity signal in the upper pickup coil would appear at the input to the amplifiers. This signal is then amplified and used to control the damping current in the suspension coils.

Figures 9.2-3 through 9.2-5 show the results of this modification. These figures show the system response to a sudden step in position. Figure 9.2-3 shows the response to a 4.0-millimeter step with no damping, $K = 0$. This is a relatively large disturbance and the resultant angular disturbance is somewhat large due to a small offset in center of mass.

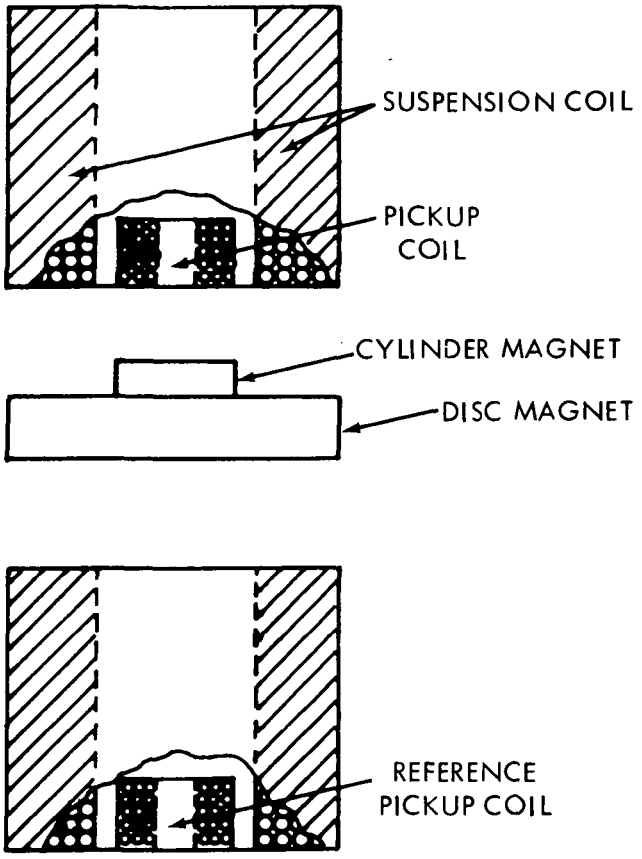

Figure 9.2-1. Concentric Velocity Pickup and Suspension Coils

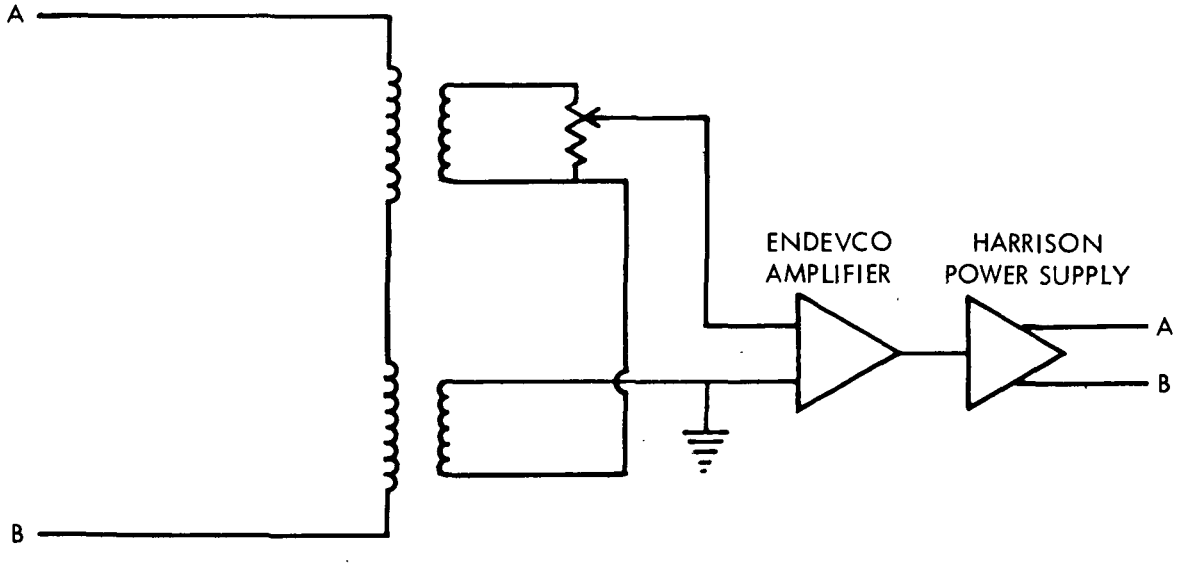

Figure 9.2-2. Electrical Schematic for Concentric Velocity Pickup and Suspension Coils

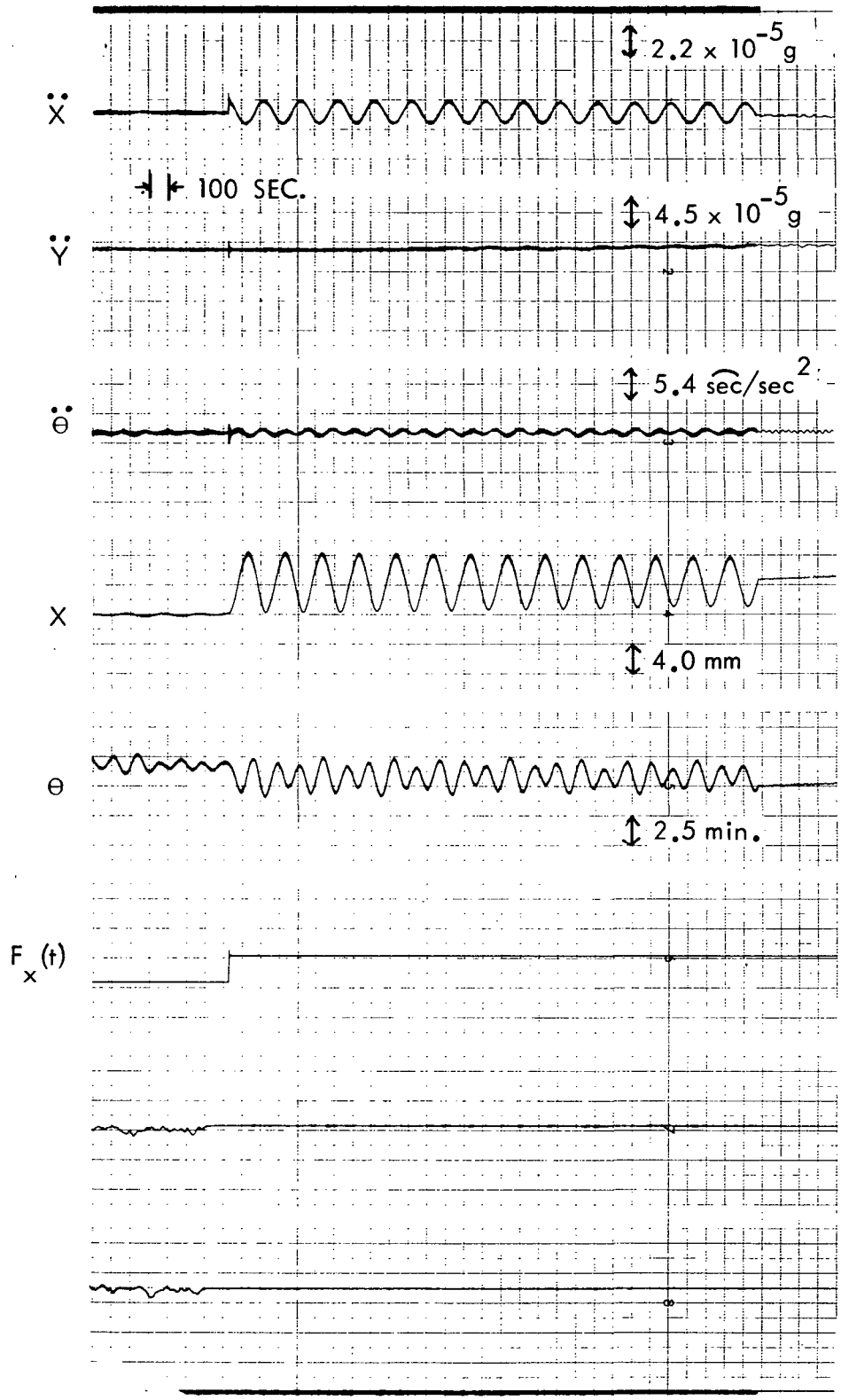

Figure 9.2-3. Response of Concentric Coil System to 4 mm Step, Zero Damping

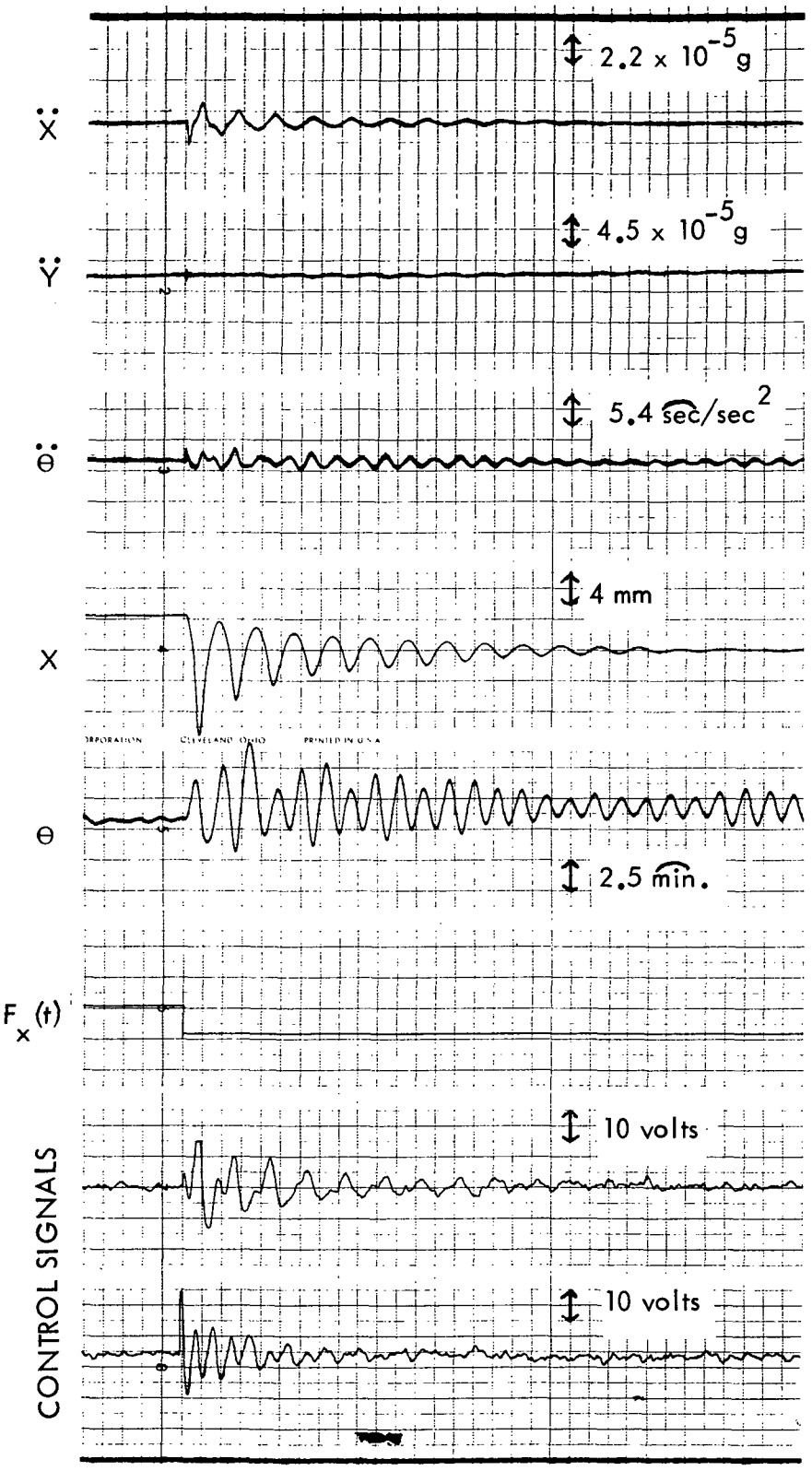

Figure 9.2-4. Response of Concentric Coil System to 4 mm Step, K = 600, 000

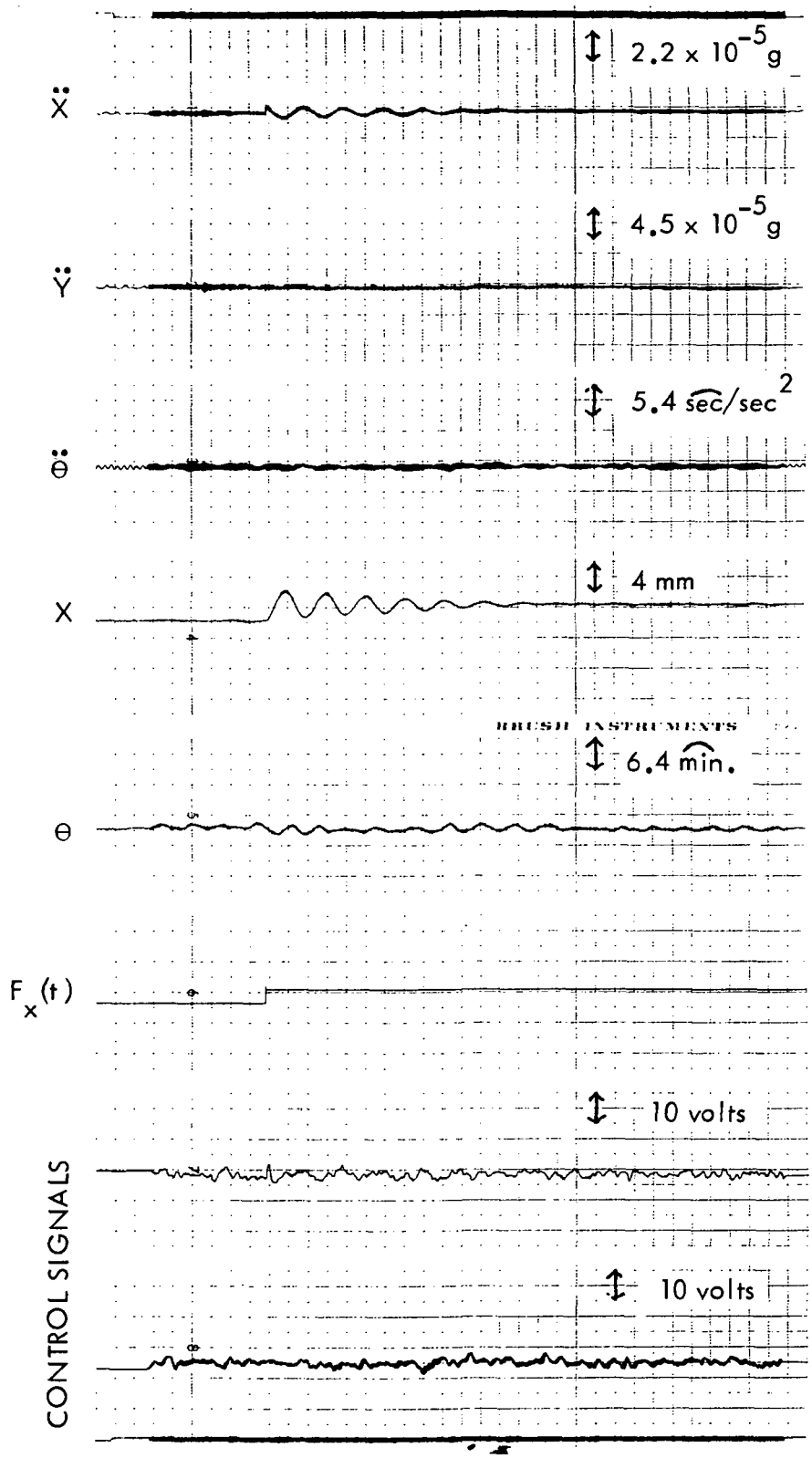

Figure 9.2-5. Response of Concentric Coil System to 2 mm Step, K = 600, 000

Figure 9.2-4 shows the response to the same 4.0-millimeter step but with a gain of K = 600,000 in the damping electronics. This large step exceeded the linear portion of the position detector in the first two cycles; however, a significant damping effect can be observed. The large angular disturbance is due to a small offset in center of mass and slightly different transient characteristics in the East and West damping electronics. These effects are becoming prominent with increasing amplifier gain.

Figure 9.2-5 is the typical 2.0-millimeter step response used to characterize the other systems in this report. The translational damping is approximately equal to a linear oscillator with a damping ratio of approximately 0.05. In agreement with the analog simulation for the basic magnetic system of section 4, there was no significant change in angular motion with the application of the step.

9.3 MODIFICATION THREE - ELIMINATION OF VELOCITY PICKUP COIL

The basic magnetic suspension and damping system is shown in figure 9.3-1. An induced voltage from the velocity pickup coil, proportional to the square of the velocity, av^2, is amplified with an amplifier of gain K, and the voltage is applied to the suspension coil. The damping force applied to the air bearing is proportional to the current i(s) through the suspension coil.

$$i(s) = \frac{V(s)}{Z} = \frac{Kav^2}{R + sL}$$

The velocity signal , av^2, is obtained from a separate external pickup coil.

The following method was used to eliminate the external velocity pickup coil and to use the suspension coil as a source of the velocity signal. A velocity signal, av^2, is also induced in the suspension coil as the air bearing and the disc magnets oscillate about the equilibrium position. However, the difficulty in using this signal is that the voltage drop caused by the changing current in the suspension coil also appears across the coil and must be separated from the induced velocity signal.

The induced velocity signal is separated from the voltage drop as shown in figure 9.3-2. A reference coil with the same resistance and inductance is placed in series with the suspension coil. The induced velocity signal appears only across the suspension coil, and the voltage drop across the reference coil is subtracted from the voltage across the suspension coil, leaving only the velocity signal. This signal is amplified and used to control the current in the suspension coil as in figure 9.3-1.

The difficulty in this method is that the reference coil cannot be exactly matched to the suspension coil. Referring to figure 9.3-3, let V_s and V_r be the voltages across the suspension and reference coils, respectively. If the two coils were identical, the difference between the two voltages would be the velocity signal. However,

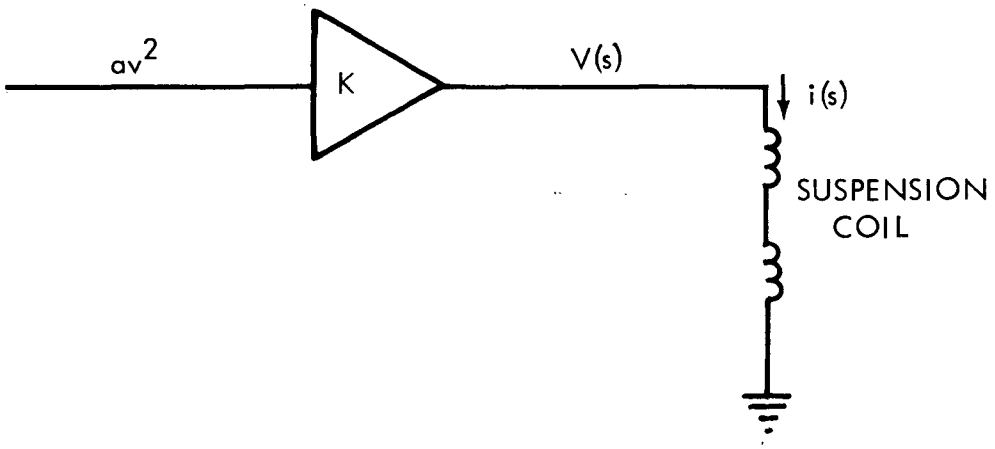

Figure 9.3-1. Basic Magnetic Damping System

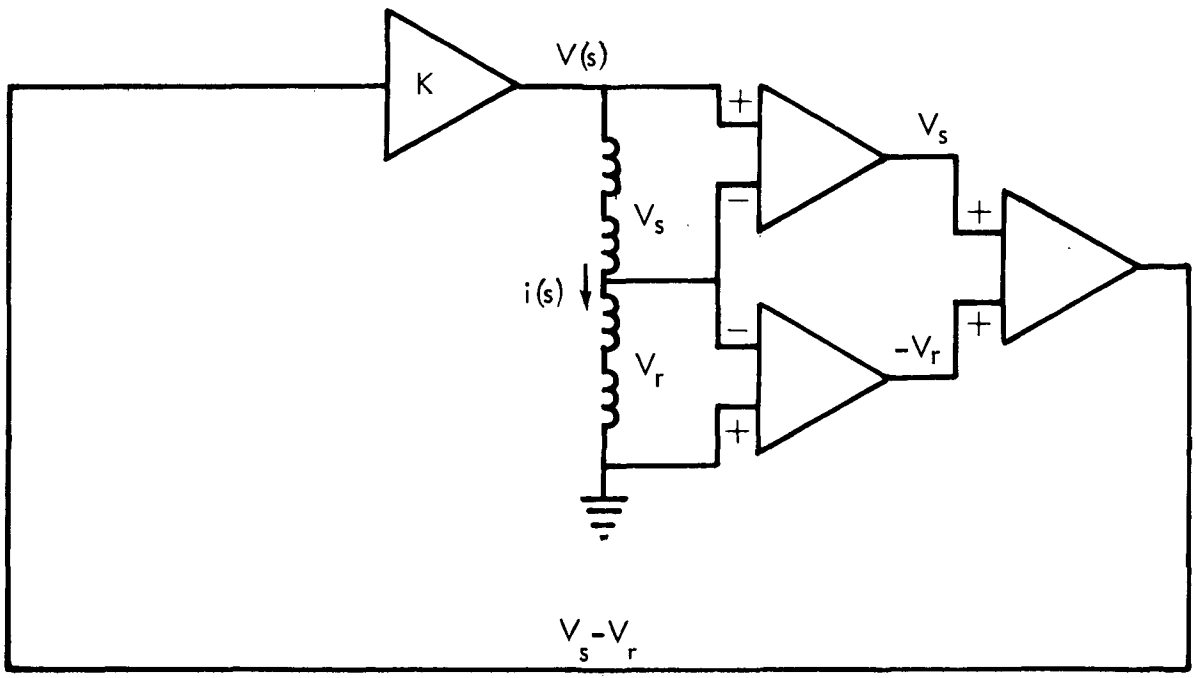

Figure 9.3-2. Elimination of Velocity Pickup Coil

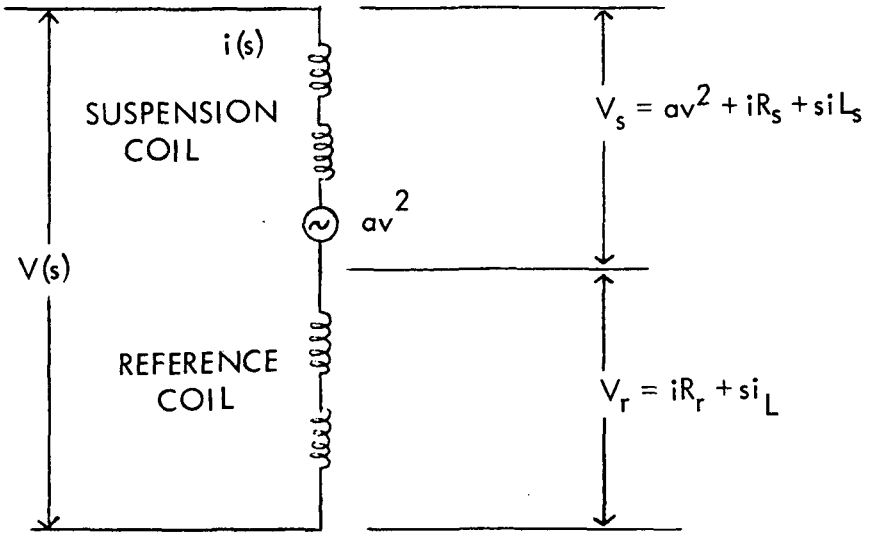

$$V(s) = K(V_s - V_r)$$

$$i(s) = K \frac{av^2 + i(R_s - R_r) + si(L_s - L_r)}{R + sL}$$

$$i(s) = K \frac{av^2}{R - K\Delta R + x(L - K\Delta L)}$$

Figure 9.3-3. Details of Suspension and Reference Coils

where they are not exactly matched, the suspension coil current, which is proportional to the damping force, is given by

$$i(s) = \frac{V}{Z} = K(V_s - V_r)$$

$$= K \frac{av^2 + iK\Delta R + siK\Delta L}{R + sL}$$

where

$$\Delta R = R_s - R_r, \quad \Delta L = L_s - L_r, \quad L = L_s + L_r, \quad R = R_s + R_r.$$

or

$$i(s) = \frac{Kav^2}{R - K\Delta R + s(L - K\Delta L)}$$

Thus, with a finite difference in the parameters of the two coils, there is a limit to the gain that can be used and still maintain a stable system.

In the present system a very large gain (K = 30,000) is necessary because of the small magnitude of the induced velocity signal. This is due to the relatively small velocity of the air bearing. The result is that the present experimental system requires that the resistance of the coils be matched to the order of an ohm to obtain the same damping as can be obtained with the basic system. The suspension and reference coils used in the air bearing simulation were matched to within 0.01 ohm. However, resistance heating by the coil current caused a greater variation in coil resistance. With this modification it was not possible to increase the amplifier gain to a value large enough to obtain significant damping.

Section 10

CONCLUSION

10.1 SUMMARY

The results of the analog simulation are indicative of the ultimate capability of the magnetic suspension and damping system. Both the analog simulation and the experimental program have demonstrated that the magnetic suspension system in two dimensions behaves similarly to a conventional spring suspension. Aside from subtle differences due to possible spring geometry variations with respect to the center of mass of the telescope, the magnetic suspension behaves almost identically to the spring system. The magnetic suspension has the additional advantages of non-physical contact between telescope and spacecraft, and real-time, continuously adjustable stiffness or spring constant. This latter property is the unique feature which allows translational and rotational energy to be removed from the telescope (i.e. damping); this energy appears in the form of dissipative heating in the power supplies of the suspension magnets.

Because of the similarity between the basic magnetic and spring suspensions this report has concentrated on defining the pertinent parameters and capabilities of the damping aspect of the magnetic suspension.

10.2 ANALOG SIMULATION

The analog simulation of section 5 illustrates the behavior of a perfectly aligned (except for center-of-mass position) and adjusted basic damping system. This illustrates the ultimate capability of the system. The most striking effect of the damping can be seen in the motion of the system after it has been released from a point, X_o, away from its equilibrium position. The damping is proportional to position (proportional to $X^2\dot{X}$ as opposed to $\dot{X}$ in a linear oscillator) and hence large amplitudes are damped much more rapidly than the smaller amplitudes. In fact, as seen from the examples in section 6, figure 6.2-7, the damping almost disappears for amplitudes below a certain value. This value is inversely proportional to the damping constant, a, or the gain in the damping electronics. This fact can be seen as an advantage since for a small amplitude about equilibrium, presumably while the telescope is operating, a smaller value of damping necessarily means a smaller value of transmissiblity for frequencies above resonance. It can,therefore be expected that the magnetic suspension with damping will have a lower transmissibility for small amplitudes than an equivalent mechanical system. Damping, and the necessarily

associated higher transmissibilities, does not take effect until the disturbance reaches some predetermined amplitude.

The results of the angular responses were mixed. The effect of damping on a previously established rotational motion was insignificant for rotations in the range of 0.5 arc-minute. Physically this is because the velocity pickup magnet extending a distance 1/2 ℓ from the center of the telescope or air bearing does not achieve an appreciable angular velocity until the angular amplitude is at least 1 arc-minute in the present example. The behavior of the rotational damping is essentially the same as the translational damping in that there is a lower amplitude below which the damping is not significant. The only parameter by which this minimum rotational amplitude can be changed without affecting the minimum translational amplitude is by changing the length, ℓ, of the arm of the velocity pickup magnet. As seen from equation 6.3, this damping term is proportional to

$$\frac{a\,\ell^4}{I_z}$$

hence, a small change in ℓ can have a very large effect on the angular motion.

10.3 EXPERIMENTAL RESULTS

In general the experimental results agreed with the analog simulation. Excellent agreement was obtained for the translational responses, once the electronic gain, K, was related to the damping constant, a, of the analog simulation. Damping ratios, as calculated by comparing the percent of first overshoot with that of a linear damped oscillator, from zero to 0.55, have been obtained experimentally for 2.0-mm step inputs. This damping is continuously variable by adjusting the electronic gain, K. This range is considered to be adequate for any anticipated astronomical telescope application, since larger values of K or "a" are accompanied by more rapid increases in rise time. Such large rise times or settling times, equal to three or four periods, would be impractical. Larger values of damping are possible, however. The value of K = 1,000,000 equivalent to a damping ratio of 0.55 was the maximum that could be conveniently obtained with the laboratory equipment and the time available. The high gains involved are not actually a problem since the control signals have frequencies comparable to the resonant frequency of the air bearing and the bandwidth can be 1.0 Hz or less. The major requirement is that the phase shift be relatively small (less than 20 degrees) for frequencies near resonance. In the present case resonance was approximately 0.03 Hz and 0.05 Hz for translation and rotation, respectively.

Major discrepancies between simulation and experimental performance occurred in the angular responses of the system with high electronic gain, K, or high damping values. This was due to a number of practical design and alignment problems and tolerances not easily controllable or measureable in the present experimental system within the time available. These problems were not foreseen and hence were not incorporated into the analog simulation; however, their effect was primarily on the angular motion, with very little effect on the translational response.

Some of the difficulties affecting the angular response of the experimental system are discussed below:

10.3.1 VALUES OF STIFFNESS

It was difficult to obtain the identical value of stiffness or spring constant, k, for each of the two sets of suspension coils on each side of the air bearing. A small difference in the two suspension systems (called East and West in this report) could introduce a small unwanted torque on the air bearing with the application of a disturbance signal to the X direction (shaker input signal). This extraneous torque would be proportional to the instantaneous value of the angular position of the air bearing.

To overcome this interaction the dimensions of the coils and their separation were matched as closely as possible. The steady-state current, I_o, through each set of suspension coils was matched to approximately 3 percent. However, there are some parameters such as stray magnetic effects, slightly different or slow decreases in the strength of each of the disc ceramic magnetics, or changes in coil resistance, which are not readily predictable and can effect the response of the system. In an actual telescope suspension the stray magnetic fields could be shielded and the disc magnets would be replaced by precision wound coils connected to a constant current source. Maintaining a very stable steady state current, I_o, in the suspension coils is not anticipated to be a problem.

10.3.2 MISMATCH OF SYSTEMS IN BOTH GAIN AND FREQUENCY RESPONSE

The high-gain amplifiers in both suspension arms should be accurately matched in both gain and frequency response. If there is a mismatch in the gains of the two systems, an unwanted torque could be exerted on the air bearing in exactly the same manner as described in paragraph 10.3.1 above. This torque is a result of interaction between the X and θ modes of oscillation under an applied disturbance $F_x(t)$; however, the effect of this mismatch is more pronounced at the higher values of gain.

In the present experimental system the gains were adjusted by applying a sinusoidal disturbance to the shaker frame and adjusting amplifier gains until the same control signal amplitude was obtained in each set of suspension coils. However, the matching could not be performed at all frequencies and hence the transient responses were not the same in both the East and West coils. This can be seen in section 8, figure 8.3-3, in which the large transient spikes in the control signals are of unequal magnitude. This mismatch created the large angular disturbance in the figure.

It should be noted, however, that even moderate mismatches such as those described in paragraphs 10.3.1 and 10.3-2 have little effect on the damping. Their major effect is the coupling of the X and θ modes of vibration, and in the absence of a driving force, both modes are still damped as predicted by the analog simulation. This damping is seen in figure 8.3-3; after the initial step input and associated transients, the disturbance quickly reduces in amplitude.

10.3.3 CENTER-OF-MASS OFFSET

Other sources of angular disturbance which were not easily measured in the present experimental system were uncertainties in the value of center of mass offset, δ , and in the actual position of the velocity pickup coils with respect to the equilibrium position of the magnetic suspension. The center of mass of the air bearing was located by inserting three force gauges at precise spots under the air bearing, and then calculating the center of mass position. However, considering the 264-kg mass of the air bearing and the difficulty of measuring some of the positions on the air bearing, the accuracy of the center-of-mass position is believed to be on the order of one millimeter. The suspension was then adjusted about this position to obtain the smallest angular disturbance with the application of a shaker disturbance.

Another alignment tolerance is the accurate positioning of the velocity pickup coil such that it is directly above the velocity pickup magnet when the air bearing is at its equilibrium position. If the velocity pickup coil is not correctly positioned, there will be some directions of motion and some amplitude below which the damping control signal will have the wrong polarity. This will result in a minimum possible amplitude for which adequate control and damping can be obtained.

These two alignment tolerances become more stringent with increased control system gain, K. It is for this reason that some of the angular disturbances measured in the laboratory were larger than indicated by the analog simulation.

10.4 GENERAL CONCLUSIONS AND RECOMMENDATIONS

The magnetic suspension system was found to have many advantages over a spring suspension, the principal advantages being non-physical contact and real-time adjustable stiffness. Basically the behavior is the same as the spring system with respect to transmissibility and dynamic response. It has been demonstrated that the suspension can reduce the transmitted disturbances to a level within the capability of the telescope pointing and stabilization systems.

The advantage of real-time adjustable stiffness allows damping to be introduced into the suspension. The damping can be controllable for translational amplitudes down to 0.1 mm or less, depending on the electronic gain. Damping for rotational amplitudes down to 30 arc-seconds has been demonstrated. Since the angular disturbance varies as $a\ell^4/I_z$, a doubling of the arm length, ℓ, to 2.0 meters would allow angular motions as small as 2.0 arc-seconds to be damped. Damping for angular motions below an arc-second should easily be attainable in a practical telescope design. The advantage of the present system for a coarse pointing and damping system is that the effective damping actually increases with amplitude. Large disturbances accidentally transmitted to the telescope are very quickly removed. The damping system is essentially inoperative for the very small amplitudes, allowing the use of a "fine" control system without concern for the usual interaction or transition between the coarse and fine servo systems.

Appendix A

DETERMINATION OF POTENTIAL WELL SHAPE AND COIL DESIGN

The purpose of this appendix is to determine the basic parameters of the suspension coil geometry and their effect on the suspension stiffness, i.e. shape of the potential function. Also illustrated in this appendix is a means to eliminate a large amount of the computer calculations which would ordinarily be involved in the force calculations. This is accomplished by using Hankel Transforms in place of the usual convolution integrals.

1.0 POTENTIAL ENERGY CALCULATIONS

A permeable body placed in a magnetic field will experience a force tending to move the body to the region of highest field. The force is proportional to the gradient of the magnetic field at the body. The potential enegy, U, of a permeable body placed in a magnetic field, $\bar{b}$, is given by (cgs units):

$$U = 1/2 \int_V \bar{m} \cdot \bar{b} \, dv$$

where $\bar{m}$ is the magnetization of the body. The magnetization $\bar{m}(x,y,z)$ at any point is usually a function of the field, $\bar{b}(x,y,z)$, at that point. However, in the case of the permanent disc magnets used in this report, the magnetization can be considered as being independent of $\bar{b}$. Referring to figure A-1, it will also be assumed that the magnetization is parallel to the z-axis, and that the magnetic field is constant across the thickness, d, of the magnet. The potential energy is then given by

$$U(x', y') = \frac{d}{2} \iint m(x,y) \, b_z(x,y) \, dx \, dy$$

the integration being performed over all space. The potential energy as a function of position (x', y') of the center of the disc magnet is

$$U(x', y') = \frac{d}{2} \int_{-\infty}^{\infty} \int_{-\infty}^{\infty} m(x - x', y - y') \, b_z(x,y) \, dx \, dy$$

Such integrals are known to be very time consuming when evaluated by digital computers.

The above equation is a special case of the two dimensional convolution integral:

$$g(x, y) = \int_{-\infty}^{\infty} \int_{-\infty}^{\infty} f_1(x - x', y - y') f_2(x', y') \, dxdy$$

$$= f_1(x, y) * f_2(x, y)$$

The above integral and the Fourier transformations have a special relationship. If

$$g(x, y) = f_1(x, y) * f_2(x, y)$$

then:

$$F[g(x, y)] = F[f_1(x, y)] \; F[f_2(x, y)]$$

where $F[\,]$ is an operator denoting the Fourier transform of the function in the brackets, i.e.

$$F\left[g(x, y)\right] = \int_{\infty}^{\infty} \int_{\infty}^{\infty} g(x, y) e^{-i(ux + vy)} \, dxdy$$

The inverse transform $F^{-1}[g]$ is given by

$$F^{-1}\left[g(u, v)\right] = \frac{1}{4\pi^2} \int_{-\infty}^{\infty} \int_{-\infty}^{\infty} g(u, v) e^{i(ux + vy)} \, dudv$$

The potential energy, U (x,y) , as a function of position (x,y) can be expressed as the convolution:

$$\frac{2U(x, y)}{d} = m(x, y) * b_z(x, y)$$

This convolution integral can be evaluated by taking the transforms of m(x, y), and $b_2(x,y)$, and then taking the inverse of their product, i.e.

$$\frac{2U(x, y)}{d} = F^{-1}\left[F[m(x, y)] \; F[b_z(x, y)]\right]$$

If the functions $f_1(x,y)$ and $f_2(x,y)$ have circular symmetry, such that

$$r^2 = x^2 + y^2$$

the convolution integral becomes

$$g\left(\sqrt{x^2 + y^2}\right) = \int_{-\infty}^{\infty}\int_{-\infty}^{\infty} f_1\left(\sqrt{x'^2 + y'^2}\right) f_2\left(\sqrt{(x - x')^2 + (y - y')^2}\right) dx'\, dy'$$

and the Fourier transforms also have circular symmetry. In such a case the Fourier transform reduces to a Hankel transform, and the convolution integral reduces to

$$g(r) = f_1(r) * f_2(r)$$

$$H[g(r)] = 2\pi H[f_1(r)]\ H[f_2(r)]$$

Therefore,

$$g(r) = H^{-1}\left[H[f_1(r)]\ H[f_2(r)]\right]$$

where $H[\ ]$ is the operator demoting the Hankel transform of the function in the brackets. The Hankel transform is defined by:

$$H[g(r)] = h(\omega) = \int_0^{\infty} r g(r) J_0(\omega r)\, dr$$

where $J_0(\omega r)$ is the Bessel function of zero order. It will be noticed that the transformation is reciprocal, and hence tables of the inverse transform are not necessary, i.e.

$$g(r) = H^{-1}H[g(r)] = \int_0^{\infty} \omega h(\omega) J_0(r\omega)\, d\omega$$

By the use of these transforms a great deal of computer time can be saved in calculating the potential energy function. If the magnetic field $b_z(r)$ and the magnetization $m(r)$ are known as functions of radial position, then the potential energy $U(r)$ is found by simply taking the inverse Hankel Transform of the product of the transforms of $b_z(r)$ and $m(r)$.

Hence,

$$U(r) = \pi d H^{-1}\left[H[m(r)]\, H[b_z(r)]\right]$$

As a simple example assume $m(r)$ is that of a permanent magnet of constant magnetization throughout its volume. Then

$$m(r) = \begin{cases} m_o & r \le r_o \\ 0 & r > r_o \end{cases}$$

$$M(\omega) = H\left[m(r)\right] = \frac{m_o r_o J_1(r_o \omega)}{\omega}$$

Assume that the magnetic field is also expressed by a similar function

$$b_z(r) = \begin{cases} b_o & r \le r_o \\ 0 & r > r_o \end{cases}$$

$$B_z(\omega) = H\left[b_z(r)\right] = \frac{b_o r_o J_1(r_o \omega)}{\omega}$$

The potential energy, $U(r)$, is obtained by taking the inverse transform of the product of two transforms above.

$$U(r) = \pi d H^{-1}\left[M(\omega)\, B_z(\omega)\right]$$

$$= \pi d r_o^2 m_o b_o H^{-1}\left[\frac{J_1^2(r_o\omega)}{\omega^2}\right]$$

$$= \pi d r_o^2 m_o b_o \begin{cases} 2\cos^{-1}\left(1/2\,\frac{r}{r_o}\right) - \frac{r}{r_o}\sqrt{1 - 1/4\left(\frac{r}{r_o}\right)^2} & r \le 2r_o \\ 0 & r > 2r_o \end{cases}$$

This function is shown in figure A-2, along with the parabolic potential function.

The force as a function of position is obtained from the derivative of the potential function:

$$f(r) = -\frac{dU(r)}{dr}$$

In this example

$$f(r) = -\frac{dU(r)}{dr} = -2\pi d r_o m_o b_o \sqrt{1 - x^2}$$

$$x = r/2r_o \le 1$$

$$= -2\pi d r_o m_o b_o \left(1 - \frac{1}{2}x^2 + \frac{1}{8}x^4 - \ldots\right)$$

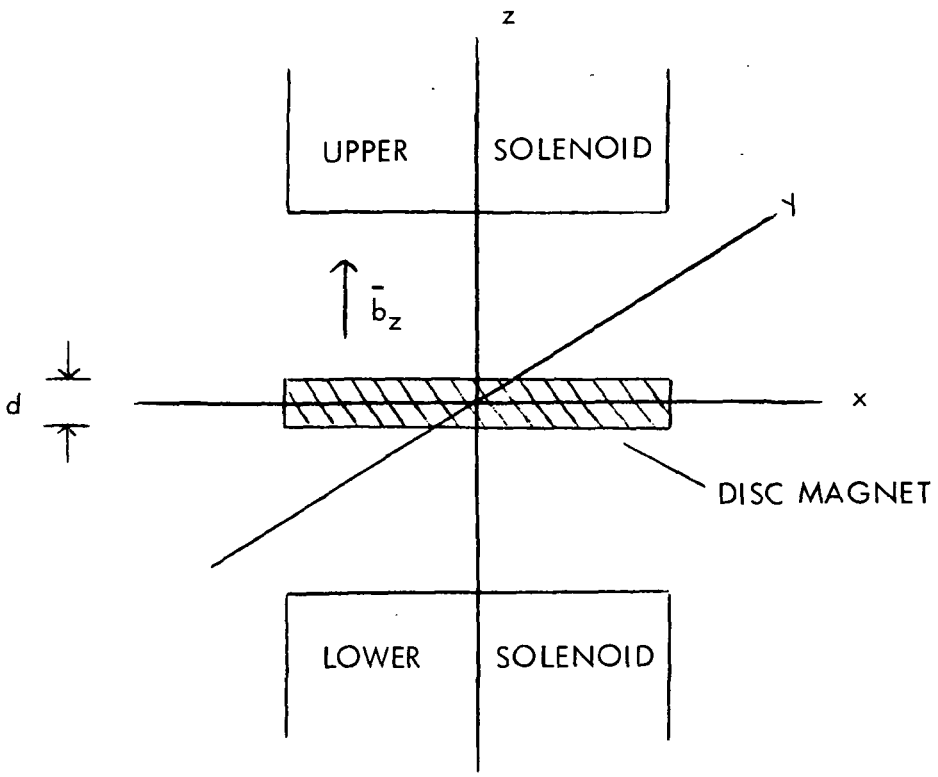

Figure A-1. Coordinate System for Suspension Coil Geometry

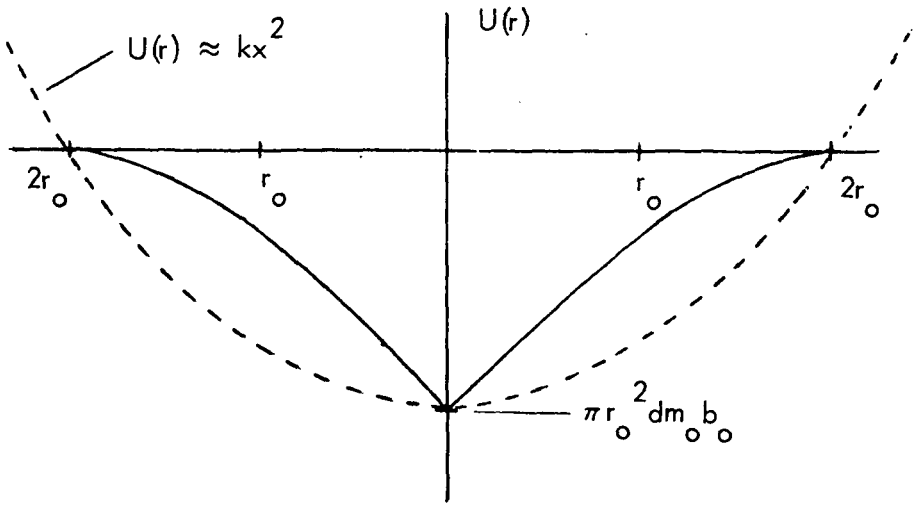

Figure A-2. Potential Energy Function for Example Discussed in Text

the force is very nearly constant for small displacement. However, this is a very simplified example, since the function assumed for $b_z(r)$ is not physically realizeable.

An excellent discussion of Hankel transforms used to evaluate convolution integrals can be found in reference 1. One of the best tables of Hankel transforms can be found in reference 2. However, some authors define the Hankel transform in slightly different manners, and this must be taken into account when using various tabulations of transforms.

The use of the transforms can be very convenient and can result in a considerable time savings in both hand and computer computations. The magnetic field, $b_z(r)$, can usually be approximated by the summation of functions for which the transforms are known. The final inverse transform, if necessary, can be easily obtained by numerical methods on a computer. The advantage is in the fact that the transform is a function of one variable and is much easier to evaluate than a two-dimensional convolution integral.

2.0 MAGNETIC FIELD CALCULATIONS AND COIL PARAMETERS

There exists a large amount of literature on the magnetic field distributions of the general Helmholtz type coil arrangement. One of the best compilations is the text by Montgomery (reference 3). Unfortunately most of the literature is concerned with the field distribution along the axis of the solenoid rather than in the central plane transverse to the axis as in the present case. However, this information can still be used, as the axial field distribution, $H_z(z, \theta = \pi/2)$, and some boundary conditions (which can be approximated) uniquely define the field at all other points. Since no closed form expression exists for the magnetic field at non-axial points for even a simple coil, the only alternative is the summation of each of the individual current loops of the coil. This necessitates the use of a computer and in most cases a fair amount of computer time. Usually, however, the transverse field distribution can be predicted with suitable accuracy, that a computer is unnecessary. Analytical rather than numerical methods are stressed in this appendix such that general trends can be more easily recognized in evaluating possible coil designs to specific applications. This will help to define the significant parameters needed as a starting point for the evaluation of suspension system characteristics or for the computer calculations if such accuracy is desired.

The basic geometry for the Helmholtz coils is shown in figure A-3. The field around the origin can be expanded in a series as follows (cylindrical coordinates are used):

$$H_z(z,O) = H_o \left[1 + h_2(z/a_1)^2 + h_4(z/a_1)^4 + \ldots\right]$$

$$H_z(r, \pi/2) = H_o \left[1 - \frac{1}{2}h_2(r/a_1)^2 + \frac{3}{8}h_4(r/a_1)^4 - \frac{5}{16}h_6(r/a_1)^6 + \ldots\right]$$

The coefficients h_2, h_4, h_6, etc. can be related to the normalized physical dimensions of the coils as shown in figure A-3. These coefficients can be found in a number of texts, although the notation used by Montgomery (reference 3) will be used here.

$$h_2 = \left[FE_2(\alpha,\beta) - F_c E_2(\alpha_c,\beta_c)\right] \div \left[F(\alpha,\beta) - F_c(\alpha_c,\beta_c)\right]$$

$$h_4 = \left[FE_4(\alpha,\beta) - F_c E_2(\alpha_c,\beta_c)\right] \div \left[F(\alpha,\beta) - F_c(\alpha_c,\beta_c)\right]$$

where

$$F = \frac{4\pi}{10}\,\beta\left(\sinh^{-1}\frac{\alpha}{\beta} - \sinh^{-1}\frac{1}{\beta}\right)$$

$$FE_2(\alpha,\beta) = \frac{4\pi}{10}\,\frac{1}{2\beta}\left(C_1^{3/2} - C_3^{3/2}\right)$$

$$FE_4(\alpha,\beta) = \frac{4\pi}{10}\,\frac{1}{24\beta^3}\left[C_1^{3/2}(2 + 3C_2 + 15C_2^2) - C_3^{3/2}(2 + 3C_4 + 15C_4^2)\right]$$

$$C_1 = \frac{1}{1+\beta^2},\quad C_2 = \frac{\beta^2}{1+\beta^2},\quad C_3 = \frac{\alpha^2}{\alpha^2+\beta^2},\quad C_4 = \frac{\beta^2}{\alpha^2+\beta^2}$$

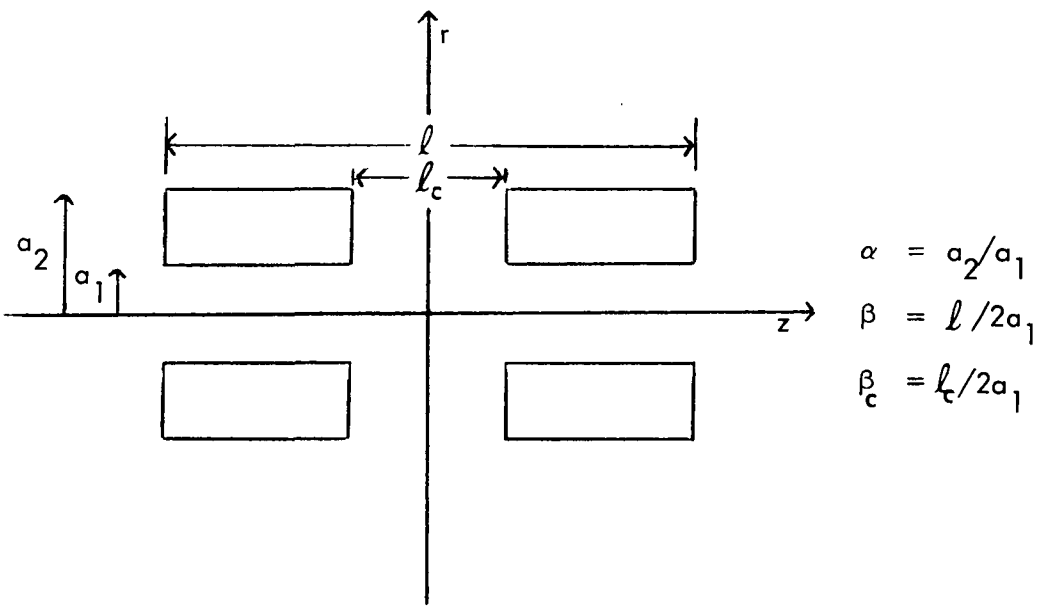

Figure A-3. Definition of Helmholtz Coil Parameters

The reader is referred to the previously cited reference for a particular coil design, since that text contains tables of the higher order coefficients and graphs of the functions $FE(\alpha,\beta)$. The graphs are especially useful for a quick first evaluation of possible coil dimensions and separations.

The axial field distribution for a typical coil geometry of $\alpha = 3$, $\beta = 1$ is shown in figure A-4. The field as a function of axial position is shown for different values of coil separation, β_c. Note that for any significant separation, the term h_2 in the expansion of the field is positive for an increasing field in the axial direction.

$$H_z(z,O) = H_o \left[1 + h_2(z/a_1)^2 + \ldots\right]$$

$$H_z(r,\pi/2) = H_o \left[1 - \tfrac{1}{2} h_2(r/a_1)^2 + \ldots\right]$$

This means that in the radial plane, $z = 0$, $\theta = \frac{1}{2}\pi$, the field is decreasing. The difference in signs for the second order terms in the two expansions is actually a consequence of a theorem by Earnshaw (reference 4). The theorem essentially states that in a region not occupied by a current distribution the field and hence the potential energy cannot have an absolute maximum or minimum. If the field is increasing in one direction, there is another direction in which the field is decreasing. The field distribution takes the form of a saddle. This theorem is usually invoked to demonstrate that a stable three dimensional electrostatic or magnetic suspension is not possible at any single point in space. (The present magnetic suspension discussed in this report is actually two separate suspensions at two different points is space).

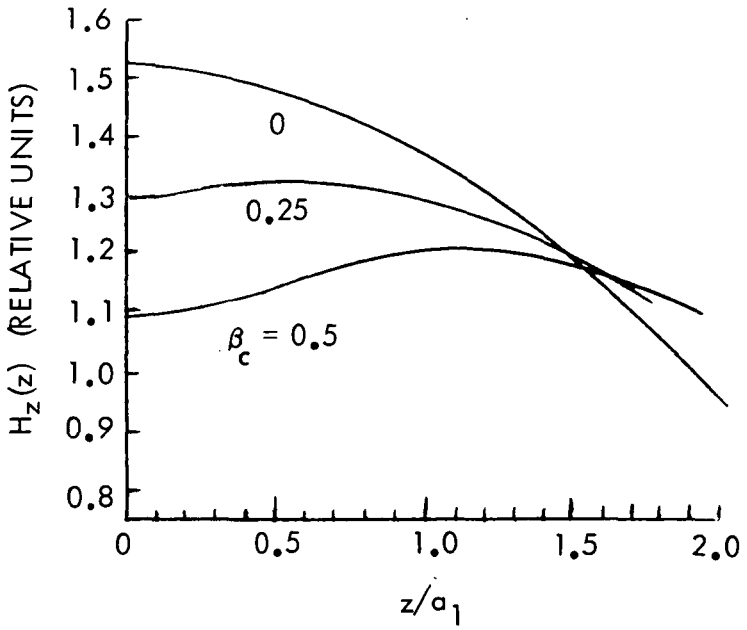

Figure A-4. Axial Field Profiles for Helmholtz Coils

In designing a suspension coil system to obtain a desired potential energy function, it is necessary to use the Hankel transforms described in the beginning of this appendix to determine the required magnetic field distribution, $H_z(r, \frac{1}{2}\pi)$, and the values of the coefficients h_2, h_4, etc. The coefficients can then be related to the coil dimensions by means of the functions FE (α, β). In most cases the behavior of the system can be adequately described by considering only the first coefficient, h_2, of the field expansion.

As a second example of a potential energy function calculation , consider the coil configuration and disc magnets used in this report. The magnetic field can adequately be approximated by considering only the first coefficient, h_2:

$$b_z(r) = \begin{cases} H_o(1 - br^2) & r \leq b^{-1/2} = r_o \\ O & r > b^{-1/2} = r_o \end{cases}$$

The magnetization of the magnet is still given by:

$$m(r) = \begin{cases} m_o & r \leq r_o \\ O & r > r_o \end{cases}$$

The Hankel transforms of these two functions are respectively

$$H_o \frac{2J_2(r_o\omega)}{\omega^2}$$

and

$$r_o m_o \frac{J_1(r_o\omega)}{\omega}$$

The potential energy, U(r) is given by the inverse transform of the product

$$U(r) = r_o H_o m_o \pi d H^{-1} \left[\frac{J_2(r_o\omega) J_1(r_o\omega)}{\omega^3}\right]$$

The product of Bessel Functions can be expanded in the following series (reference 5 page 360):

$$J_\nu(z)J_\mu(z) = (\tfrac{1}{2}z)^{\nu+\mu} \sum_{k=o}^{\infty} \frac{(-1)^k \Gamma(\nu+\mu+2k+1) (\frac{1}{4}z^2)^k}{\Gamma(\nu+k+1) \Gamma(\mu+k+1) \Gamma(\nu+\mu+k+1) k!}$$

For $\nu = 2$, and $\mu = 1$,

$$J_2(z)J_1(z) = (\tfrac{1}{2}z)^3 \left[1/2 - (5/48)z^2 + (7/768)z^4 - \ldots\right]$$

$$z = r_o\omega$$

Consistent with the approximations made with the magnetic field, the terms higher than second order can be neglected, and the potential energy can be written:

$$U(r) = 1/16\ \pi d r_o H_o m_o H^{-1} \left[r_o^3 (1 - \frac{10}{48} r_o^2 \omega^2) \right]$$

On taking the transform,

$$U(r) = \frac{r_o^2 d H_o m_o}{16\gamma^2} \quad \frac{J_2(r/\gamma r_o)}{(r/\gamma r_o)^2} \qquad \gamma = (10/48)^{1/2}$$

$$\approx \frac{r_o^2 d H_o m_o}{128\gamma^2} \quad \left[1 - (1/12)\ (r/\gamma r_o)^2 + \ldots \right]$$

for small values of r about equilibrium.

For most Helmholtz coil arrangements the potential function is to a first approximation parabolic; and hence the basic magnetic suspension discussed in this report should behave as a linear oscillator. (Of course the suspension becomes non-linear as soon as the electronic damping is applied). The approximations made here are considered to be adequate since the coefficients of the higher order terms in the series expansions are rapidly decreasing. Therefore, keeping only the terms up to second order is a reasonable approximation.

In summary, if the diameter of the disc magnet is approximately equal to the diameter of the helmholtz coils, then the potential function will be approximately parabolic regardless of the other dimensions of the coils within reasonable limits. Major departures from a parabolic function, if desirable, would necessitate nonuniform current distributions in the magnet coils. However, there is one major departure from a nonlinear system that can easily be obtained. If the disc magnet is made to have a diameter much smaller then the extent of the magnetic field, then there would exist a small region about equilibrium in which the disc magnet would experience little or no force. This would be due to the fact that the force is proportional to the gradient of the field in the vicinity of the magnet. If the field is relatively constant over a particular region, then the force would be zero. It would therefore be simple to fabricate a system having a generally parabolic potential but with a small "dead space" near equilibrium which would have a constant or very slowly changing potential.

REFERENCES FOR APPENDIX A

R1. Papoulis, Athanasios: Systems and Transforms with Applications in Optics. McGraw Hill, 1968.

R2. Bateman, Harry: Tables of Integral Transforms, Vol. II. McGraw Hill, 1954.

R3. Montgomery, Bruce: Solenoid Magnet Design. John Wiley and Sons, 1969.

R4. Smythe, William: Static and Dynamic Electricity. McGraw Hill, 1950.

R5. Abramowitz, Milton and Irene Stegun ed., Handbook of Mathematical Functions. National Bureau of Standards, 1964.

GOVERNMENT FIELD PRINTING PLANT
(UNDER CONTRACT NAS 8-26887)
NASA-MICHOUD ASSEMBLY FACILITY 1972
NEW ORLEANS, LOUISIANA 70129